The genetic and evolutionary basis for somatic cell differentiation in the multicellular alga *Volvox carteri*: investigations into the regulation of *regA* expression

by

Stephan König

Diplom in Biology, University of Heidelberg, 2005

A Dissertation Submitted in Partial Fulfillment
of the Requirements for the Degree of

Doctor of Philosophy

in the Graduate Academic Unit of Biology

Supervisor: Aurora Nedelcu, PhD Biology

Examining Board: Andreas Decken, PhD, Chemistry, Chair
Adrian Reyes-Prieto, PhD, Biology
Shawn MacLellan, PhD, Biology

External Examiner: Stephen Miller, PhD Biology, University of Maryland, Baltimore County

This dissertation is accepted by the
Dean of Graduate Studies

THE UNIVERSITY OF NEW BRUNSWICK

November, 2014

©Stephan König (2015)

ABSTRACT

The evolution of life is characterized by a series of major transitions in the complexity of biological systems. One such transition was from unicellular to multicellular organisms and involved the evolution of sterile somatic cells—a premier example of cooperation. The goal of this thesis was to investigate the genetic and evolutionary basis for somatic cell differentiation in *Volvox carteri*, a simple multicellular green alga composed of ca. 2,000 somatic cells and up to 16 reproductive cells (gonidia). In *V. carteri*, the terminal differentiation of small somatic cells involves the expression of *regA*, a gene coding for a transcription factor thought to repress nuclear genes required for chloroplast biogenesis and, thus, for cell growth and division. *regA* induction is likely dependent on cell size, but the molecular mechanism whereby cell size is translated into *regA* expression remains to be elucidated. This study focused on the regulation of *regA* expression by employing mechanistic and evolutionary approaches. Using a *regA*$^{-}$/gonidialess double mutant strain characterized in this study, I showed for the first time that in addition to its developmental expression, *regA* can be induced by environmental stimuli, and this induction is also dependent on cell size. These findings provide support for a previously proposed hypothesis that *regA* evolved from an ancestral stress-response gene. Furthermore, in mutants expressing a non-functional RegA protein, the conditions that trigger *regA* expression also induce programmed cell death, which points towards a dual function for *regA* in cell fitness: to decrease cell reproduction (by repressing cell growth) and to increase cell survival (by conferring resistance to stress). Genes with antagonistic pleiotropic effects on fitness have been proposed to stabilize cooperation, and *regA* is the first such example in multicellular organisms with unitary development (i.e., developed

from a single cell). To identify transcription factors binding to *cis*-regulatory elements of *regA* I have used yeast one-hybrid assays. No potential candidates were identified, suggesting that cooperative binding of proteins or multi-protein complexes are involved in the regulation of *regA*. Overall, this study provides novel insights into our understanding of somatic cell differentiation, from both a mechanistic and an evolutionary perspective.

DEDICATION

To my parents:

Among countless things, I owe you an open mind and stubbornness.

ACKNOWLEDGEMENTS

Like with any grand undertaking this thesis would not have been possible without the help of many others.

I would like to thank my supervisor Dr. Aurora Nedelcu for introducing me to *Volvox*, for the opportunity and support to realize my own project, and for showing me how to find a compelling story in a tangle of data.

My thanks also go to the members of my supervisory committee, Drs. Bryan Crawford, Cheryl Patten, and Dion Durnford; their ideas and guidance greatly helped me to shape this project and to find the next steps.

I am grateful to Drs. Linley Jesson, Dave Kubien, and Laura Weir for their help with my brief foray into statistics, and to Susan Belfry and Steven Cogswell for their insights and training related to microscopy and image analysis.

I would also like to thank Chris Wile, Polly Brinkman, and Tanya Moore for helping me out with resources or hunting them down, John Tidswell for his untiring dedication to keep our incubators at bay and our cultures alive, and Brian Titus and Murray Olive for taking the culturing of *Volvox* to the next level.

Thanks to Dr. David Taplin for a surreal encounter like in a movie scene, and for encouragement on the last stretch of the writing.

Karen Gordon and Dr. Mike Duffy, I greatly appreciate your help in becoming a better teacher.

My brothers and sisters in arms Jon Neilson, Maria Davis, Jonas Leichsenring, Christian Tudorache, Amanda Cavanagh, Chris Jackson, Lauren Scopel, Tom Coulson, Sarah

Hamsher, Katy Hind, Meghan Bruce, and Ryan O'Neill: my thanks go to you for braving the waters of science together with coffee in hand and a song on our lips.

And thank you, Bridgette Clarkston: you make any journey more exciting and less daunting.

Table of Contents

ABSTRACT ii
DEDICATION iv
ACKNOWLEDGEMENTS v
Table of Contents vii
List of Tables xiii
List of Figures xv
Abbreviations xviii
Chapter 1 General introduction 1
1.1 General background 1
1.2 The volvocine algae as a model system 2
1.3 Hypotheses on the selective advantages of multicellularity and cell differentiation in *Volvox carteri* 3
1.4 Cells of two different sizes are formed during embryogenesis of *Volvox carteri* 6
1.5 Cell size determines cell fate 7
1.6 Somatic cells escape terminal differentiation in regenerator mutants 8
1.7 RegA is a putative transcription repressor 10
1.8 Goal and objectives of this study 11
1.9 References 15
Chapter 2 Characterization of a new gonidialess mutant as a model-system for *regA* expression studies 18
2.1 Introduction 18
2.1.1 Goal and objectives of this study 20
2.2 Material and Methods 21

2.2.1 Strains and culturing conditions 21

2.2.2 Experimental cultures 21

2.2.3 Isolation of early EVE embryos 22

2.2.4 Cell size measurements 22

2.2.5 Genomic DNA extraction 22

2.2.6 Amplification of *regA* regions 23

2.2.7 RNA extraction and quantification 24

2.3 Results 26

2.3.1 *regA* expression in the dmTAM gonidialess mutant 26

2.3.2 Characterization of the dmAMN gonidialess mutant 27

2.3.3 Characterization of the *regA* mutation in the dmAMN mutant 27

2.3.4 Initial studies of *regA* expression in dmAMN 28

2.3.5 *regA* expression in the dmAMN gonidialess mutant grown in a standard light regime 28

2.3.6 *regA* expression in dmAMN as a function of cell size 29

2.3.7 *regA* expression in the wild-type EVE strain grown in a standard light regime 30

2.4 Discussion 31

2.4.1 *regA* expression pattern in EVE 31

2.4.2 Loss of *regA* expression in the dmTAM mutant 33

2.4.3 dmAMN is a suitable mutant to investigate *regA* induction 33

2.5 References 49

2.6 Appendix 51

2.6.1 Determination of a suitable reference gene 51

2.6.2 Additional sequencing of dmAMN *regA* locus 55

2.6.3 Sequencing of the *regA* RT-qPCR product 58

Chapter 3 Environmental induction of *regA*: a new role for the RegA protein 59
3.1 Introduction 59

3.1.1 The effects of cell size on gene expression 60

3.1.2 The closest *regA* homolog in *C. reinhardtii*, *RLS1*, is expressed in response to stress 62

3.1.3 Gene co-option and the evolution of *regA* 64

3.1.4 Signaling pathways and *regA* induction 66

3.1.5 Goal and objectives of this study 69

3.2 Material and Methods 70

3.2.1 Strains and culturing conditions 70

3.2.2 *regA* expression and cell viability under different light regimes 71

3.3 Results 76

3.3.1 *regA* expression in dmAMN 76

3.3.2 *regA* expression in *V. carteri* wild type strain EVE 80

3.4 Discussion 82

3.4.1 Photoreceptors are likely not involved in *regA* induction 82

3.4.2 *regA* is induced by a specific combination of environmental cues, genetic background and cell size 85

3.4.3 Conditions that trigger *regA* expression also induce PCD 86

3.4.4 RegA protein confers stress-resistance 88

3.4.5 The environmental induction of *regA* likely involves a chloroplast-related redox signal 90

3.4.6 The potential effects of cell size on CEF and ROS production 93

3.4.7 A model for *regA* induction 95

3.4.8 *regA* evolved to deal with drastic changes in chloroplast size due to multiple fission 96

3.4.9 *regA* as a cooperation gene 97

3.5 References 116

3.6 Appendix 123

Chapter 4 Yeast one-hybrid screens to identify *trans*-acting factors binding to *cis*-regulatory elements in *regA*'s introns 125

4.1 Introduction 125

4.1.1 Brief overview of gene regulation 125

4.1.2 Differential *regA* expression involves intronic elements 126

4.1.3 Hypothesis and objectives of this study 128

4.2 Material and Methods 130

4.2.1 *Volvox carteri* strain and culturing conditions 130

4.2.2 Molecular Cloning 130

4.2.3 Yeast one-hybrid assays 132

4.3 Results 140

4.3.1 Y1H assays for specific interactions between *cis*-regulatory elements predicted by bioinformatics approaches and their *trans*-acting factors 140

4.3.2 Y1H screen of *regA* intron 3 143

4.3.3 Intron 7 145

4.3.4 Intron 5 146

4.4 Discussion 146

4.4.1 Technical difficulties of Y1H screens 146

4.4.2 Testing of specific *trans*-acting factors for interaction with *regA* intron 3 ... 147

4.4.3 *trans*-acting factors might bind to *regA* introns cooperatively or they might be covalently modified 149

4.5 References 169

Chapter 5 Conclusions 172

5.1 Evolution of multicellularity and cell differentiation 172

5.2 Evolution of cooperation 175

5.3 Future directions 177

5.4 References 178

Curriculum Vitae

List of Tables

Table 2.1 Regenerator mutant strains used in this study 35

Table 2.2 PCR primers and conditions 36

Table 2.3 Gene-specific primer (GSP) for reverse transcription and qPCR primers (F, forward; R, reverse) 37

Table 2.4 dmAMN cells almost doubled in size during the first light period of the light cycle. 38

Table 2.5 Additional qPCR primers (F, forward; R, reverse) for the amplification of *tbpA* and *actA* 53

Table 2.6 Gene stability of *rps18*, *tbpA* and *actA* for selected time points 54

Table 3.1 Gene-specific primer (GSP) for reverse transcription and qPCR primers (F, forward; R, reverse) 98

Table 3.2 Light and cell size influence the viability of dmAMN cells (Effect Test for data in Figure 3.9A–B) 99

Table 3.3 Phenotype and light affect viability of *V. carteri* cells 100

Table 3.4 Summary of conditions for *regA* expression and PCD 101

Table 3.5 Gonidial genes and putative targets of *regA* regulation (Tam and Kirk 1991a; Choi, Przybylska, and Straus 1996; Meissner et al. 1999) 102

Table 4.1 *E. coli* strains used in this study 150

Table 4.2 *S. cerevisiae* strains used in this study 151

Table 4.3 Bait plasmids (and other plasmids used for their construction) used in this study 152

Table 4.4 PCRs used for construction of bait plasmids 153

Table 4.5 Prey plasmids and other plasmids used in this study 154

Table 4.6 RT-PCR and PCR for prey 155

Table 4.7 Summary of cDNA library screens of *regA* introns 156

Table 4.8 Single gene screens 157

Table 4.9 Interaction of prey protein DofA with bait sequence *regA* intron 3. 158

Table 4.10 interaction of B3TF DBD with *regA* intron 3 or AE box 2. 159

Table 4.11 Summary of Y1H screens of *regA* intron 3 160

Table 4.12 Sequenced positives of Y1H screen of *regA* intron 3. 161

Table 4.13 Summary of Y1H screens of *regA* intron 7 162

Table 4.14 Sequenced positives of Y1H screen of *regA* intron 7. 163

List of Figures

Figure 1.1 A subset of volvocine green algae that show a progressive increase in cell number, volume of extracellular matrix per cell, division of labor between somatic and reproductive cells, and proportion of vegetative cells. 13

Figure 1.2 The asexual life cycle of *Volvox carteri* (adapted from Hallmann et al. 1998). 14

Figure 2.1 Original *regA* expression data (adapted from Kirk et al. 1999) 39

Figure 2.2 The asexual life cycle of a *regA*$^-$/*gls*$^-$ mutant (adapted from Tam and Kirk 1991) 40

Figure 2.3 *regA* transcripts in several *regA*$^-$ mutant strains. 41

Figure 2.4 A dmAMN gonidialess mutant during the first (10 h), second (34 h), and third (58 h) day of its life cycle. 42

Figure 2.5 The *regA* locus of dmAMN contains an insertion in exon 6. 43

Figure 2.6 *regA* transcript level in dmAMN gonidialess mutant in a standard 16L:8D regime 44

Figure 2.7 *regA* transcript levels in dmAMN gonidialess mutant in standard conditions or in continuous darkness. 45

Figure 2.8 *regA* expression only peaks once within the first 48 h of the EVE life cycle, and its expression is independent of light. 46

Figure 2.9 *regA* expression in continuous dark in EVE 47

Figure 2.10 Comparison of *regA* expression in dmAMN gonidialess mutant and EVE in standard 16L:8D regime. 48

Figure 2.11 The *regA* locus of dmAMN does not contain any mutations in the promoter or any other regions that likely contain regulatory sequences. 55

Figure 2.12 *regA* RT-qPCR specifically amplifies the *regA* locus and not other homologs in the *VARL* gene family. 58

Figure 3.1 Different models for the evolution of *regA* regulation. 103

Figure 3.2 Linear electron flow (LEF, blue solid arrows) and cyclic electron flow (CEF, red solid arrows) in the photosynthetic electron transport chain and chlororespiration (orange solid arrow); adapted from Joliot and Johnson (2011), and Peltier et al. (2010). 104

Figure 3.3 (A) Cool white light spectrum and (B) transmittance of red, green or blue filter (#027, 735, and 071 respectively, LEE Filters). 105

Figure 3.4 In small dmAMN cells, *regA* expression is induced by light after extended periods of darkness. 106

Figure 3.5 In large dmAMN cells, light only weakly induces *regA* expression. 107

Figure 3.6 Light quality does not affect the level of *regA* induction in dmAMN. 108

Figure 3.7 Light intensity does not influence *regA* expression levels. 109

Figure 3.8 SYTOX Green staining of large dmAMN cells. 110

Figure 3.9 After 31 h of darkness, light causes higher levels of PCD in small than in large dmAMN cells. 111

Figure 3.10 Only small cells enter PCD after 31 h of darkness followed by 4 h of light. 112

Figure 3.11 In EVE, *regA* is only slightly induced by light after extended period of darkness 113

Figure 3.12 Light after extended darkness does not cause detectable levels of PCD in EVE. 114

Figure 3.13 Two different models for the role of RegA in stress resistance, with RegA either in a (A) preventative or (B) responsive role. 115

Figure 3.14 Light after extended darkness causes cell death in UTEX1877 at levels similar to dmAMN. 123

Figure 3.15 After 31 h of darkness, light causes increasing levels of cell death in dmAMN over time. 124

Figure 4.1 *regA* gene structure (adapted from Stark, Kirk, and Schmitt 2001). 164

Figure 4.2 Model for *regA* regulation (based on Stark, Kirk, and Schmitt 2001). 165

Figure 4.3 The principle of the yeast one-hybrid assay. 166

Figure 4.4 AE box 2 adapter 167

Figure 4.5 Potential binding sites (red boxes) of transcription factors in *regA* intron 3. 168

Abbreviations

16L:8D	light regime of 16 h of light and 8 h of dark
3'UTR	3' untranslated region
3AT	3-amino-1,2,4-triazole
5'UTR	5' untranslated region
A	adenine
AA	amino acids
AD	activation domain
ADP/ATP	adenosine diphosphate/ adenosine triphosphate
B3TF	B3 domain transcription factor
bp	base pairs
C	cytosine
cDNA	complementary deoxyribonucleic acid
CEF	cyclic electron flow
cyt b_6f	cytochrome b_6f complex
DBD	DNA binding domain
ddH_2O	double-distilled water
DEPC	diethylpyrocarbonate
DF	degrees of freedom
DNA	deoxyribonucleic acid
DTT	dithiothreitol
dNTP	deoxyribonucleotide
ECM	extracellular matrix
EDTA	ethylenediaminetetraacetic acid
Fd	ferredoxin
FNR	ferredoxin $NADP^+$ reductase
G	guanine
gDNA	genomic deoxyribonucleic acid
HDAC3	histone deacetylase 3
LB	lysogeny broth
LD-PCR	long-distance polymerase chain reaction
LEF	linear electron flow
LHCI and II	light-harvesting complex I and II
M	mean
MAPK	mitogen-activated protein kinase
MAPKKK	mitogen-activated protein kinase kinase kinase
MRTF-A	myocardin-related transcription factor A
N:C ratio	nuclear to cytoplasmic volume ratio
NaCl	sodium chloride
$NADPH/NADP^+$	nicotinamide adenine dinucleotide phosphate
Nda2	type II NAD(P)H dehydrogenase
NTC	no template control
NRT	no reverse transcriptase control
OD_{600}	optical density at 600 nm

OEB	Oligotex elution buffer
ORF	open reading frame
PCD	programmed cell death
PCR	polymerase chain reaction
Pc	plastocyanin
PEG	polyethylene glycol
pETC	photosynthetic electron transport chain
PGC	progenitor germ cells
PGR1	PGR5 Like 1
PQ/PQH_2	plastoquinone/plastoquinol
PSI and II	photosystem I and II
PTOX	plastid terminal oxidase
RE	regulatory element
RNA	ribonucleic acid
ROS	reactive oxygen species
RT	reverse transcription
RT-qPCR	reverse transcription quantitative polymerase chain reaction
S:V ratio	surface to volume ratio
SAND domain	domain of Sp100, AIRE-1, NucP41/75 and DEAF-1
SD medium	synthetically defined medium
SDS	sodium dodecyl sulfate
SE	standard error
SOC	super optimal broth with catabolite repression
SRE	serum response element
SVM	standard *Volvox* medium
T	thymine
TE	Tris EDTA
U	units
VARL	volvocine algal *regA*-like
Y1H	yeast one-hybrid
YPDA	yeast extract, peptone, dextrose, adenine

Chapter 1 General introduction

1.1 General background

Looking at the diversity of life it is striking how much organisms differ in complexity, from simple bacteria, to single-celled eukaryotes (with mitochondria and chloroplasts derived from previously endosymbiotic bacteria), to multicellular organisms and the complex societies they form. The different levels of complexity are the result of a series of major evolutionary transitions during which lower-level individuals were integrated into a higher-level individual (Michod 2007). These higher-level individuals also act as new evolutionary individuals, i.e. they possess variable and heritable traits at this new level of organization on which natural selection can act (Michod 2007).

One major evolutionary transition led single cell individuals to form highly integrated multicellular organisms, and its hallmark is the rise of cells specialized for either reproduction or vegetative functions (Michod 2007). In general terms, the fitness of an organism is defined by its ability to survive and reproduce (Michod 2007). Differential investment in these two components results in a tradeoff that is thought to reflect in the different life-history strategies and traits of extant organisms. The transition to multicellularity required the reorganization of the two fitness components, between soma (specialized in survival) and germ (specialized in reproduction; Michod 2007). Because somatic cells forgo their own reproduction for the benefit of the whole organism they are expressing a behavior known as reproductive altruism.

1.2 The volvocine algae as a model system

Multicellularity evolved at least 25 times independently. In addition to the lineages leading to animals and land plants, multicellular forms evolved among bacteria (e.g., cyanobacteria, myxobacteria), green, red, and brown algae, slime molds, fungi, and several other groups (Grosberg and Strathmann 2007). In this context, the chlorophyte green algae have a special place as 9 out of 11 orders contain multicellular forms that each evolved multicellularity independently (Kirk 2005). Among chlorophytes, the order Volvocales has members that represent all different levels of organizational complexity leading to multicellularity (examples of representative species are in parenthesis): unicellular algae (*Chlamydomonas reinhardtii*), groups of uniform unspecialized cells (*Gonium pectorale*, *Eudorina elegans*), spherical algae with somatic cells but no specialized reproductive cells (*Pleodorina californica*), and spherical algae with terminally differentiated somatic cells and specialized reproductive cells known as gonidia (*Volvox carteri*; Figure 1.1). Complexity increased several times independently in this group, and this might be an indication that only a small number of changes was necessary to increase in complexity from a simpler ancestor (Kirk 2003).

Volvocine algae without specialized cells are characterized by a biphasic life-cycle (Kirk 2003). During the vegetative phase, they are motile (as each cell possesses a pair of flagella) and grow (each cell grows 2^n in size); during the reproduction phase each cell loses the flagella as they enter a series of n divisions in quick succession, a process called multiple fission (Kirk 2003). In algae with germ-soma differentiation this temporal biphasic pattern (the ancestral program) is instead realized in a spatial context, i.e. the somatic cells are specialized in vegetative functions and confer motility throughout the

entire life-cycle, while the gonidia are not involved in motility and are specialized in reproduction (Kirk 2003).

In the volvocine algae, multicellularity evolved more recently than in many other lineages, so it is more likely that the origin of the program for multicellular development can be traced back to the co-opted pathways in the unicellular ancestors (Kirk 2003). For instance, recent estimates indicate that the lineages leading to the multicellular *V. carteri* and the unicellular *C. reinhardtii* diverged from each other about 235 million years ago (Herron et al. 2009).

Both *C. reinhardtii* and *V. carteri* are well-developed experimental model systems and their genomes have been sequenced (Merchant et al. 2007; Prochnik et al. 2010). Furthermore, the presence of different organizational complexity levels and the availability of developmental mutants allow us to test various hypotheses that may explain the drivers of the evolution of germ-soma differentiation (Kirk 2003). Altogether, these make volvocine algae an interesting model system with which to study the transition to multicellularity.

1.3 Hypotheses on the selective advantages of multicellularity and cell differentiation in *Volvox carteri*

The evolution of multicellular (also referred to as colonial) volvocine algae is thought to have been driven by predation, as the increase in size helped to avoid the major predators, mostly invertebrate filter feeders (e.g. rotifers and small crustaceans; Bell 1985). Indeed, the size of almost all of the multicellular volvocine algae is above the predation threshold of these predators (Kirk 1998).

Another advantage of the colonial form in volvocine algae might lie in the production of an extracellular matrix (ECM), which is the modified form of the cell wall found in *C. reinhardtii* (Kirk 2005). Most volvocine algae live in shallow and transient pools of water, in which multiple species are often represented and compete with each other for nutrients, including minerals such as phosphates (Kirk 2003). Volvocine algae are efficient at scavenging and storing phosphorous and the size of their internal phosphorous stores influences algal growth (Rhee 1973). It has been postulated that while unicellular algae are mostly limited to the intracellular storage of phosphorous, colonial algae also store phosphorous as phosphorylated components of the ECM; since the amount of ECM produced increases with cell number, algae with large cell numbers accumulate greater phosphate reserves (Bell 1985).

The ECM might not only explain the rise of colonial forms of volvocine algae but also the evolution of germ-soma differentiation, as proposed in the "source-sink" hypothesis (Bell 1985). In this scenario, the somatic cells act as scavengers for phosphorous which is deposited as phosphorylated components of the ECM (they act as source for nutrients), and the gonidia use the phosphorous for growth (they act as sink). Because uptake is dependent on a concentration gradient between the inside and outside of the colony, consumption of the internal products by reproductive cells decreases the nutrient concentration in the ECM and maintains fast uptake from the environment (Bell 1985). Indeed, gonidia of *V. carteri* grow faster in the presence of an intact soma, than in isolation (Koufopanou and Bell 1993).

In volvocine algae, somatic cells might also increase nutrient uptake due to the flagellar stirring of the boundary layer. Nutrient uptake leads to nutrient depletion in the

boundary layer, and mixing of the boundary layer increases the transport of nutrients closer to the cells than diffusion of nutrients alone (Solari et al. 2006).

Interestingly, germ-soma differentiation is only observed in volvocine species with larger cell numbers (Herron and Michod 2008). A larger body size can be advantageous to avoid predation, but can result in an increase in drag making it important that the colony maintains mobility throughout the life cycle (Solari, Kessler, and Michod 2006). While an increase in colony size might increase fitness for the reasons described above, the multiple fission type of division that characterizes the developmental program of most volvocine algae increases the cost of reproduction. This is because in this group of algae, flagellar activity is negatively affected during cell division—the so-called "flagellar constraint" (Koufopanou 1994). The flagellar roots are connected to basal bodies that are not only important for flagellar function but also act as centrioles during cell division. Due to the presence of a cell wall, the flagella cannot move laterally, and the basal bodies cannot act as centrioles during mitosis. Consequently, the basal bodies dissociate from the flagellar root. The flagella remain functional—although beating is weakened and more uncoordinated—for about 5 embryonic divisions (which will result in a colony comprised of 32 cells), but then the flagella detach and the colony loses its motility. The division of labor between germ and soma might have evolved in order for some cells (the somatic cells) to maintain their flagella and the motility of the colony (which will ensure an optimal position in the water column for light or nutrient uptake), while reproductive cells continue to grow and divide (Koufopanou 1994). Indeed, cell differentiation is only observed in volvocine algae of 64 or more cells.

1.4 Cells of two different sizes are formed during embryogenesis of *Volvox carteri*

V. carteri is a spherical multicellular green alga consisting of two different cell types: about 2000 biflagellated somatic cells with no division or re-differentiation potential, and up to 16 non-flagellated reproductive cells called gonidia (Kirk 1998). During the asexual life cycle (Figure 1.2), each mature gonidium develops into an embryo (by a rapid succession of cell divisions known as cleavage) that forms a new individual (aka spheroid). In *V. carteri* asexual spheroids, cell fate is established in three steps: 1) formation of large and small cells by asymmetric divisions during embryonic development; 2) cytodifferentiation of small cells and large cells into somatic cells and gonidia, respectively; and 3) terminal differentiation of somatic cells.

During the cleavage phase of embryogenesis, each gonidium undergoes a series of symmetric and asymmetric cell divisions that generate a cohort of either large or small cells. Specifically, a gonidium first undergoes 5 symmetric divisions resulting in 32 cells (blastomeres) identical in size and differentiation potential. Then, the anterior 16 cells start dividing asymmetrically, each producing a large and a small cell; the large cells continue to divide asymmetrically twice more to produce 16 large cells (presumptive gonidia) of ca. 10.5 μm in diameter (Kirk et al. 1993). All other cells (i.e., the small cells formed by asymmetric divisions and all cells of the posterior hemisphere) divide symmetrically up to a total of 11–12 times, to produce cells of ca. 3.3 μm in diameter. At the end of the cleavage, the embryo turns inside out (a process called inversion) and the newly formed spheroid is called a juvenile. In the presence of light, cells differentiate (a process known as cytodifferentiation) into gonidia and somatic cells (Kirk and Kirk 1985); large cells differentiate as gonidia by resorbing their flagella, becoming spherical

and forming large vacuoles, whereas small cells become somatic by flagellar elongation and formation of the eyespot (important for light perception; Coggin and Kochert 1986; Kirk 2001). Gonidia start out about 32-fold larger than somatic cells and increase about 140-fold during the life cycle; in contrast somatic cells only increase ca. 9-fold (Kirk 1998). Two general explanations can be invoked to account for the different fates undertaken by the two cell types at the end of cleavage: differences in cell size or the unequal distribution of a cytoplasmic factor.

1.5 Cell size determines cell fate

A series of studies showed that cell size alone (regardless of whether cells originated from symmetric or asymmetric cell divisions) determines cell fate in *V. carteri*; cells that are below 8 μm in diameter develop into somatic cells, whereas cells above 8 μm differentiate as gonidia (Kirk et al. 1993). For instance, if a heat shock was applied during embryogenesis, cells continued to divide for 1–2 times, and then stopped dividing (Kirk et al. 1993). When the heat shock was applied early, spheroids with fewer but larger cells were formed, whereas spheroids with more but smaller cells were produced when the shock was applied later. In spheroids with fewer but larger cells, more cells differentiated as gonidia. Similarly, a temperature sensitive mutant with a cleavage defect divided fewer times when shifted to the restrictive temperature generating cells of various sizes; the percentage of cells above 8 μm directly correlated with the percentage of cells differentiating as gonidia (Kirk et al. 1993). Also, two mutant strains randomly stopped cleavage after an average of 5–6 divisions, forming a wide range of cell sizes and numbers for each spheroid; tracking the cell fate of cells of various sizes showed that

cells below 6 μm cell diameter always differentiated as somatic cells and above 9 μm always as gonidia (Kirk et al. 1993).

Microsurgery experiments corroborate the studies mentioned above. The posterior hemisphere never develops gonidia in an undisturbed, whole spheroid. When an embryo was separated into the posterior and anterior hemispheres at the 16-cell stage, 1–2 large cells were formed both in the anterior and posterior half by early cessation of cleavage or by a number of asymmetric divisions (Kirk et al. 1993). This cannot be explained by assuming an asymmetric distribution of a cytoplasmic factor, because the posterior hemisphere should not contain this factor since gonidia are usually not formed there. Furthermore, cells larger than 8 μm were generated by microsurgery (i.e., cell fusions) in the posterior hemisphere; these cells always differentiated as gonidia (Kirk et al. 1993). Regardless of how cells with a diameter above 8 μm were formed or of their position within the embryos, they always differentiated as gonidia; if cells were below 8 μm they differentiated as somatic cells.

1.6 Somatic cells escape terminal differentiation in regenerator mutants

The terminal differentiation of nonreplicative/sterile somatic cells is disrupted in the so-called regenerator mutants in which somatic cells regain their reproductive potential (Starr 1970; Kirk et al. 1999). Small cells initially differentiate as somatic cells, but after one day they redifferentiate and resemble gonidia: they lose their flagella and eyespot, start growing in size, become vacuolated and by the 3rd day they start dividing to form new spheroids.

Three different classes of regenerator mutants have been described in *V. carteri* (Huskey and Griffin 1979): in class I mutants all somatic cells regenerate; in class II mutants only somatic cells in the posterior region regenerate (about 75% of all somatic cells); and in class III mutants about 50% of somatic cells regenerate with a random distribution across the spheroid. Crossing experiments among more than one hundred mutants of all three classes always mapped the mutation to the same locus and it was concluded that they all are affected by the same gene (Huskey and Griffin 1979), which was later identified as *regA* (Kirk et al. 1999). Subsequently, it was revealed that *regA* actually belongs to a group of genes encoding a common DNA binding domain (see below), known as the *VARL* (volvocine algal *regA*-like) gene family. Furthermore, it was found that three *regA*-like genes are found in close proximity to *regA* (forming the so-called *regA* cluster), which allows for the possibility that the early crossing experiments might not have resolved mutations among these clustered genes (Duncan et al. 2006; Duncan et al. 2007). On the other hand, all characterized regenerator mutants (1 bleomycin-induced deletion mutant and 28 transposon-mediated insertion mutants) mapped to *regA* only (Kirk et al. 1999; Duncan et al. 2006). In addition, a temperature-sensitive regenerator mutant showed all of the three phenotypic classes described above (depending on the duration of incubation at the restrictive temperature; i.e. when the regenerator protein is not functional), making it likely that the mutations causing the different classes all map to the same gene (Huskey and Griffin 1979). Taken together, the regenerator phenotype is likely only caused by mutations in *regA*.

A number of regenerator mutants are available in culture collections. In addition to regenerator mutants exhibiting single mutations mapping to *regA*, a series of mutants that

carry additional mutations in other cell differentiation-related genes have been isolated and described, including the so-called gonidialess mutants in which all cells first resemble somatic cells for one day but redifferentiate into gonidia later (discussed in Chapter 2, Table 2.1).

1.7 RegA is a putative transcription repressor

regA is thought to encode a transcriptional repressor (Kirk et al. 1999). Several lines of evidence are consistent with this functional assignment. The RegA protein contains three glutamine-, two alanine-, and two proline-rich regions, often in the form of homopolymeric runs (Kirk et al. 1999). Such regions are found in known or predicted transcriptional repressors that directly prevent transcription initiation as opposed to modulating the activity of a transcriptional activator or chromatin structure (Hanna-Rose and Hansen 1996; Kirk et al. 1999). When these regions are fused to DNA binding domains they act as a repressor domain, i.e. they down-regulate transcription of a gene next to the respective DNA binding site. The proposed DNA binding domain of RegA is a SAND domain—found in transcription factors such as ULTRAPETALA in *Arabidopsis thaliana* and SP100 in humans (Bottomley et al. 2001; Carles and Fletcher 2010)—and is contained in the ca. 100 AA long VARL domain shared by the members of the *VARL* gene family (Duncan et al. 2006; Duncan et al. 2007). The only published *regA* mutation in a regenerator strain results in the loss of the SAND domain. Specifically, in the strain HB11A, the *regA* locus has a 284 bp deletion upstream of the coding region corresponding to the SAND domain; this deletion causes a frameshift that introduces a premature stop codon 12 bp downstream of the deletion site, which results in a short

291 AA gene product (and lacking a SAND domain) instead of the 1049 AA wild type product (Kirk et al. 1999).

regA is specifically expressed in somatic cells and its product localizes to their nucleus; on the other hand, at least 18 other genes are specifically expressed in the gonidia (gonidial genes) but not in somatic cells (Tam and Kirk 1991a; Kirk et al. 1999). In contrast, in a *regA*$^{-}$/gonidialess mutant gonidial genes are expressed in small cells, and their transcript levels exhibit a pattern that is similar to that of gonidial genes in wild-type gonidia, suggesting that these genes can be expressed in small cells in the absence of a functional RegA protein (Tam and Kirk 1991b). Because all of the 18 gonidial genes are nuclear-encoded chloroplast proteins—15 of which are directly involved in photosynthesis—RegA is thought to directly or indirectly repress these genes (Choi, Przybylska, and Straus 1996; Kirk et al. 1999; Meissner et al. 1999).

Taken together, RegA is thought to establish a non-reproductive state in somatic cells by repressing nuclear-encoded chloroplast proteins, preventing chloroplast biogenesis (and thus further development of the small embryonic chloroplast) and—since *V. carteri* is an obligate photoautotroph—by extension cell growth, and consequently cell division (Kirk et al. 1999). The differential expression of *regA* is thought to be related to the size of cells at the end of embryogenesis; however, the mechanistic basis for the connection between cell size and *regA* expression has never been investigated.

1.8 Goal and objectives of this study

To gain a better understanding of the evolutionary transition to multicellularity it is crucial to understand how the somatic cell fate is established. The goal of this study is to

investigate the mechanistic basis for somatic cell differentiation in *V. carteri*; specifically, to gain a deeper understanding of the signaling pathways (and their evolution) involved in the regulation of *regA*. The objectives of this study were: 1) to establish a *regA*$^{-}$/gonidialess mutant as a model system for *regA* expression studies (Chapter 2); 2) to investigate the *regA* expression pattern in *V. carteri* under various conditions (Chapter 3); and 3) to identify *trans*-acting factors that bind *regA* regulatory sequences (Chapter 4).

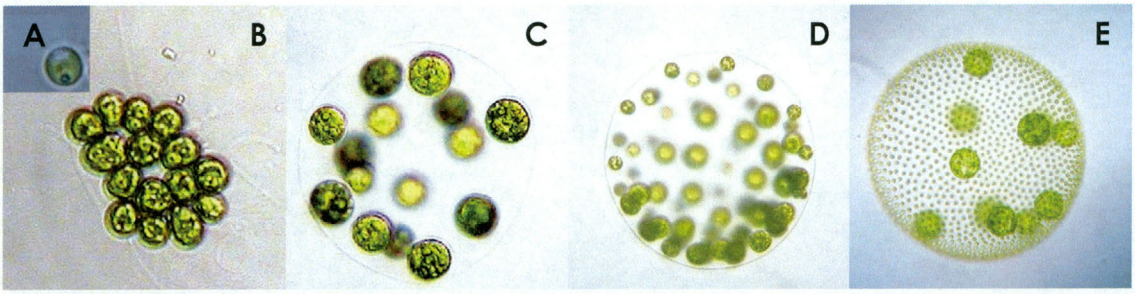

Figure 1.1 A subset of volvocine green algae that show a progressive increase in cell number, volume of extracellular matrix per cell, division of labor between somatic and reproductive cells, and proportion of vegetative cells.

(**A**) *Chlamydomonas reinhardtii*; (**B**) *Gonium pectorale*; (**C**) *Eudorina elegans*; (**D**) *Pleodorina californica*; (**E**) *Volvox carteri*. Where two cell types are present, the smaller cells are the vegetative (somatic) cells, whereas the larger cells are the reproductive cells (gonidia). Photo credit: Aurora Nedelcu.

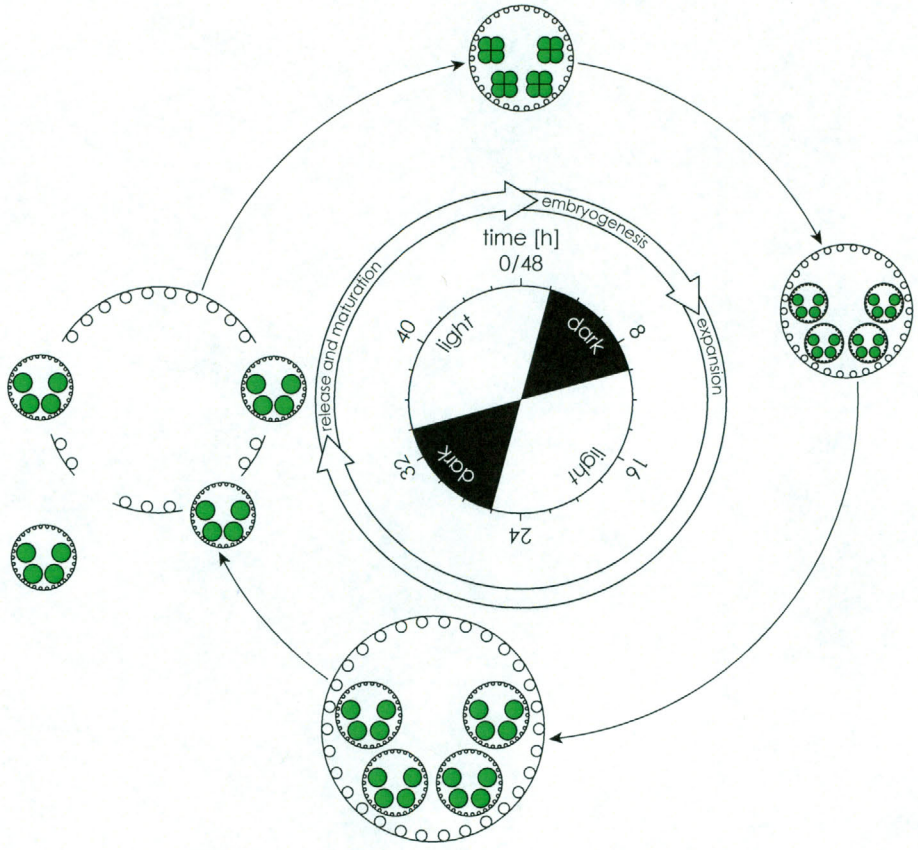

Figure 1.2 The asexual life cycle of *Volvox carteri* (adapted from Hallmann et al. 1998).

The life cycle of *Volvox carteri* takes 48 h when synchronized using a 16L:8D regime. The first cleavage division of embryogenesis is defined as time point 0 h and occurs ca. 2 h before the next dark period. Embryogenesis takes about 8 h, and after transition back into the light, both the parent and the newly formed juveniles expand in size as somatic cells synthesize the extracellular matrix. After a full day of growth, juveniles hatch from their parents, and the parental somatic cells undergo senescence and die. The gonidia of the released juveniles mature and enter the next round of embryogenesis towards the end of the light period, concluding the 48 h life cycle.

1.9 References

Bell G. 1985. The origin and early evolution of germ cells as illustrated by the Volvocales. In: Halvorson HO, Monroy A, editors. The origin and evolution of sex. New York. pp. 221–256.

Bottomley MJ, Collard MW, Huggenvik JI, Liu Z, Gibson TJ, Sattler M. 2001. The SAND domain structure defines a novel DNA-binding fold in transcriptional regulation. Nat Struct Biol 8:626–633.

Carles CC, Fletcher JC. 2010. Missing links between histones and RNA Pol II arising from SAND? Epigenetics 5:381–385.

Choi G, Przybylska M, Straus D. 1996. Three abundant germ line-specific transcripts in *Volvox carteri* encode photosynthetic proteins. Curr Genet 30:347–355.

Coggin S, Kochert GD. 1986. Flagellar Development and Regeneration in *Volvox carteri* (Chlorophyta). J Phycol 22:370–381.

Duncan L, Nishii I, Harryman A, Buckley S, Howard A, Friedman NR, Miller SM. 2007. The *VARL* gene family and the evolutionary origins of the master cell-type regulatory gene, *regA*, in *Volvox carteri*. J Mol Evol 65:1–11.

Duncan L, Nishii I, Howard A, Kirk DL, Miller SM. 2006. Orthologs and paralogs of *regA*, a master cell-type regulatory gene in *Volvox carteri*. Curr Genet 50:61–72.

Grosberg RK, Strathmann RR. 2007. The Evolution of Multicellularity: A Minor Major Transition? Annu Rev Ecol Evol Syst 38:621–654.

Hallmann A, Godl K, Wenzl S, Sumper M. 1998. The highly efficient sex-inducing pheromone system of *Volvox*. Trends Microbiol 6:185–189.

Hanna-Rose W, Hansen U. 1996. Active repression mechanisms of eukaryotic transcription repressors. Trends Genet 12:229–234.

Herron MD, Hackett JD, Aylward FO, Michod RE. 2009. Triassic origin and early radiation of multicellular volvocine algae. PNAS 106:3254–3258.

Herron MD, Michod RE. 2008. Evolution of complexity in the volvocine algae: transitions in individuality through Darwin's eye. Evolution 62:436–451.

Huskey RJ, Griffin BE. 1979. Genetic control of somatic cell differentiation in *Volvox* analysis of somatic regenerator mutants. Dev Biol 72:226–235.

Kirk DL. 1998. *Volvox*: the molecular genetic origins of multicellularity and cellular differentiation. Cambridge.

Kirk DL. 2001. Germ–Soma Differentiation in *Volvox*. Dev Biol 238:213–223.

Kirk DL. 2003. Seeking the ultimate and proximate causes of *Volvox* multicellularity and cellular differentiation. Integ Comp Biol 43:247–253.

Kirk DL. 2005. A twelve-step program for evolving multicellularity and a division of labor. Bioessays 27:299–310.

Kirk MM, Kirk DL. 1985. Translational regulation of protein synthesis, in response to light, at a critical stage of *Volvox* development. Cell 41:419–428.

Kirk MM, Ransick A, McRae SE, Kirk DL. 1993. The relationship between cell size and cell fate in *Volvox carteri*. J Cell Biol 123:191–208.

Kirk MM, Stark K, Miller SM, Müller W, Taillon BE, Gruber H, Schmitt R, Kirk DL. 1999. *regA*, a *Volvox* gene that plays a central role in germ-soma differentiation, encodes a novel regulatory protein. Development 126:639–647.

Koufopanou V, Bell G. 1993. Soma and germ: an experimental approach using *Volvox*. Proc Biol Sci 254:107–113.

Koufopanou V. 1994. The evolution of soma in the Volvocales. Am Nat 143:907–931.

Meissner M, Stark K, Cresnar B, Kirk DL, Schmitt R. 1999. *Volvox* germline-specific genes that are putative targets of RegA repression encode chloroplast proteins. Curr Genet 36:363–370.

Merchant SS, Prochnik SE, Vallon O, Harris EH, Karpowicz SJ, Witman GB, Terry A, Salamov A, Fritz-Laylin LK, Maréchal-Drouard L, et al. 2007. The *Chlamydomonas* genome reveals the evolution of key animal and plant functions. Science 318:245–250.

Michod RE. 2007. Evolution of individuality during the transition from unicellular to multicellular life. PNAS 104 Suppl 1:8613–8618.

Prochnik SE, Umen JG, Nedelcu AM, Hallmann A, Miller SM, Nishii I, Ferris P, Kuo A, Mitros T, Fritz-Laylin LK, et al. 2010. Genomic analysis of organismal complexity in the multicellular green alga *Volvox carteri*. Science 329:223–226.

Rhee G-Y. 1973. A continuous culture study of phosphate uptake, growth rate and polyphosphate in *Scenedesmus* sp. J Phycol 9:495–506.

Solari CA, Ganguly S, Kessler JO, Michod RE, Goldstein RE. 2006. Multicellularity and the functional interdependence of motility and molecular transport. PNAS 103:1353–1358.

Solari CA, Kessler JO, Michod RE. 2006. A hydrodynamics approach to the evolution of multicellularity: flagellar motility and germ-soma differentiation in volvocalean green algae. Am Nat 167:537–554.

Starr RC. 1970. Control of differentiation in *Volvox*. Symp Soc Dev Biol 29:59–100.

Tam L-W, Kirk DL. 1991a. Identification of cell-type-specific genes of *Volvox carteri* and characterization of their expression during the asexual life cycle. Dev Biol 145:51–66.

Tam L-W, Kirk DL. 1991b. The program for cellular differentiation in *Volvox carteri* as revealed by molecular analysis of development in a gonidialess/somatic regenerator mutant. Development 112:571–580.

Chapter 2 Characterization of a new gonidialess mutant as a model-system for *regA* expression studies

2.1 Introduction

As discussed in Chapter 1, the differential expression of *regA* is likely a function of cell size. However, it is not known what triggers the expression of *regA* in somatic cells and how this signal is transduced to control the expression of *regA*. Previous studies using the wild-type *V. carteri* strain EVE grown in a standard 16L:8D light regime showed that *regA* has a bimodal expression pattern (Figure 2.1; Kirk et al. 1999). *regA* transcripts were first detected in newly formed somatic cells 12 h after the onset of embryogenesis (during the first light period; see Chapter 1, Figure 1.2), peaked at 18 h (in the middle of the first light period) and then diminished gradually, reaching their lowest point in the middle of the second dark period (30 h; Figure 2.1A). During the second light period, *regA* mRNA levels in somatic cells increased again and after some fluctuation were highest towards the end of the second light period (48 h) before falling again. In contrast, *regA* was never expressed in gonidia.

Despite the strong interest in understanding the mechanistic basis for somatic cell differentiation in *V. carteri*, the 1999 study mentioned above is the only that has addressed the expression pattern of *regA*. Three aspects related to the biology of *V. carteri* make *regA* expression studies (especially with respect to its induction in newly formed somatic cells) challenging: 1) the embryos/juveniles and thus the newly formed somatic cells are embedded in the parental spheroid that possesses its own set of somatic

cells, such that *regA* expression studies in early somatic cells require the forced release of the embryos/juveniles from the parental spheroids (or the *ex vivo* development of juveniles from isolated mature gonidia or early embryos); 2) newly formed somatic cells have to be separated from the gonidia of the embryo/juvenile (this is because although gonidia do not appear to express *regA* during development, the possibility that they might express *regA* in some conditions has not been investigated); 3) the stress associated with cell separation might influence the expression of *regA* and/or of the reference genes.

To avoid these potential issues, I decided to use the so-called gonidialess mutants; these mutants carry a mutation in a class of genes called *gls* whose products are essential for the asymmetric divisions during embryogenesis (Kirk et al. 1991). In the absence of asymmetric divisions, all cells start small and act as somatic cells during the first day of their life cycle. A *gls* mutation on a wild type background would prove lethal as no reproductive cells are produced; but in combination with a mutation in *regA*, the small cells start growing during the following 2 days, lose their flagella, and become reproductive. When grown as synchronous cultures, such mutants provide the advantage of homogenous populations of cells, thus circumventing the need for cell separation and fractionation. However, *regA*'s expression pattern has not been characterized in such mutants.

The best studied gonidialess mutant is a bleomycin-induced $regA^{-}/gls^{-}$ double mutant (here referred as dmTAM, i.e. double mutant isolated by Tam; Tam and Kirk 1991; Kirk et al. 1999), which in addition to having the mutated *regA* locus of the only well characterized $regA^{-}$ mutant (strain HB11A) has an uncharacterized *gls* mutation (Table 2.1 and Figure 2.2). In this mutant, during embryogenesis, all cells divide

symmetrically to produce 64–256 small cells (Tam and Kirk 1991). Consequently, all cells start as flagellated somatic cells, but—due to their nonfunctional RegA protein—they start growing and re-differentiate into gonidia (i.e., they lose their flagella and become vacuolated) during the second day, and by the 3rd day they produce new individuals (see Figure 2.2). Previous studies have shown that when the *regA*$^-$ mutant strain 153-68 containing the mutant *regA* locus of HB11A (which is the one also present in the dmTAM mutant; Kirk et al. 1999) was rescued with a constitutively expressed *regA* gene construct, the mutant allele was still expressed in a cell type specific manner (i.e., only in somatic cells but not gonidia); this indicates that the regulation of this mutated locus was not affected (Stark, Kirk, and Schmitt 2001). Nevertheless, the expression of *regA* in the dmTAM was not investigated, as the gene had not been characterized at that time.

In addition to the bleomycin-induced dmTAM mutant, a spontaneous gonidialess double mutant (dmAMN, i.e. double mutant isolated by Aurora M. Nedelcu) has been recently isolated on the background of the *regA*$^-$ strain UTEX LB 1877 (Table 2.1). However, this mutant has not been characterized and the location and nature of the *regA* mutation or the expression pattern of *regA* in this mutant was not known.

2.1.1 Goal and objectives of this study

The goal of this project was to develop a model system with which to investigate the molecular mechanisms involved in the differential expression of *regA* in *V. carteri*. The specific objectives of this study were to 1) characterize the phenotype and *regA*$^-$ mutation of the gonidialess dmAMN mutant, and 2) investigate the expression pattern of *regA* in

gonidialess mutants (relative to EVE), during their life cycle and as a function of cell size.

2.2 Material and Methods

2.2.1 Strains and culturing conditions

The wild-type strain EVE (Adams et al. 1990) and all *regA*$^-$ strains (Table 2.1) were maintained in 20 mL of standard *Volvox* medium (SVM; Kirk and Kirk 1983), in Petri dishes, under standard growth conditions (in a 16L:8D photoperiod either at 30°C for EVE or 32°C for all other strains). Illumination was provided by cool white fluorescent light bulbs at 260 μmol photons m^{-2} s^{-1} of photosynthetically active radiation (Kirk and Kirk 1985) as measured with a Laboratory Quantum Scalar Irradiance Meter QSL-100 (Biospherical Instruments Inc.). Cultures were diluted ca. 1:20 into fresh SVM every 2 days.

2.2.2 Experimental cultures

Gonidialess or EVE cultures for *regA* expression kinetics were grown in aerated SVM, under the conditions above. In preparation for each experiment, fresh cultures were started at the onset of embryogenesis (time point 0 h) at a density of 0.625 spheroids/mL for EVE or 0.67 spheroids/mL for gonidialess strains. Cultures were grown for one generation (2 d for EVE and 3 d for gonidialess strains) before initiating the experimental cultures for a given experiment. Experimental cultures were started at the 1 h time point (after start of embryogenesis) and grown in 150 mL SVM at starting densities of 25–60 embryos/mL for EVE and 5–15 spheroids/mL for gonidialess strains; cultures

remained in 16L:8D, or were switched to continuous darkness at the end of the light period (time point 2 h).

2.2.3 Isolation of early EVE embryos

Experimental cultures were started with early embryos/juvenile cells that were separated from the maternal somatic cell sheets. Specifically, EVE spheroids containing 2-celled embryos (at the 0 h time point) were collected on a 100 μm Nitex filter and resuspended in 40 mL fresh SVM in a 40 mL Dounce homogenizer (Kontes) at ≤ 300 spheroids/mL density. Spheroids were broken with one down-and-up stroke of the loose fitting pestle A, and the cell suspension was incubated for 10 min at room temperature so embryos could fully dissociate from the somatic cell sheets. The cell suspension was poured onto a 100 μm Nitex filter; the embryos passed the filter in the flow-through, were collected on a 30 μm Nitex filter, washed with 100 mL SVM to remove any loose somatic cells, and used to start experimental cultures.

2.2.4 Cell size measurements

For cell size measurements, 10 cells from at least 20 random spheroids were observed using a Leica DM R upright microscope and a Leica DC 500 digital camera; cell sizes were determined using the Fiji image processing package.

2.2.5 Genomic DNA extraction

For genomic DNA (gDNA) extractions, cultures were collected on a 30 μm Nitex filter. Approximately 1 mL of concentrated culture was then transferred to a 15 mL screw cap tube, washed twice with 9 mL saline EDTA (50 mM Tris-HCl, pH 8.0; 50 mM NaCl;

5 mM EDTA), centrifuged for 5 min at 1380 g at room temperature, and the supernatant discarded. Cells were lysed in 6 mL Buffer A (10 mM Tris-HCl, pH 7.6; 10 mM EDTA; 10 mM NaCl) supplemented with SDS and Proteinase K (final concentrations of 0.5% and 20 mg/mL, respectively) for 1 h at 50°C. The cell lysate was mixed with 6 mL phenol (equilibrated with 10 mM Tris-HCl, pH 8.0, 1 mM EDTA, Sigma) on a rotary shaker for 10 min at 200 rpm, followed by phase separation by centrifugation for 10 min at 1380 g. Nucleic acids in the aqueous phase were purified by phenol:chloroform extraction and overnight ethanol:sodium acetate precipitation at 4°C (Sambrook and Russel 2001). The nucleic acid pellet was dissolved in 500 µL TE, pH 8.0 containing 25 µg/mL RNase A (Sigma), and the solution was incubated for 15 min at 37°C to remove any RNA contamination. To pellet and remove any polysaccharides, 250 µL of 7 M ammonium acetate were added, the solution was mixed well and centrifuged for 15 min at 13,000 g. The supernatant containing DNA was transferred to a fresh microcentrifuge tube; the DNA was precipitated with ethanol and resuspended in 250 µL TE, pH 8.0.

2.2.6 Amplification of *regA* regions

Various regions of *regA* (spanning different introns and exons) were amplified with the primers given in Table 2.2; PCR reactions contained gDNA as template and the components indicated in Table 2.2, and were run in a RoboCycler Gradient 96 (Stratagene). PCR products were sequenced at the McGill University and Génome Québec Innovation Centre using a 3730x DNA Analyzer (Applied Biosystems).

2.2.7 RNA extraction and quantification

For RNA extraction, cultures were first concentrated on a 30 μm Nitex filter and then transferred in 1 mL fresh SVM to a microcentrifuge tube; cells were pelleted by centrifugation for 1 min at 3000 g at room temperature, and the supernatant was discarded. After flash-freezing the samples in liquid nitrogen, they were stored at −80°C until RNA extraction. RNA was extracted with the RNeasy Plant Mini Kit (Qiagen) using Buffer RLC, and eluted in 50 μL ddH_2O. RNA concentration was measured with a NanoVue (GE) or a SpectroMax M5 spectrophotometer (Molecular Devices).

2.2.7.1 RNA gel electrophoresis to assess RNA integrity

RNA was separated for 1.5 h at 4 V/cm on a 1X SB gel (5 mM disodium borate decahydrate, pH adjusted to 8.5 with solid boric acid) containing 1.2% agarose, 20 mM guanidine thiocyanate and 0.5X SYBR Safe (Invitrogen; Goda and Minton 1995; Brody and Kern 2004). To remove any RNA secondary structures prior to electrophoresis, the RNA samples were added to 1X Blue Gel Loading Dye (NEB) and 20 mM guanidine thiocyanate in a total volume of 15 μL, incubated for 10 min at 70°C, and then cooled on ice for 2 min. RNA bands were visualized using the Gel Doc 2000 System and Quantity One Imaging Software (Version 4.2.1, Bio-Rad).

2.2.7.2 DNase treatment

gDNA contamination was removed by treating RNA with 2 U RQ1 DNase in 1X RQ1 DNase Reaction Buffer (Promega) in a total volume of 20 μL for 1 h at 37°C; all samples within one experiment contained the same amount of RNA. After adding 2 μL RQ1 Stop

Solution to the reaction, the DNase was inactivated by a 10 min incubation at 65°C, and then the RNA was kept on ice.

2.2.7.3 Reverse transcription

cDNA was synthesized from 4 µL DNase-treated RNA by 100 U SuperScript III Reverse Transcriptase (Invitrogen) in 1X First-Strand Buffer, 0.5 mM each dNTPs, 5 mM DTT, and either 2.5 µM oligo$(dT)_{20}$ for *rps18* (the reference gene) or 0.1 µM gene-specific primer for *regA* (the gene of interest) in 10 µL total volume (Table 2.3). *rps18* was the most stable reference gene tested (Appendix, Table 2.6) and had been used as reference gene for *V. carteri* in numerous studies including the initial *regA* expression studies (Kirk et al. 1999; Miller and Kirk 1999; Shimizu, Inoue, and Shiraishi 2001; Cheng et al. 2006; Ferris et al. 2010). The No-RT controls contained no reverse transcriptase or primers (used as template for –RT in qPCR). Samples were incubated for 1 h at 50°C, followed by 5 min at 85°C.

2.2.7.4 Quantitative real-time PCR

For each biological replicate, two +RT replicates and one −RT were prepared. A 20 µL reaction contained 2 µL template in 1X KAPA SYBR FAST Master Mix Universal (Kapa Biosystems), and 0.2 µM of each primer (Table 2.3). A no template control (NTC) was also prepared. The PCR was run in a Rotor-Gene 6000 (Corbett Research) with an initial denaturation at 95°C for 3 min followed by either 40 (*rps18*) or 45 (*regA*) PCR cycles (95°C/3 sec; 55°C/30 sec; 72°C/3 sec), and ended with a melt curve analysis from 72 to 95°C.

2.2.7.5 Data analysis

Data collected with Rotor-Gene 6000 software (Version 1.7.87, Corbett Research) were exported to LinRegPCR (Version 12.17; Ramakers2003a, Ruijter2009a); average PCR efficiency and threshold cycle (C_T) were calculated, C_T for technical replicates was averaged, and all data entered into the REST2009 software (Version 2.0.13, Qiagen) to determine relative expression of the gene of interest between samples.

2.2.7.6 Sequencing of qPCR products

regA qPCR products were first purified by gel-electrophoresis and gel-extraction, and then subcloned with the CloneJET PCR Cloning Kit (Thermo Scientific); *regA* clones and *rps18* qPCR products were then sequenced (for *regA* see Appendix, Figure 2.12).

2.3 Results

2.3.1 *regA* expression in the dmTAM gonidialess mutant

RT-qPCR was initially used to detect *regA* transcripts and confirm the expression of *regA* in the dmTAM mutant; however, no *regA* transcripts were detected (data not shown). The wild-type strain of *V. carteri* f. *nagariensis* (EVE) and several other *regA* mutants (see Table 2.1) were then used as positive controls. Unexpectedly, although *regA* transcripts were detected in EVE as well as in six *regA*$^-$ mutant strains (Figure 2.3)—including the strains HB11A and 153-68 that share the same mutant *regA* locus as dmTAM (i.e., an out-of-frame deletion of 284 bp in exon 6 from C5016 to C5299; Tam and Kirk 1991; Kirk et al. 1999)—no *regA* transcripts were identified in the dmTAM mutant, despite extensive attempts (data not shown).

2.3.2 Characterization of the dmAMN gonidialess mutant

A new gonidialess strain, dmAMN, had been recently isolated in our lab based on its phenotype (Table 2.1); this is a spontaneous *gls* mutant on the background of the *regA*$^-$ strain UTEX LB 1877 (Table 2.1). Cultures of the dmAMN gonidialess mutant were grown in standard conditions and examined using both a dissecting and a compound microscope. Microscopic observations showed that dmAMN has a similar 72 h life cycle (Figure 2.4) to that of the dmTAM mutant (Tam and Kirk 1991). After embryogenesis and hatching, all cells were flagellated, about 4 μm in diameter and resembled somatic cells (Figure 2.4A), but in the next 24 h they grew to almost 8 μm at the end of the first day light period (similar in size to wild-type gonidia just after embryogenesis; Table 2.4) and then lost their flagella (Figure 2.4B). During the last 24 h cells increased further in size, became vacuolated (similar to gonidia; Figure 2.4C), and a new round of embryogenesis was initiated at 72 h into the life cycle.

2.3.3 Characterization of the *regA* mutation in the dmAMN mutant

To identify the *regA* mutation in the dmAMN gonidialess mutant, various regions of the gene were PCR-amplified (see Table 2.2). A 365 bp insertion downstream position +5222 (in exon 6) was detected (Figure 2.5); the insertion introduces several potential premature stop codons and should result in a truncated chimeric protein consisting of the first 355 AA (of 1049 AA) of the RegA protein and at least 33 AA encoded by the insertion. No additional mutations were identified in regions that are known to contain regulatory sequences involved in the control of *regA* expression (i.e., promoter, introns 3, 5, and 7; see Appendix, Figure 2.11; Stark, Kirk, and Schmitt 2001).

2.3.4 Initial studies of *regA* expression in dmAMN

To confirm that *regA* is still expressed in the dmAMN mutant, RT-qPCR was performed using the *regA* F and R primers listed in Table 2.3. A PCR product of the right size (101 bp) was detected (Figure 2.3) and its sequencing confirmed that it is a *regA* transcript (Appendix, Figure 2.12). These results indicated that *regA* is indeed transcribed in this strain, and rendered this gonidialess mutant a suitable system for further gene expression studies.

2.3.5 *regA* expression in the dmAMN gonidialess mutant grown in a standard light regime

To further characterize *regA* expression in dmAMN, synchronized cultures were grown in the standard 16L:8D light regime; under these conditions, embryogenesis is initiated 2 hours before the end of the light period and continues for another 6 hours in the dark (Figure 2.2). If the onset of embryogenesis is considered as reference point (time 0), embryogenesis is complete around time point 8 h.

In an initial experiment, RNA was extracted from the dmAMN at several time points during the first 49 hours of its life cycle (i.e., 1 h, 9 h, 25 h, 33 h, 38 h, 49 h). As expected, *regA* transcripts were the lowest at 1 h (early during embryogenesis) and reached the highest levels at 9 h (at the end of embryogenesis), after which *regA* transcript levels decreased dramatically to almost the initial levels by the end of the second light period (Figure 2.6A). However, in contrast to the pattern of *regA* expression reported in EVE (Figure 2.1), a second peak of expression during the second light period was not detected. Additional experiments using different time points (9 h, 11 h, 22 h,

33 h, and 35 h in Figure 2.6B; 9 h, 14 h, 26 h, 33 h, and 37 h; Figure 2.6C), including one carried out in triplicate confirmed the lack of a second expression peak (Figure 2.6C). Also, the data indicate that *regA* is already transcribed at highest levels before the first light period (time point 9 h—i.e., 1 hour before light; Figure 2.6A–C), which suggest that the developmental induction of *regA* is not light-dependent (to be further discussed later).

2.3.6 *regA* expression in dmAMN as a function of cell size

One possible explanation for the absence of a second peak of *regA* expression during the second light period in the dmAMN mutants could be the fact that, in contrast to EVE, dmAMN cells continue to grow and increase in size (Figure 2.4). To address the possibility that the continuous drop in *regA* transcript levels is due to the increase in cell size above the 8 μm threshold for *regA* induction, dmAMN cultures were kept in continuous darkness following the onset of embryogenesis; under these conditions, cells cease to grow and maintain their initial size. RNA was extracted at several time points (i.e., 1 h, 9 h, 25 h, 33 h, 38 h, 49 h) from cultures grown in either standard conditions or continuous darkness (Figure 2.7A), and changes in *regA* transcript levels in the two treatments were compared. In continuous darkness (and thus in the absence of cell growth) *regA* mRNA levels dropped in a fashion similar to that observed under regular light:dark conditions, but transcript levels were maintained at a higher level. Nevertheless, in contrast to EVE, a second peak was not been detected during the second day (Figure 2.7B).

2.3.7 *regA* expression in the wild-type EVE strain grown in a standard light regime

To address the inconsistency in *regA* expression patterns between the dmAMN mutant and EVE, I have investigated the expression of *regA* in EVE using the same conditions and approaches as those used for the dmAMN mutant. Furthermore, I focused on specific time points during either the first or the second light period after embryogenesis (Figure 2.8A & B respectively) in an attempt to confirm the expression peaks reported by Kirk et al. (1999; Figure 2.1).

As observed for the dmAMN mutant, in a standard 16L:8D light regime, *regA* transcript levels in EVE increased sharply at the end of embryogenesis (at 6 h) peaking one hour before the light came on (9 h); *regA* transcript levels then dropped quickly to low levels by the end of the first light period and stayed low during the following dark phase. However, in contrast to Kirk et al. (1999; Figure 2.1), *regA* transcript levels remained low in the dark and there was no second peak during the second light period of the life cycle (Figure 2.8B). The same general trends were observed when the experiment was repeated with triplicates for a different set of time points (Figure 2.8C). Thus, in a standard 16L:8D regime, the *regA* expression patterns in the first 48 h of the life cycle are similar between dmAMN and EVE (Figure 2.6 and 2.8).

To further compare *regA* expression patterns between dmAMN and EVE, I also investigated the *regA* expression pattern in EVE in continuous darkness. *regA* transcript levels in EVE peaked once at 9 h, decreasing quickly until 14 h and then more slowly up to 39 h (Figure 2.9). This pattern is similar to that as observed for EVE in a standard light regime and for dmAMN in continuous darkness.

2.4 Discussion

2.4.1 *regA* expression pattern in EVE

Interestingly, in contrast to the data reported for EVE, a second peak of *regA* expression was not observed during the second day in neither light nor dark conditions. Our multiple attempts to reproduce the data reported by Kirk et al. (1999) indicate that—at least under our growth conditions—there is not a second peak of *regA* transcript accumulation in EVE. Differences in experimental procedures could account for the observed differences in expression pattern between the two studies. An important difference is the use of total RNA of whole spheroids (i.e. somatic cells and gonidia) for this study instead of RNA from only somatic cells in the original study. Since gonidia grow in size during the light period, their amount of RNA is also expected to increase, while that of somatic cells is not; consequently, the contribution of gonidial RNA in samples containing both somatic and gonidia cells (such as in this study) would be higher/greater, potentially diluting the *regA* transcripts exclusively expressed in somatic cells. Within the same experiment, total RNA amounts were normalized to the number of spheroids in each sample. Any change in the total RNA amount among time points could probably be attributed to an increased contribution of gonidial RNA. Nonetheless, total RNA amounts never increased more than 2–3-fold between time points during the first light period, and less than 2-fold during the second light period of the life cycle (*data not shown*); thus, it is unlikely that any hypothetical increases in *regA* levels in somatic cells were masked by being diluted in the total RNA pool by gonidial RNA. For example, *regA* levels increased 8-fold from time point 30 h to 48 h in the original study (Figure 2.1, Kirk et al. 1999); during the

same time period total RNA amounts only increased 1.5-fold in this study. That is, even if this increase in total RNA was solely due to an increase of gonidial RNA it would not have sufficed to dilute out an 8-fold increase in *regA* transcript levels. Also, in contrast to the original data of Kirk et al. (1999; Figure 2.1), in this study, *regA* transcript levels did not drop during the second dark period (when gonidia were not growing) of the life cycle (Figure 2.8). Taken together, the actual decrease in *regA* transcript levels in somatic cells might be slower than the apparent decrease in this study due to dilution with increasing amounts of gonidial RNA in the samples, but the overall trends probably still reflect the actual *regA* expression pattern in somatic cells.

Another difference between the two studies is the use of mechanical means (a Dounce homogenizer) to disrupt embryos and juveniles, as well as filtration and centrifugation for cell fractionation during the isolation and purification of somatic cell populations in the Kirk et al. study. Wounding and mechanical stress have been shown to induce the expression of many genes in *V. carteri*, including metalloproteinases involved in biochemical modification of the extracellular matrix (ECM) and pherophorins—which are components of the ECM (Hallmann et al. 2001; Hallmann 2006). Accordingly, the mechanical means used in Kirk et al. (1999) to separate somatic cells and gonidia after embryogenesis might have also affected *regA* expression levels.

It is important to note that the *regA* expression pattern reported here for EVE (Figure 2.8) is actually consistent with the expression pattern reported previously for the RegA protein in somatic cells (Kirk et al. 1999). A recombinant hemagglutinin-tagged RegA protein was first detected 16 h after the first cleavage division, increased for 2 h and then stayed constant (Kirk et al. 1999). The peak in *regA* transcript levels at 9 h

might help to establish this initial RegA protein population, and after transcript levels fall to a lower basal level these transcripts might suffice for synthesis of new RegA proteins to compensate for protein turnover.

2.4.2 Loss of *regA* expression in the dmTAM mutant

The data presented here revealed that *regA* is not expressed in the dmTAM mutant, although the same mutant allele (the HB11A *regA* locus, Table 2.1) is expressed in related strains, including HB11A, 153-68 (Figure 2.3) and another strain (Stark, Kirk, and Schmitt 2001). This finding suggests that following the initial deletion in the *regA* coding sequence, the dmTAM mutant has accumulated additional mutations (as expected when selection is relaxed or lacking), and these mutations also affected regions involved in *regA* regulation. The identification and characterization of such mutations would be of great interest, since the *cis*-regulatory sequences involved in *regA* regulation remain to be identified (Stark, Kirk, and Schmitt 2001; see Chapter 4). However, extensive efforts to amplify different *regA* regions (including the promoter) failed, suggesting that dmTAM might have incurred additional extensive mutations (possibly including large deletions) since its initial isolation.

2.4.3 dmAMN is a suitable mutant to investigate *regA* induction

Since the previously described gonidialess mutant was not suitable for *regA* expression studies, a new mutant was characterized in this study. The newly isolated gonidialess dmAMN mutant shares the same life cycle progression as the dmTAM mutant (Figure 2.4; Tam and Kirk 1991) but, in contrast to dmTAM, dmAMN still expresses *regA* (Figure 2.3). The specific mutation that inactivates *regA* was also identified. The

365 bp insertion in exon 6 is predicted to result in a truncated protein containing only the first 355 AA (of 1049 AA) of the RegA protein, similar to the 291 AA long truncated protein encoded by the mutant HB11A *regA* locus (Kirk et al. 1999). Since the dmAMN mutant does not contain any mutations in *regA*'s promoter or its known *cis*-regulatory regions, it is likely that the regulation of *regA* expression is unaffected, just like for the HB11A *regA* locus (Appendix, Figure 2.11, Stark, Kirk, and Schmitt 2001).

Indeed, during the first day, *regA* expression in dmAMN (Figure 2.6) followed the expected pattern: as in EVE, *regA* transcript levels were low at the onset of embryogenesis (when cells are above the 8 μm threshold), peaked at 9 h after the end of embryogenesis when cells were around 4 μm in diameter (Table 2.4), and then dropped abruptly by the end of the first day. The difference in transcript levels between cells growing in regular light:dark conditions and cells growing in continuous dark at time point 34 h (i.e., corresponding to the end of the second dark period; Figure 2.7B) suggests that cell size might influence (to some extent) the expression of *regA*; specifically, relative to large cells, small cells show a higher basal level of *regA* transcripts. Alternatively, this difference could be explained by higher global transcription rates (i.e., the amount of *regA* transcripts is the same in the two treatments but due to higher global transcription rates in the light:dark treatment *regA* transcripts get diluted in the total RNA population) or by differences in transcript stability between the two conditions.

Overall this study shows that *regA* expression patterns are very similar between the dmAMN gonidialess mutant and EVE (Figure 2.10). These findings argue for the suitability of the dmAMN mutant as a model-system for *regA* expression studies (Chapter 3).

Table 2.1 Regenerator mutant strains used in this study

Strain	Phenotype	Derivative of	Description
HB11A	*regA*$^-$/*nitA*$^-$	EVE	bleomycin-induced *regA*$^-$ mutation (Adams et al. 1990)
153-68	*regA*$^-$/*nitA*$^-$	HB11A × PM1	*regA*$^-$ mutation inherited from HB11A (Kirk et al. 1999)
UTEX LB 1877	*regA*$^-$	UTEX 1978 × UTEX 1886	Starr (1970)
RegAMN	*regA*$^-$	EVE	spontaneous *regA*$^-$ mutant isolated by Aurora M. Nedelcu
Reg/Lag	*regA*$^-$/late-gonidia$^-$	w153 k3	spontaneous *regA*$^-$ mutant isolated by Cristian A. Solari; the original late-gonidia (Lag) strain w153 k3 strain was isolated by David L. Kirk
dmTAM	*regA*$^-$/*gls*$^-$	HB11A × PM1	*regA*$^-$ mutation inherited from HB11A; spontaneous gonidialess mutant (status of *nitA* not reported; strain referred to as Gls/Reg in Tam and Kirk 1991)
dmAMN	*regA*$^-$/*gls*$^-$	UTEX LB 1877	*regA*$^-$ mutation inherited from UTEX LB 1877; spontaneous gonidialess mutant isolated by Aurora M. Nedelcu

Table 2.2 PCR primers and conditions

All PCRs were run in a RoboCycler Gradient 96 (Stratagene); additional primers used for sequencing of PCR products are also listed; F, forward primer; R, reverse primer; SP, sequencing primer.

regA* region	**Primer sequences (5' to 3', artificial sequences are in red†) and conditions**
Promoter–Exon 5 (−125 to +2498 bp)	F CCTGTCCGTATCTGGCATTGG R CTCCTGTCCCAATCACGCAGG 50 µL PCR mix: 0.2 µM each Primer, Platinum PCR SuperMix High Fidelity PCR program: 94°C/2 min—[94°C/0.5 min; 55°C/0.5 min; 68°C/2 min]×45—68°C/10 min SP GGATTGAGAATCGCCATTTCG *attB1* SP GGGGACAAGTTTGTACAAAAAAGCAGGCTGTAAGCCTGTTCCGCTTCC *attB2* SP GGGGACCACTTTGTACAAGAAAGCTGGGTCTGCAGACAATGCAAAAAGC
Part of Intron 5 (+2885 to +3830 bp)	*attB1* F GGGGACAAGTTTGTACAAAAAAGCAGGCTCATTGATATCAGATGTAAC *attB2* R GGGGACCACTTTGTACAAGAAAGCTGGGTGGATATCCGATTGAGGCAGG 50 µL PCR mix: 0.2 µM each Primer, 1 U *Taq*, 1X HB, 2 mM $MgSO_4$, 0.2 mM each dNTPs PCR program: 94°C/2 min—[94°C/0.5 min; 50°C/1 min; 68°C/2 min]×45—68°C/10 min
Part of Exon 6‡ (+4860 to +5609 bp)	F TTGGGAGCCGACCTGCCAT R AGCGTGACCTCGCATGTATC 50 µL PCR mix: 0.2 µM each Primer, 1 U *Taq*, 1X AB, 1X ES, 1.5 mM $MgSO_4$, 0.2 mM each dNTPs PCR Program: 94°C/2 min—[94°C/0.5 min; 55°C/1 min; 68°C/2 min]×45—68°C/10 min
Intron 7 (+7280 to + 8539 bp)	*attB1* F GGGGACAAGTTTGTACAAAAAAGCAGGCTGGCGGCTCTTCCGGCAGTG *attB2* R GGGGACCACTTTGTACAAGAAAGCTGGGTTGCGGAACCTGCGACGGTG 50 µL PCR mix: 0.2 µM each Primer, 2.5 U *Taq*, 1X AB, 1X ES, 1.5 mM $MgSO_4$, 0.2 mM each dNTPs PCR program: 94°C/2 min—[94°C/0.5 min; 55°C/1 min; 68°C/2 min]×45—68°C/10 min SP CTCCTGCAACAGCACCAACG SP CCTGAAGGTCAAGGTGAAGC

Taq, Platinum *Taq* DNA Polymerase High Fidelity; HB, High Fidelity PCR Buffer; AB, PCRx Amplification Buffer; ES, PCRx Enhancer Solution (all reagents Invitrogen); all oligonucleotides were provided by Sigma Genosys

*relative to gDNA

†Primers with artificial sequences were originally designed for cloning in Chapter 4; artificial sequences were not relevant in this study

‡Primers from Stark et al. (2001)

Table 2.3 Gene-specific primer (GSP) for reverse transcription and qPCR primers (F, forward; R, reverse)

Region*	Primer sequences (5' to 3')	
rps18† (+225 to +362 bp)	F	TCGCGCTTACAAGATTCCG
	R	TGGTTGCGGATCTTCTTCAG
regA‡ (+1503 to +1603 bp)	GSP	CGACGCTCCTGTCGAGGC
	F	CAATGGCAGCAAATGGATGTC
	R	GTTCCAAATCAGGCAACACG

all oligonucleotides were provided by Sigma Genosys
*relative to cDNA position
†primers designed with IDT SciTools PrimerQuest program, IDT, Coralville, USA. Retrieved 12 December, 2012. http://www.idtdna.com/Scitools.
‡GSP from Stark et al. (2001); F & R from Nematollahi et al. (2006)

Table 2.4 dmAMN cells almost doubled in size during the first light period of the light cycle.

The average diameter was calculated from measurements of 10 cells of at least 10 random spheroids.

Time [h]	Average cell diameter ± SD [µm] (total cell number measured)
10	4.3 ± 0.7 (220)
14	4.8 ± 0.9 (380)
18	5.6 ± 0.8 (470)
22	5.7 ± 0.7 (200)
27	7.6 ± 1.3 (370)

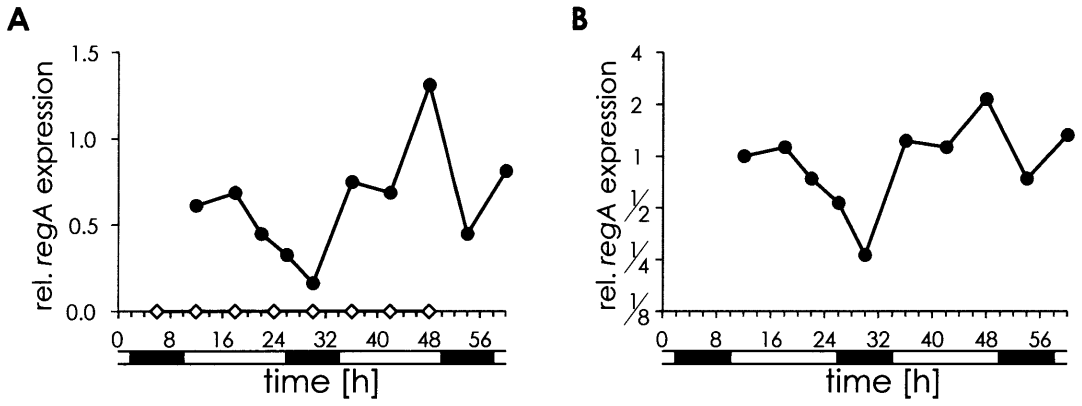

Figure 2.1 Original *regA* expression data (adapted from Kirk et al. 1999)

(**A–B**) EVE was grown in a standard 16L:8D light regime; time point 0 h corresponds to the onset of embryogenesis. *regA* RNA transcript levels in EVE somatic cells (circles) and gonidia (diamonds) were measured using semi-quantitative RT-PCR. Each plotted value represents the ratio of *regA* PCR product to *rps18* PCR product (average of 6 technical replicates each, amplified from the same cDNA pool) at each time point. White bars, light periods; black bars, dark periods. (**A**) Original representation of data. (**B**) The same *regA* expression data of somatic cells on a $\log_2$ scale after linear transformation so that the *regA* level at the first time point (12 h) is 1; this representation was chosen to make comparisons to *regA* expression data in this study easier.

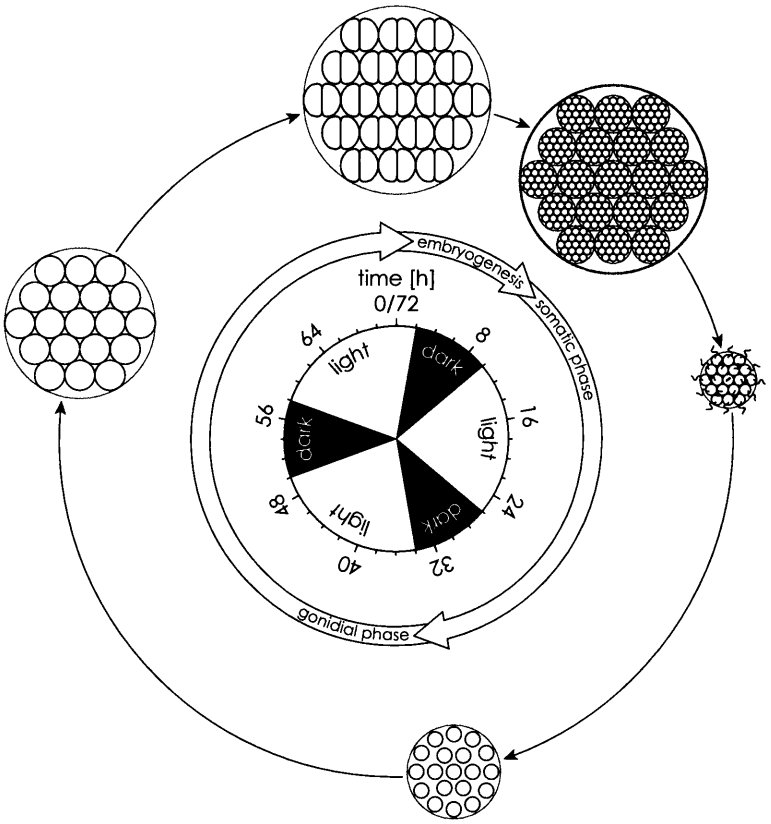

Figure 2.2 The asexual life cycle of a *regA*$^{-}$/*gls*$^{-}$ mutant (adapted from Tam and Kirk 1991)

When a *regA*$^{-}$/*gls*$^{-}$ mutant is synchronized by a 16L:8D light cycle, the life cycle takes 72 h to complete and is divided into three phases. After the onset of **embryogenesis** (the first cleavage division defines the 0 h time point), each cell undergoes 6–8 symmetric divisions and the newly formed spheroids (called juveniles) turn inside out in a process called inversion. Juveniles then enter the **somatic phase** as cells develop somatic features like flagella and an eyespot, but in contrast to the wild-type somatic cells they continue to grow in size. About 24 h later, spheroids enter the **gonidial phase**; cells re-differentiate, lose their flagella and eyespot, grow faster and become increasingly vacuolated resembling wild-type gonidia. After 72 h, cells have reached maturity and enter a new round of embryogenesis; juveniles hatch and are free-swimming.

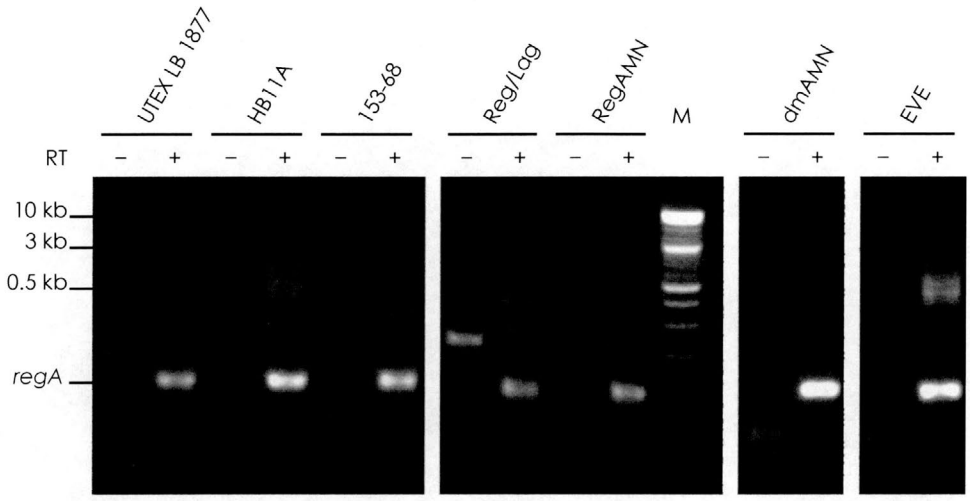

Figure 2.3 *regA* transcripts in several *regA*$^-$ mutant strains.

Unsynchronized *V. carteri* cultures were grown in a standard 16L:8D light regime. RNA was extracted from samples 7 h into the dark period and either treated with reverse transcriptase (+RT) or not (−RT). *regA* transcripts were amplified using RT-qPCR and the primers listed in Table 2.3; the expected product size was 101 bp. An EVE sample from the same time point was included for reference. M, DNA marker.

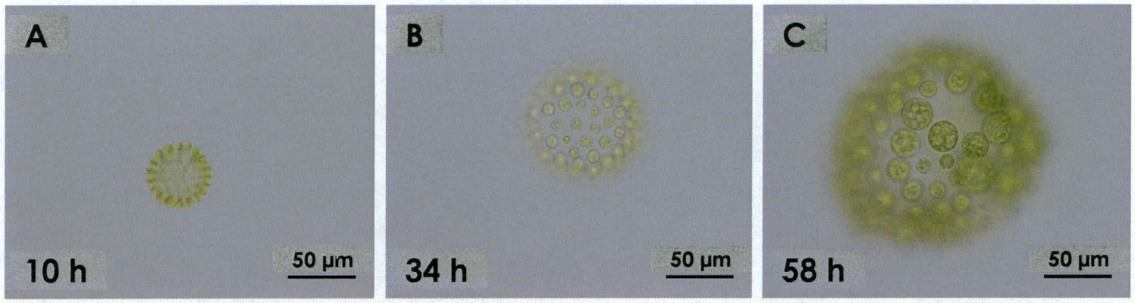

Figure 2.4 A dmAMN gonidialess mutant during the first (10 h), second (34 h), and third (58 h) day of its life cycle.

(**A, 10 h**) A juvenile spheroid shortly after embryogenesis composed of small flagellated cells. (**B, 34 h**) After one day of growth most of the cells have lost their flagella. (**C, 58 h**) After two days of growth the cells resemble gonidia and are clearly vacuolated.

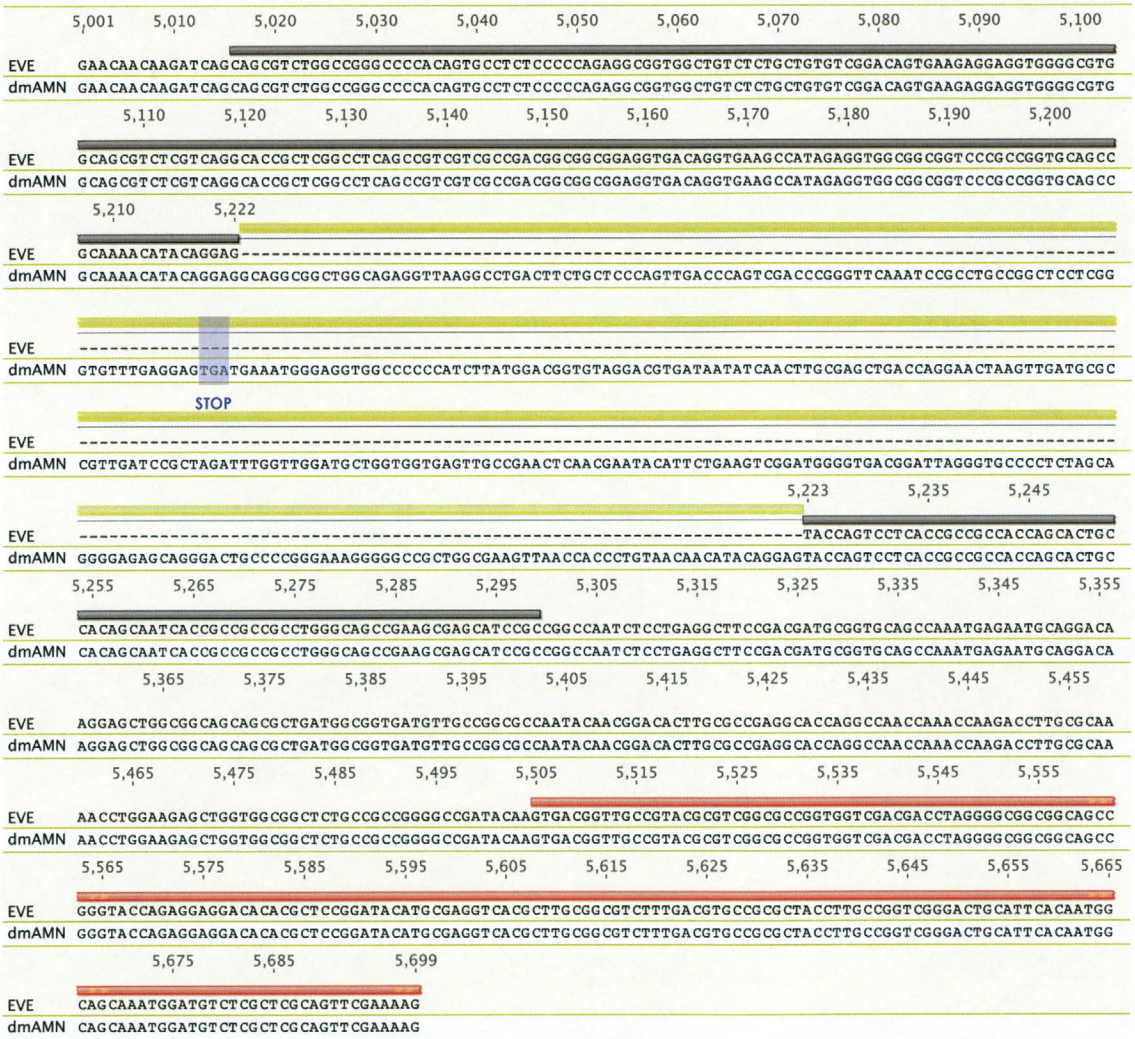

Figure 2.5 The *regA* locus of dmAMN contains an insertion in exon 6.

Part of *regA* exon 6 is shown and the EVE sequence is given as wild-type reference. dmAMN is a derivative of UTEX LB 1877 and their *regA* locus contains a 365 bp insertion (green bar) after position +5222 relative to transcription start site; the insertion contains a premature stop codon (indicated in blue) and the VARL domain (red bar) is not translated. For comparison the deletion in the *regA* locus of the *regA* mutant strain HB11A and its derivates is also given (black bars); the deletion causes a frame shift mutation resulting in a premature stop codon and the VARL domain is not translated either (Kirk et al. 1999).

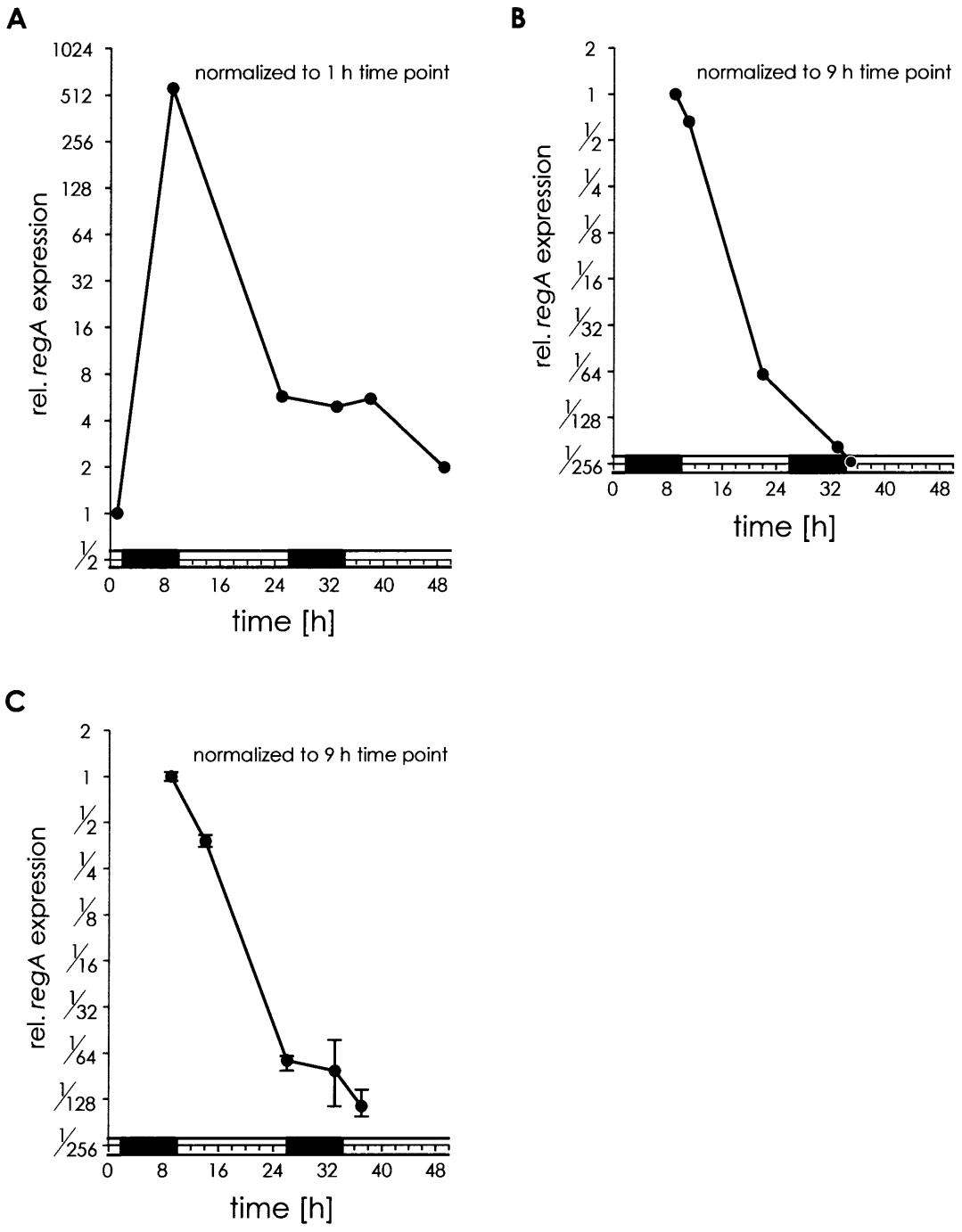

Figure 2.6 *regA* transcript level in dmAMN gonidialess mutant in a standard 16L:8D regime

dmAMN cultures were grown in a standard 16L:8D light regime; under these conditions the onset of embryogenesis (time point 0 h) takes place 2 hours before the end of the light period. *regA* transcript levels were measured using RT-qPCR and are given relative to the first time point in each experiment. (**A–B**) Initial ($n = 1$) and (**C**) replicated ($n = 3$, bars indicate SE) experiments. Along x-axis: black bars, dark periods; white bars, light periods.

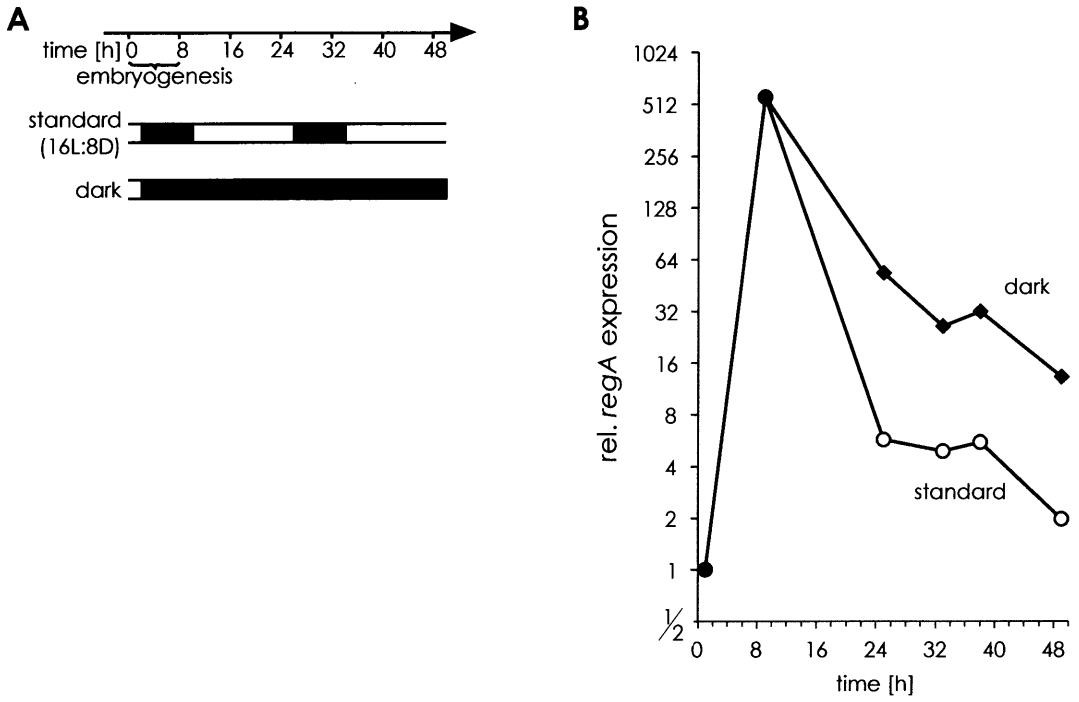

Figure 2.7 *regA* transcript levels in dmAMN gonidialess mutant in standard conditions or in continuous darkness.

(**A**) dmAMN cultures were grown in a standard 16L:8D light regime; under these conditions the onset of embryogenesis (time point 0 h) takes place 2 hours before the end of the light period. For the dark treatment, cultures were maintained in continuous darkness. White bars, light periods; black bars, dark periods. (**B**) *regA* expression was measured using RT-qPCR and is given in reference to the sample under standard light:dark conditions at the first time point (1 h). Initial experiment (n = 1) of dmAMN in standard light:dark regime (standard, open circles) or continuous darkness (dark, closed diamonds).

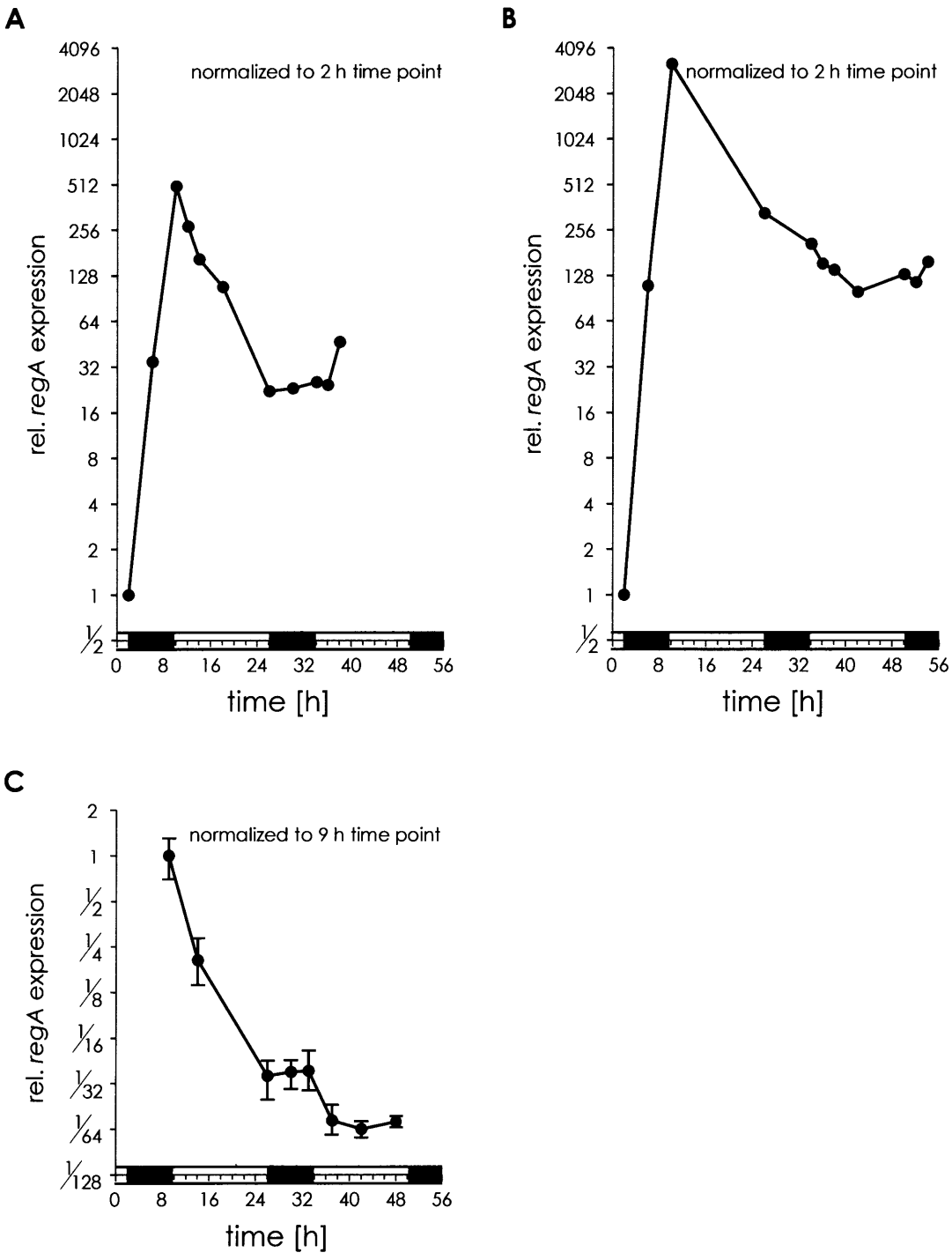

Figure 2.8 *regA* expression only peaks once within the first 48 h of the EVE life cycle, and its expression is independent of light.

EVE was grown in standard16L:8D regime. After the first cleavage division of embryogenesis, parental somatic cells were removed and the isolated embryos were further cultivated. *regA* transcript levels in embryos (time point 2 h) or newly formed juvenile spheroids (containing somatic cells and gonidia; all other time points) were measured by RT-qPCR and shown relative to the first time point in each experiment. (**A–B**) Initial (n = 1) and (**C**) replicated experiments (n = 3, bars indicate SE). Along x-axis: black bars, dark periods; white bars, light periods.

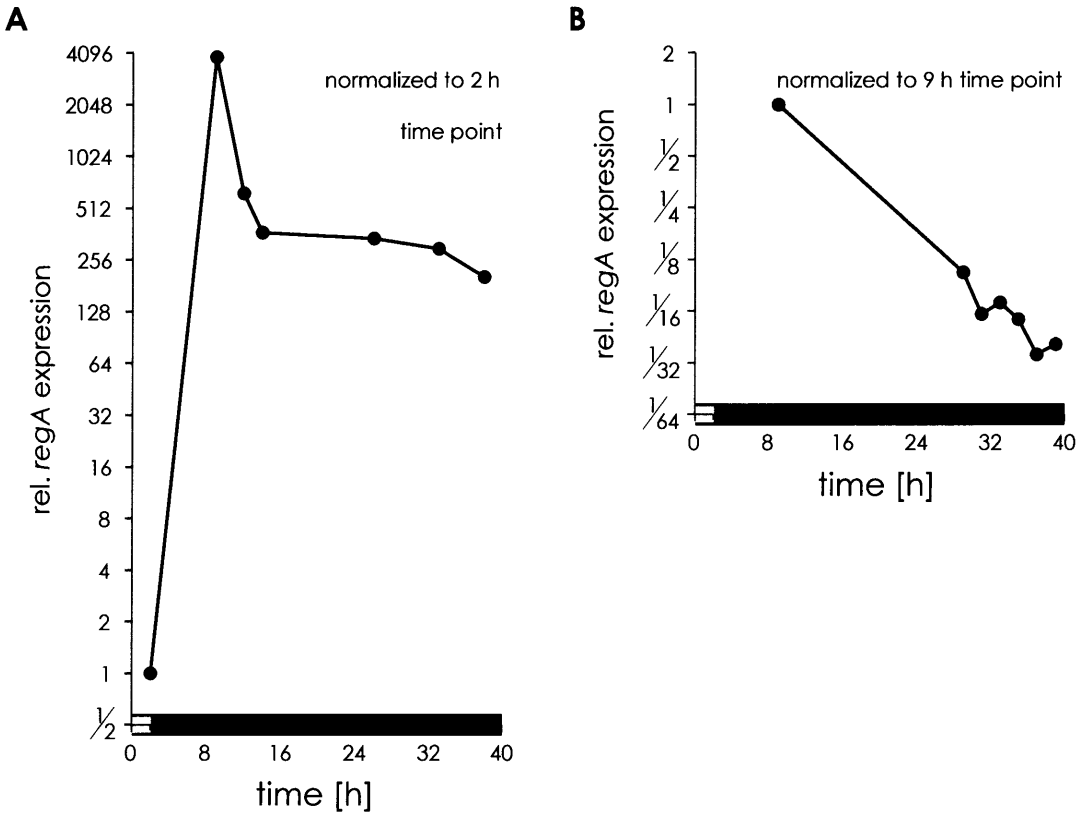

Figure 2.9 *regA* expression in continuous dark in EVE.

(**A-B**) EVE cultures were first grown in a standard 16L:8D light regime. After the onset of embryogenesis (time point 0 h) and at the end of the current light period (time point 2 h), cultures of isolated embryos were switched to continuous darkness. *regA* transcript levels in embryos (time point 2 h) or newly formed juveniles (containing both somatic cells and gonidia; all other time points) were measured using RT-qPCR. Two independent initial experiments ($n = 1$) using different time points show the *regA* transcript levels relative to first time point in each experiment. Along *x*-axis: black bars, dark periods; white bars, light periods.

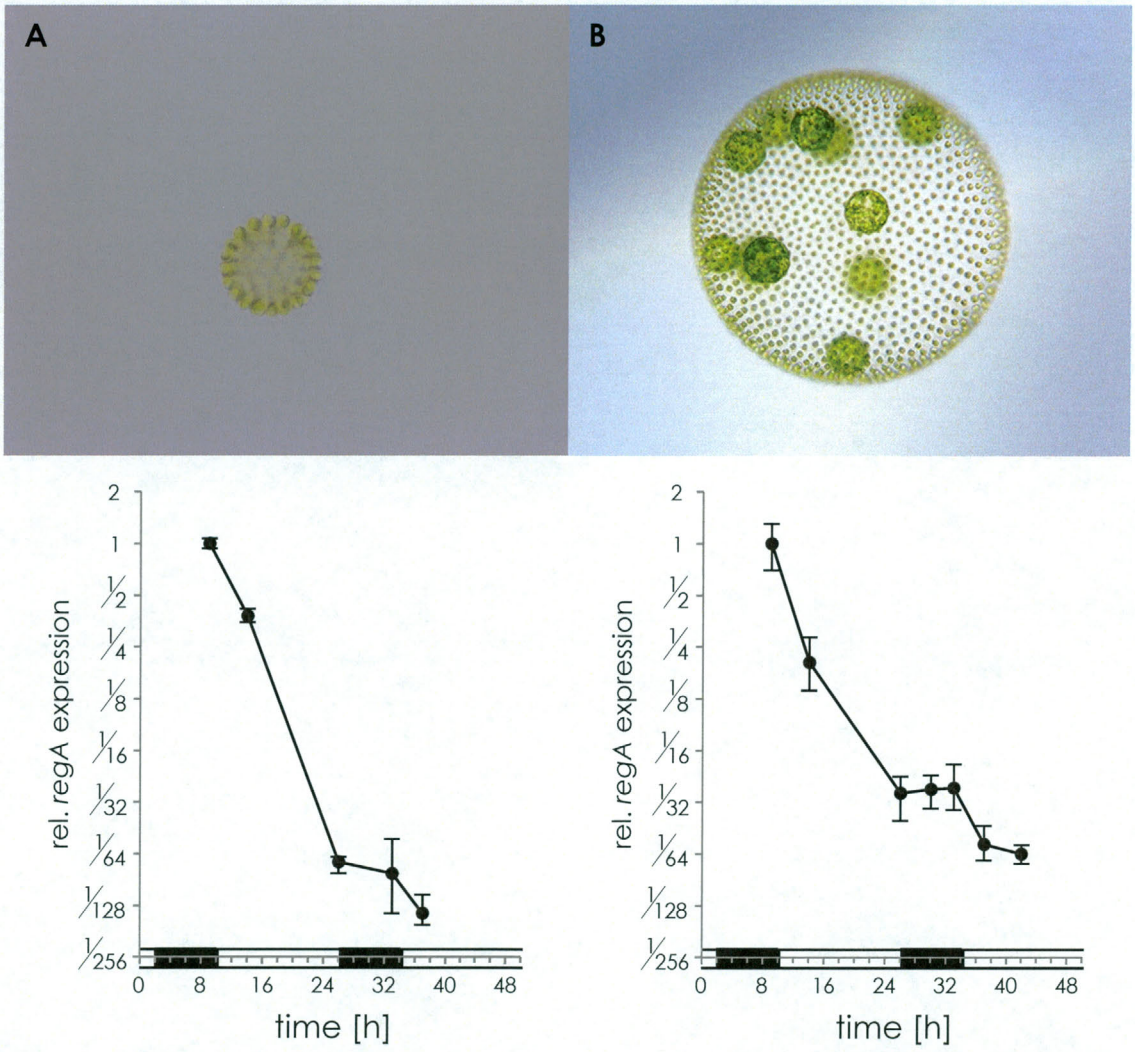

Figure 2.10 Comparison of *regA* expression in dmAMN gonidialess mutant and EVE in standard 16L:8D regime.

Side by side comparison of *regA* expression in standard light regime in (**A**) dmAMN (Figure 2.6C) and (**B**) EVE (Figure 2.8C). Along *x*-axis: black bars, dark periods; white bars, light periods. Photo credit for EVE: Aurora Nedelcu.

2.5 References

Adams CR, Stamer KA, Miller JK, McNally JG, Kirk MM, Kirk DL. 1990. Patterns of organellar and nuclear inheritance among progeny of two geographically isolated strains of *Volvox carteri*. Curr Genet 18:141–153.

Brody JR, Kern SE. 2004. Sodium boric acid: a Tris-free, cooler conductive medium for DNA electrophoresis. BioTechniques 36:214–216.

Cheng Q, Hallmann A, Edwards L, Miller SM. 2006. Characterization of a heat-shock-inducible *hsp70* gene of the green alga *Volvox carteri*. Gene 371:112–120.

Ferris P, Olson BJSC, De Hoff PL, Douglass S, Casero D, Prochnik SE, Geng S, Rai R, Grimwood J, Schmutz J, et al. 2010. Evolution of an expanded sex-determining locus in *Volvox*. Science 328:351–354.

Goda SK, Minton NP. 1995. A simple procedure for gel electrophoresis and northern blotting of RNA. Nucleic Acids Res 23:3357–3358.

Hallmann A, Amon P, Godl K, Heitzer M, Sumper M. 2001. Transcriptional activation by the sexual pheromone and wounding: a new gene family from *Volvox* encoding modular proteins with (hydroxy)proline-rich and metalloproteinase homology domains. Plant J 26:583–593.

Hallmann A. 2006. The pherophorins: common, versatile building blocks in the evolution of extracellular matrix architecture in Volvocales. Plant J 45:292–307.

Kirk DL, Kaufman MR, Keeling RM, Stamer KA. 1991. Genetic and cytological control of the asymmetric divisions that pattern the *Volvox* embryo. Dev Suppl 1:67–82.

Kirk DL, Kirk MM. 1983. Protein synthetic patterns during the asexual life cycle of *Volvox carteri*. Dev Biol 96:493–506.

Kirk MM, Kirk DL. 1985. Translational regulation of protein synthesis, in response to light, at a critical stage of *Volvox* development. Cell 41:419–428.

Kirk MM, Stark K, Miller SM, Müller W, Taillon BE, Gruber H, Schmitt R, Kirk DL. 1999. *regA*, a *Volvox* gene that plays a central role in germ-soma differentiation, encodes a novel regulatory protein. Development 126:639–647.

Miller SM, Kirk DL. 1999. *glsA*, a *Volvox* gene required for asymmetric division and germ cell specification, encodes a chaperone-like protein. Development 126:649–658.

Nematollahi G, Kianianmomeni A, Hallmann A. 2006. Quantitative analysis of cell-type specific gene expression in the green alga *Volvox carteri*. BMC Genomics 7:321.

Pfaffl MW, Tichopad A, Prgomet C, Neuvians TP. 2004. Determination of stable housekeeping genes, differentially regulated target genes and sample integrity: BestKeeper—Excel-based tool using pair-wise correlations. Biotechnol Lett 26:509–515.

Sambrook J, Russel DW. 2001. Molecular cloning: A laboratory manual. 3rd ed.

Shimizu T, Inoue T, Shiraishi H. 2001. A senescence-associated S-like RNase in the multicellular green alga *Volvox carteri*. Gene 274:227–235.

Stark K, Kirk DL, Schmitt R. 2001. Two enhancers and one silencer located in the introns of *regA* control somatic cell differentiation in *Volvox carteri*. Genes Dev 15:1449–1460.

Starr RC. 1970. Control of differentiation in *Volvox*. Symp Soc Dev Biol 29:59–100.

Tam L-W, Kirk DL. 1991. The program for cellular differentiation in *Volvox carteri* as revealed by molecular analysis of development in a gonidialess/somatic regenerator mutant. Development 112:571–580.

Thompson JD, Higgins DG, Gibson TJ. 1994. CLUSTAL W: improving the sensitivity of progressive multiple sequence alignment through sequence weighting, position-specific gap penalties and weight matrix choice. Nucleic Acids Res 22:4673–4680.

Vandesompele J, De Preter K, Pattyn F, Poppe B, Van Roy N, De Paepe A, Speleman F. 2002. Accurate normalization of real-time quantitative RT-PCR data by geometric averaging of multiple internal control genes. Genome Biol 3:RESEARCH0034.

2.6 Appendix

2.6.1 Determination of a suitable reference gene

To select the most stable reference gene for *regA* expression studies I investigated several genes, including ribosomal protein 18 (*rps18*, GenBank# XM_002946177), TATA-box binding protein (*tbpA*, GenBank# AY787798), and actin (*actA*, GenBank# M33963). Synchronous cultures of EVE were grown in SVM at 30°C in a photoperiod of 16L:8D. At −6 h (6 hours before the onset of embryogenesis—used as time 0), cultures were diluted to 40 spheroids/mL in a final volume of 40 mL and either maintained in 16L:8D, or switched to continuous darkness at the end of the current light period (Figure 2.7A). Samples were collected at time points 9 h and 15 h, and RNA was extracted as described above. To remove any gDNA contamination, 670 ng RNA were treated with 2 U DNase I, Amp Grade in 1X DNase I Reaction Buffer (Invitrogen) in a total volume of 20 µL for 15 min at room temperature; the reaction was stopped by adding 2 µL of 25 mM EDTA and a 10 min incubation at 65°C, and then kept on ice. cDNA was synthesized from 4 µL DNase-treated RNA using 15 U ThermoScript RT and 40 U RNase Out in 1X cDNA Synthesis Buffer (all Invitrogen), 1 mM each dNTPs, 5 mM DTT, and 2.5 µM oligo$(dT)_{20}$ in 20 µL total volume; the reaction was incubated for 1 h at 60°C, and then terminated for 5 min at 85°C. The newly synthesized cDNA was further treated with 4 U RNase H (Invitrogen) for 20 min at 37°C. qPCR (using additional primers listed in Table 2.5) and data analysis to calculate C_T was performed as described above, then gene stability was determined with BestKeeper and geNorm (Vandesompele et al. 2002; Pfaffl et al. 2004). The *rps18* was chosen as reference gene for both its stability (Table 2.6) and

its prior use as reference gene for *V. carteri*, in particular for the initial *regA* expression studies (Kirk et al. 1999; Miller and Kirk 1999; Shimizu, Inoue, and Shiraishi 2001; Cheng et al. 2006; Ferris et al. 2010).

Table 2.5 Additional qPCR primers (F, forward; R, reverse) for the amplification of *tbpA* and *actA*

Region*		Primer sequences (5' to 3')
tbpA† (+531 to +636 bp)	F	TGCTCATCTTTGTGTCGGG
	R	TGCGTCTCCTTTCTTGTACTG
actA‡ (+560 to +867 bp)	F	TGACGGACTACCTGATGAAG
	R	GACATCGCACTTCATGATGC

all oligonucleotides were provided by Sigma Genosys
*relative to cDNA position
†primers designed with IDT SciTools PrimerQuest program, IDT, Coralville, USA. Retrieved 12 December, 2012. http://www.idtdna.com/Scitools.
‡from Hallmann et al. (2001)

Table 2.6 Gene stability of *rps18*, *tbpA* and *actA* for selected time points

	rps18	*tbpA*	*actA*
C_T of samples @			
9 h	16.158	26.206	18.834
15 h (16L:8D)	16.331	26.724	17.814
15 h (cont. darkness)	16.357	27.547	20.399
Gene stability (the lower the more stable)*			
BestKeeper†	0.067	0.467	0.933
geNorm‡	0.557	0.557	0.925

*using RefFinder (http://www.leonxie.com/referencegene.php)
†Pfaffl et al. (2004)
‡Vandesompele et al. (2002)

2.6.2 Additional sequencing of dmAMN *regA* locus

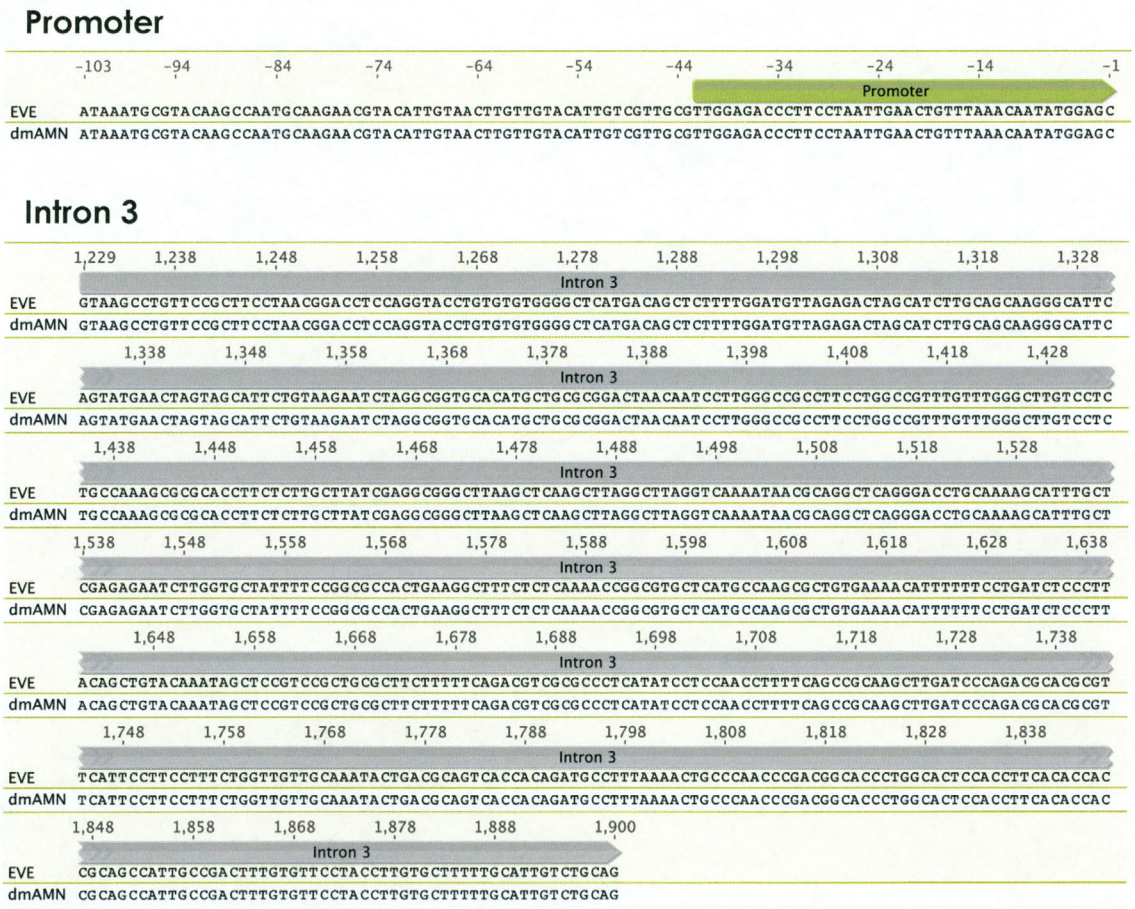

Figure 2.11 The *regA* locus of dmAMN does not contain any mutations in the promoter or any other regions that likely contain regulatory sequences.

Alignment between wild-type EVE and dmAMN sequences of promoter, intron 3, part of intron 5 between two *Eco*RV restriction sites, and intron 7; base numbers are given relative to *regA* transcription initiation site.

Part of Intron 5

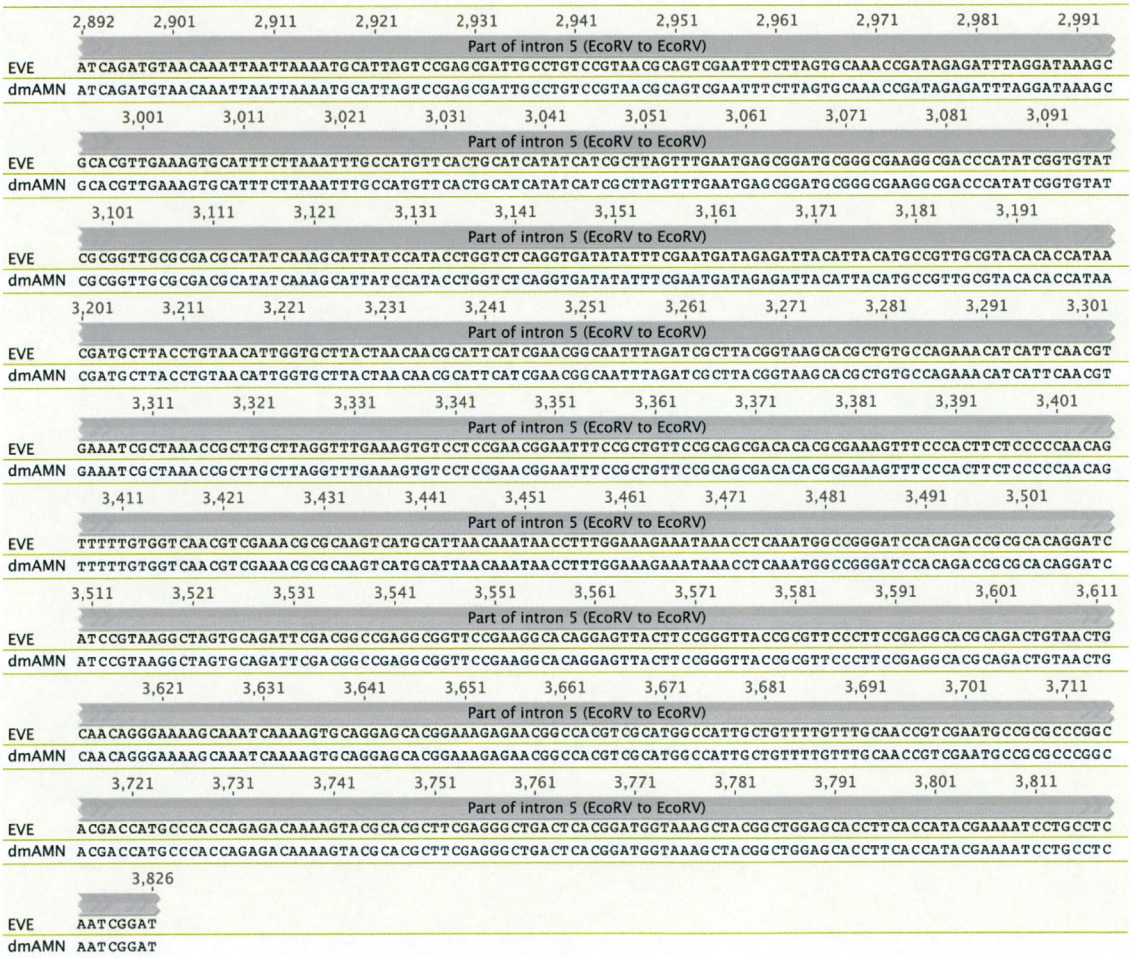

Figure 2.11 continued.

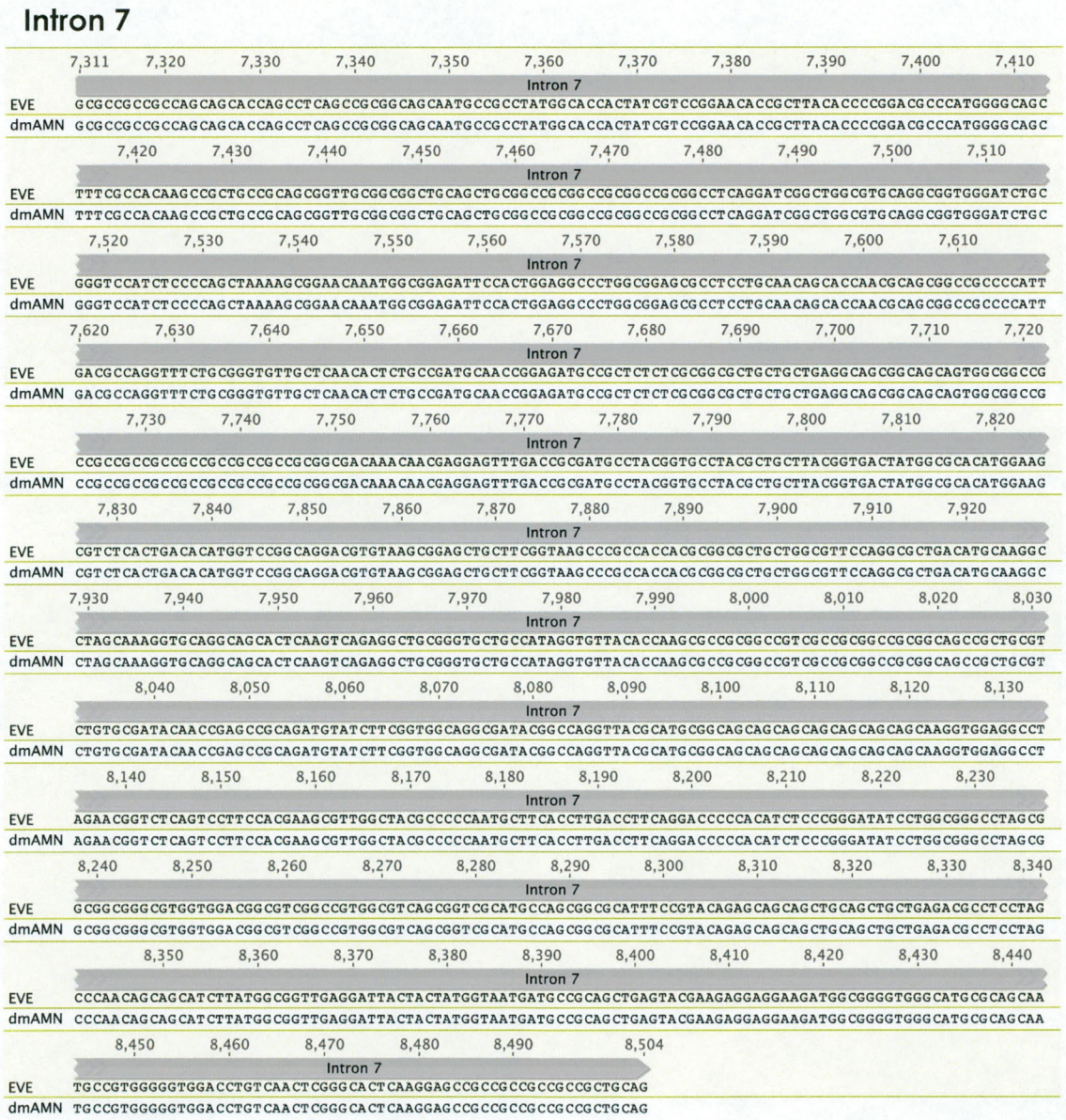

Figure 2.11 continued.

2.6.3 Sequencing of the *regA* RT-qPCR product

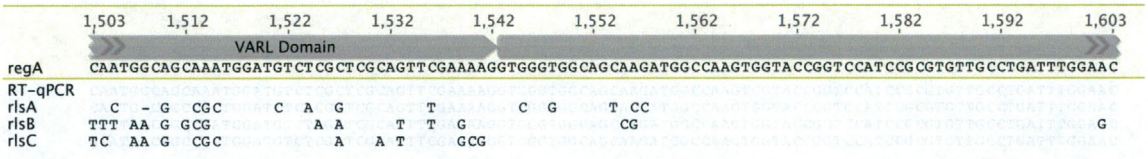

Figure 2.12 *regA* RT-qPCR specifically amplifies the *regA* locus and not other homologs in the *VARL* gene family.

The cDNA sequences encoding the VARL domain (a putative DNA binding domain) of *regA* and its three closest homologs, *rlsA*, *rlsB*, and *rlsC* were aligned using ClustalW (Thompson, Higgins, and Gibson 1994) as part of Geneious 6.0 (Biomatters); base numbers are given relative to the *regA* cDNA, the exon border is after 1542 bp. The sequenced *regA* RT-qPCR product is identical to the *regA* sequence only.

Chapter 3 Environmental induction of *regA*: a new role for the RegA protein

3.1 Introduction

Somatic cell differentiation is a basic process in the development of most multicellular organisms. However, with the exception of some animal lineages, the mechanisms involved in the separation of germ and soma are not well understood. In animals, a set of cells is separated in early embryogenesis to form the germline. The asymmetric distribution of germ granules determines germ fate in most animals (Voronina et al. 2011). The differentiation of germ cells involves three general phases (Cinalli, Rangan, and Lehmann 2008): 1) Transcriptional repression of somatic cell programs in progenitor germ cells (PGC); 2) Migration of PGCs to the somatic gonad, which forms a microenvironment for the maintenance of germ cells; 3) Posttranscriptional regulation of gene regulatory networks—which represses somatic functions on the one hand and might promote germ cell-specific functions (including meiosis and gametogenesis) on the other hand. In stark contrast, in flowering plants, germ cells differentiate late, from somatic cells of the mature plants (Yang, Shi, and Chen 2010). Specifically, the germline develops from the so-called archesporial cells, which will enter meiosis to form gametophytes and ultimately gametes, a process that also depends on complex intercellular signaling between somatic and germline cells (Feng, Zilberman, and Dickinson 2013).

Volvox carteri provides a great model-system with which to investigate the mechanistic basis for somatic cell differentiation due to its simple development and the fact that one gene (*regA*) is necessary and sufficient to establish the somatic cell fate in this species. Interestingly, although the germline is segregated early during embryogenesis (as in animal systems), cell size—and not cytoplasmic composition—is responsible for determining cell fate in *V. carteri* (discussed in Chapter 1 and 2). However, the exact mechanism that converts information about cell size into cell fate and differential *regA* expression is unknown; specifically, the signal that induces *regA* expression in cells that fall under the 8 μm threshold has not been identified.

3.1.1 The effects of cell size on gene expression

Changes in cell size can have various biological consequences. For instance, as cell size increases the cell surface to volume (S:V) ratio decreases, which might limit nutrient/gas uptake or waste removal as well as affect signal reception at the cell surface (Wu et al. 2010). If the nuclear to cytoplasmic volume (N:C) ratio remains constant as cells grow, the nuclear surface to cell volume ratio also decreases (similar to the S:V ratio) and might limit the transport of molecules (e.g. transcription factors) across the nuclear envelope (Wu et al. 2010). So far, a constant N:C ratio has been reported for budding and fission yeast (Jorgensen et al. 2007; Neumann and Nurse 2007), and more recently for *C. reinhardtii* whose nuclear volume halves with each cell division (Dianyi Liu and James Umen, personal communications). In *V. carteri*, whether the N:C ratio remains constant during embryogenesis (or during gonidial growth when the gonidial nucleus increases in size; Coleman and Maguire 1982) is not known, but if so, the somatic cells

should have a smaller nucleus than gonidia (since progenitors leading to somatic cells undergo more cell divisions than those leading to gonidia the nucleus of somatic cells would have decreased more), and ultimately the nuclear import and export kinetics might be different between the two cell types just due to their cell size (Wu et al. 2010).

With an increase in cell size, the DNA to cytoplasm ratio decreases as well (Umen 2005), and to support their larger mass cells need to synthesize larger quantities of mRNA and protein that can only be provided by an increase in global transcription (Marguerat and Bähler 2012). Beyond global changes, examples of specific genes regulated by cell size are scarce. In budding yeast, regardless of the cause for an increase in cell size (either by polyploidy or haploid cell size mutations), a set of genes is repressed in large cells, more than half of which encode proteins of the cell wall, extracellular space or plasma membrane (Wu et al. 2010). Many of the repressed genes are regulated by the mating and filamentation mitogen-activated protein kinase (MAPK) pathways and their repression due to cell size might be mediated by the transcriptional repressor *DIG1* (Wu et al. 2010). Both MAPK pathways start with membrane-bound G-proteins that activate further downstream a cytoplasmic MAPKKK (MAPK kinase kinase; Chen and Thorner 2007; Saito 2010), and this initial step might be modulated by cell size via a change in the S:V ratio; i.e. the ratio of G-protein to MAPKKK (Wu et al. 2010). Since the relative nuclear surface area is smaller in larger cells, another step in the MAPK pathways, namely the transport of MAPK into the nucleus, might also be limited (Wu et al. 2010).

Jain et al. (Jain et al. 2013) recently described a model for mouse fibroblast cells on how cell geometry—including cell size—results in differential expression of a set of

actin-related genes. Larger cells show an increase in actomyosin contractility that results in the translocation of histone deacetylase 3 (HDAC3) from the nucleus to the cytoplasm. The decrease of HDAC3 in the nucleus causes a global increase of acetylated histones and results in chromosome decondensation, thus making genes more accessible to transcription factors. At the same time, the myocardin-related transcription factor (MRTF-A) is transported from the cytoplasm into the nucleus where it upregulates genes containing serum response elements (SRE).

Both studies above used transcriptome analyses (either microarrays or RNA-seq) to identify genes whose expression is affected by a change in cell size; gene ontology analyses were then used to determine what regulatory elements—and by extension what signaling pathways—were shared among these genes. Evolutionary approaches can provide alternative ways to address functional questions about what signaling pathways are involved in converting cell size into differential gene expression, and this study has taken advantage of what is currently known about the evolutionary history of *regA*.

3.1.2 The closest *regA* homolog in *C. reinhardtii*, *RLS1*, is expressed in response to stress

regA belongs to the *VARL* (Volvocine Algal *RegA* Like) gene family (Duncan et al. 2006; Nedelcu and Michod 2006; Duncan et al. 2007; Hanschen, Ferris, and Michod 2014). *VARL* genes are characterized by the presence of the VARL domain, a ~100 AA region including a DNA binding motif called the SAND domain (Bottomley et al. 2001; Duncan et al. 2006; Duncan et al. 2007; Carles and Fletcher 2010). With the exception of the SAND domain, *VARL* genes are quite diverged in gene structure (exon-intron

organization) and predicted amino acid sequences (Duncan et al. 2006; Duncan et al. 2007; Hanschen, Ferris, and Michod 2014), suggesting that the SAND domain is the only region under strong negative/purifying selection.

As *VARL* genes have been identified in both *V. carteri* (14 genes) and *C. reinhardtii* (12 genes), *VARL* genes must have already been present in the unicellular ancestor of *C. reinhardtii* and *V. carteri* (Nedelcu and Michod 2006; Duncan et al. 2007). More recently, orthologs (i.e., homologous sequences related via speciation) of *regA* have been identified in several distant *Volvox* species suggesting that *regA* evolved in multicellular volvocine algae before the evolution of somatic cell differentiation (Hanschen, Ferris, and Michod 2014). Under this scenario, a *regA* gene was later co-opted for a new function in the lineage leading to *V. carteri* (note that whether *regA* is involved in somatic cell differentiation in other *Volvox* species is not known).

Interestingly, the closest homolog of *regA* in *C. reinhardtii*, *RLS1*, has been shown to be expressed in response to stress (Nedelcu and Michod 2006; Nedelcu 2009). Specifically, *RLS1* was induced during stationary phase, extended darkness, deprivation of sulfur or phosphorus, or in response to an inhibitor of the photosynthetic electron transport that causes acclimation-like responses (Nedelcu 2009). These findings suggest that the ancestral *RLS1*-like gene was likely environmentally induced and one of its descendants was later co-opted into a developmental context in the lineage leading to *V. carteri*.

3.1.3 Gene co-option and the evolution of *regA*

Gene co-option is an important evolutionary mechanism involved in the evolution of both physiological and morphological traits (True and Carroll 2002). Genes can be co-opted by changing their pattern of regulation (via mutations in their regulatory elements), by altering the function of the encoded protein (involving structural mutations), or by both. The relative contribution of structural and regulatory mutations to the evolution of morphological traits is still a controversial matter (Hoekstra and Coyne 2007), but changes in gene regulation are considered the main contributors to morphological evolution (Carroll 2000; Ohta 2003; Carroll 2008; Wittkopp and Kalay 2012). Two main arguments are used in support of regulatory changes as playing the main role in the evolution of morphological innovations. First, mutations in *cis*-regulatory elements (i.e. DNA-binding sites of transcription factors) are thought to have less negative pleiotropic effects as such mutations will only affect the spatiotemporal expression of the respective gene (Hoekstra and Coyne 2007). Second, *cis*-regulatory elements can easily evolve *de novo* because binding sequences are usually pretty short (5–10 bp; Ohta 2003). In contrast, mutations in sequences coding for proteins in general and transcription factors in particular might lead to complete loss of function or impair more than one phenotypic trait (i.e. pleiotropy; Hoekstra and Coyne 2007). Nevertheless, gene duplication can circumvent such negative effects as structural mutations in one gene copy can accumulate while the other copy retains it original function (Hoekstra and Coyne 2007). The advent of next generation sequencing facilitates the comparison of whole genomes among species and promises new insights into the contributions of structural and regulatory mutations to morphological evolution (Stapley et al. 2010).

In volvocine algae, since *RLS1* is expressed in response to environmental stress, it has been suggested that the evolution of somatic cells involved a change in the regulation of an *RLS1*/*regA*-like gene, from a temporal/environmental context into a spatial/developmental context (Nedelcu and Michod 2006). Three potential scenarios (with distinct predictions) can be envisioned for such a change in regulation (Figure 3.1): (**A**) no new regulatory elements evolved; rather, the same ancestral environmentally-induced signaling pathway was also induced during development in multicellular volvocine algae (prediction: *regA* can be induced both environmentally and developmentally by the same signal); (**B**) an additional layer of regulation evolved as part of a new (developmentally-induced) signaling pathway and both mechanisms have been maintained (prediction: *regA* can be induced both environmentally and developmentally, but the signals are different); or (**C**) new regulatory elements evolved and the ancestral regulation was replaced or lost (prediction: *regA* can be only be induced developmentally). Notably, the former two scenarios predict that *regA* can still be induced in an environmental context. However, scenario **A** also predicts that the unknown intracellular signal triggered by environmental stimuli (e.g., reactive oxygen species, Ca^{2+}, ATP/ADP, NADPH/$NADP^{+}$, ATP/NADPH) is also induced in small cells at the end of embryogenesis, and any conditions that abolish the shared intracellular signal should affect both environmental and developmental induction of *regA*. Thus, learning about the factors that can induce *regA* expression outside its developmental context could provide clues as to the signal that triggers *regA* induction at the end of embryogenesis.

Recently, the Jun N-Terminal Kinase (JNK) pathway involved in both development and stress response in *Drosophila melanogaster* has also been proposed to have originated as a stress response pathway that was later co-opted for development (Ríos-Barrera 2013). Several important developmental steps involve the JNK pathway and depend on the activation of basket (Bsk) regulating cell elongation: dorsal closure, follicle cell morphogenesis and thorax closure during embryogenesis as well as male genitalia disc rotation/closure during metamorphosis (Ríos-Barrera 2013). But Bsk is not only activated in a developmental context but also as stress response, such as UV exposure, irradiation, wound healing, oxidative stress, and immune challenges (Ríos-Barrera 2013). One hypothesis regarding the JNK pathway is that it is perpetually "on" but silenced by negative regulators of Bsk; this enables the pathway to quickly respond to unpredictable stimuli like stresses.

3.1.4 Signaling pathways and *regA* induction

Compared to heterotrophic organisms, photosynthetic organisms are faced with additional challenges that are related to the presence of a second electron transport chain—the photosynthetic electron transport chain (pETC)—whose imbalance can result in oxidative stress. Light causes the flow of electrons through the pETC (Figure 3.2), and its energy is ultimately converted into ATP and NADPH (i.e. light reactions); ATP and NADPH are then used to reduce inorganic carbon (i.e. carbon-fixation reactions). Under normal conditions, the electrons flow through both photosystem (PS) II and I, and are eventually used to reduce $NADP^+$ to NADPH; this is known as the linear electron flow (LEF; Figure 3.2). However, when imbalances lead to excess excitation energy in the

pETC and the potential production of reactive oxygen species (ROS), electrons are redirected via the cyclic electron flow (CEF). CEF describes the electron flow around PSI from stromal electron carriers to plastoquinone (PQ) forming plastoquinol (PQH_2). PQH_2 is then oxidized by the cytochrome b_6f complex (cyt b_6f), building a proton gradient across the thylakoid membrane that drives the chloroplastic ATPase; this results in ATP production but no net production of NADPH (Figure 3.2; Alric 2010).

In *C. reinhardtii*, LEF does not provide sufficient ATP for the carbon-fixation reactions and ATP is supplemented by CEF, which might constitute up to 50% of the total electron flow (Forti et al. 2003). In this alga, the components for CEF are recruited into a supercomplex consisting of PSI and its own light-harvesting complex (LHCI), the PSII light harvesting complex (LHCII), cyt b_6f, ferredoxin-$NADP^+$ reductase, and the integral membrane protein PGR5-Like 1 (PGRL1; Iwai et al. 2010). The formation of the supercomplex depends on the reducing power of the chloroplast (i.e. the chloroplast redox poise), i.e when availability of ATP limits the carbon fixation reaction NADPH is not depleted by carbon fixation reactions leading to overreduction of the stroma; in this way the amount of CEF is modulated to metabolic demands (Takahashi et al. 2013).

This energy balance, called photostasis, can be disrupted by environmental changes; consequently, photosynthetic organisms evolved mechanisms (i.e., short-term and long-term acclimation responses) to maintain an intracellular redox balance and avoid oxidative damage (Scheibe et al. 2005). For instance, during sulfur or phosphorus deprivation ATP and NADPH consumption is reduced, leading to excess excitation energy in the pETC and the formation of ROS (Wykoff et al. 1998); these changes to the redox poise of the chloroplast that cause short- and long-term acclimation responses

reducing photosynthetic efficiency likely include a switch to CEF and culminate in cessation of cell growth (Wykoff et al. 1998; Pfannschmidt et al. 2009). Since the conditions that induce *RLS1* in *C. reinhardtii* affect photostasis it is likely that *RLS1* is induced by changes in redox status.

If the ancestral signaling pathway that is now associated with *RLS1* induction in response to various environmental stresses in *C. reinhardtii* is still present in *V. carteri*, creating conditions that will induce the same signal in *V. carteri* might result in *regA* expression. Previous studies in *C. reinhardtii* indicated that several factors including dark, nutrient stress and an inhibitor of the pETC induce *RLS1* expression (Nedelcu and Michod 2006; Nedelcu 2009), suggesting that they all converge in triggering a common intracellular signal or secondary messenger. However, *C. reinhardtii* and *V. carteri* are very different in their metabolic capabilities: while the former is mixotrophic (i.e., it can grow both autotrophically and heterotrophically; note that *RLS1* studies have been performed with cultures grown mixotrophically), the latter is strictly autotrophic. Thus, the environmental conditions that induce *regA* in *V. carteri* might be different than the ones that trigger *RLS1* expression in *C. reinhardtii*.

As mentioned above, *RLS1* can be induced in *C. reinhardtii* cultures grown heterotrophically in the dark. Two electron transfer pathways—namely, CEF and chlororespiration (see below)—might be active under heterotrophic conditions in the dark; both pathways are also involved in the stress response of plants and depend on a reduced PQ pool (Rumeau, Peltier, and Cournac 2007; Alric 2010; Peltier et al. 2010; Johnson and Alric 2012). Based on a model by Houille-Vernes et al. (2011), the redox state of the PQ pool in *C. reinhardtii* might be regulated by a process called

chlororespiration in which electron flow to PQ pool is mediated by the type II NAD(P)H dehydrogenase (Nda2) and plastid terminal oxidase 2 (PTOX2). Chlororespiration is thought to act as a safety valve for excitation pressure (and thus to contribute to photoprotection) as electrons get redirected from the pETC to O_2 forming H_2O (Figure 3.2), but also takes place in the dark (Peltier et al. 2010).

However, in contrast to *RLS1* expression in *C. reinhardtii*, extended dark periods did not induce *regA* expression in *V. carteri* (Chapter 2, Figure 2.7 and 2.9). The difference in expression pattern between *RLS1* and *regA* could be due to the different lengths of dark periods used (35 hours for *V. carteri* vs. 3 days for *C. reinhardtii*) and/or differences in metabolic states as, in contrast to *C. reinhardtii*, *V. carteri* lacks the ability to utilize organic substrates and to grow in the dark. Nevertheless, exposure to light after long periods of darkness could induce a metabolic imbalance in these dark-adapted cultures; this might be the case especially in small cells, in which the S:V ratio is higher than in large cells and as a result the ratio of membrane bound pETC components to electron carriers is higher. Consequently, small cells might be prone to the overreduction of the electron carriers and the excess excitation energy might cause to the formation of ROS.

3.1.5 Goal and objectives of this study

The goal of this study was to identify experimental conditions that trigger *regA* expression outside its developmental context to gain information on the signaling pathway(s) and genetic mechanisms involved in the differential expression of *regA* in somatic cells and gonidia in *V. carteri*. To induce changes in redox status several combinations of extended dark periods followed by light exposures of various times have

been used. However, if light is involved in the induction of *regA* two potential mechanisms can be envisioned. 1) Light induces a photosynthesis/redox-mediated signal; in this case *regA* expression levels should correlate with light intensity and be lower in green light as it not as efficiently absorbed by photosynthetic pigments. 2) Light induces a photoreceptor-mediated signal; in this case *regA* induction would show wavelength dependency (Kirk and Kirk 1985). The specific objectives of this study were: 1) to test whether *regA* can be induced by a combination of extended dark followed by exposure to light; and 2) if so, to distinguish between photosynthesis-dependent or independent light induction. To this end, *regA* expression in dmAMN cultures grown in various conditions was investigated using RT-qPCR. To confirm the main findings, several of the experiments were also carried out in EVE. For ease of presentation the results are presented for each strain separately. The results are then discussed in the context of the models presented in Figure 3.1.

3.2 Material and Methods

3.2.1 Strains and culturing conditions

The two *Volvox carteri* strains used in this study were: the gonidialess strain dmAMN and the wild type strain EVE (Adams et al. 1990). dmAMN is a spontaneous gonidialess mutant derived from the *regA*$^-$ strain UTEX1877. The *regA* mutation was characterized previously as a 365 bp insertion after position +5222 in exon 6; the mutation is predicted to result in a truncated and chimeric protein containing the first 355 AA (of 1049 AA) of the RegA protein and 33 AA encoded by the insertion (see Chapter 2 and Appendix).

Under standard culturing conditions, synchronous cultures of both strains were grown in aerated standard *Volvox* medium (SVM, Kirk and Kirk 1983) at 30°C (EVE) or 32°C (dmAMN) and a photoperiod of 16L:8D. Light was provided by cool white fluorescent tubes at 260 μmol photons m^{-2} s^{-1} photosynthetically active radiation (Kirk and Kirk 1985)—as measured with a Laboratory Quantum Scalar Irradiance Meter QSL-100 (Biospherical Instruments Inc.; for light spectrum, see Appendix Figure 3.3A). Under these conditions, the generation time was 48 h for EVE and 72 h for dmAMN. Stock cultures were transferred every generation at the start of embryogenesis during the light period (the 0 h time point), and grown in 300 mL SVM with starting densities at 0.625 spheroids/mL for EVE or 0.67 spheroids/mL for dmAMN.

3.2.2 *regA* expression and cell viability under different light regimes

3.2.2.1 Isolation of early EVE embryos

EVE spheroids containing 2-celled embryos (defined as 0 h time point) were collected on a 100 μm Nitex filter and resuspended in 40 mL fresh SVM in a 40 mL Dounce homogenizer (Kontes) at ≤ 300 spheroids/mL density. Spheroids were broken with one down-and-up stroke of the loose fitting pestle A, and the cell suspension was incubated for 10 min at room temperature so embryos could fully dissociate from the somatic cell sheets. The suspension was poured on a 100 μm Nitex filter; the embryos passed through the filter in the flow-through, were collected on a 30 μm Nitex filter, washed with 100 mL SVM to remove any loose somatic cells, and used to start the experimental cultures.

3.2.2.2 Experimental cultures under different light regimes

Experimental cultures were started at the 1 h time point (after the onset of embryogenesis) and grown in 150 mL SVM at densities of 25–60 embryos/mL for EVE and 5–15 spheroids/mL for dmAMN. Cultures remained in 16L:8D, or were switched to continuous darkness at the end of either the light period (time point 2 h, for experiments with early EVE juveniles or small dmAMN cells) or the following light period (time point 26 h, for experiments with late EVE juveniles or large dmAMN cells). After 16–35 h of continuous darkness, cultures for *regA* light induction experiments or cell viability studies were then exposed to 2–6 h of light (Figure 3.4A and 3.5A). Light intensity was manipulated by wrapping culture flasks in black fiberglass screen and by placing them at various distances from lamps. To adjust light quality, culture flasks were wrapped in red, green or blue filters (#027, 735, and 071 respectively, LEE Filters; see Appendix Figure 3.3B); the transmitted photosynthetically active radiation was 5 μmol photons m^{-2} s^{-1}.

3.2.2.3 Measuring *regA* mRNA levels with reverse transcription quantitative real-time PCR

3.2.2.3.1 RNA extraction and quantification

dmAMN or EVE cultures were collected on a 30 μm Nitex filter and resuspended in 1 mL fresh SVM in a microcentrifuge tube; the sample was centrifuged for 1 min at 3000 g at room temperature, and the supernatant discarded. The pellet was flash-frozen in liquid nitrogen, and stored at −80°C. RNA was extracted with the RNeasy Plant Mini Kit (Qiagen) using Buffer RLC, and eluted in 50 μL ddH2O. RNA concentration was

determined either with a NanoVue (GE) or a SpectroMax M5 spectrophotometer (Molecular Devices).

3.2.2.3.2 RNA integrity testing

RNA integrity was tested on RNA gels; each sample contained up to 1 µg RNA, 1X Blue Gel Loading Dye (NEB), and 20 mM guanidine thiocyanate in a total volume of 15 µL. Samples were incubated for 10 min at 70°C to remove any RNA secondary structures, cooled on ice for 2 min, then loaded on a 1X SB gel (5 mM disodium borate decahydrate, pH adjusted to 8.5 with solid boric acid) containing 1.2% agarose, 20 mM guanidine thiocyanate (Goda and Minton 1995; Brody and Kern 2004) and 0.5X SYBR Safe (Invitrogen). The gel was run in 1X SB conductive medium for 1.5 h at 4 V/cm. RNA bands were visualized using the Gel Doc 2000 System and Quantity One Imaging Software (Version 4.2.1, Bio-Rad).

3.2.2.3.3 DNase treatment

Equal RNA amounts were used for all samples within one experiment. To remove genomic DNA contamination, up to 2 µg RNA were treated with 2 U RQ1 DNase in 1X RQ1 DNase Reaction Buffer (Promega) in a total volume of 20 µL for 1 h at 37°C. The reaction was stopped by adding 2 µL RQ1 Stop Solution, followed by heat-inactivation of DNase for 10 min at 65°C, and then kept on ice.

3.2.2.3.4 Reverse transcription

A reverse transcription (RT) reaction contained 4 µL DNase-treated RNA (up to 360 ng) and 100 U SuperScript III Reverse Transcriptase (Invitrogen) in 1X First-Strand Buffer,

5 mM DTT, and either 2.5 µM oligo(dT)$_{20}$ for reference gene *rps18* or 0.1 µM gene-specific primer for gene of interest *regA* (Table 3.1) in 10 µL total volume. No-RT controls (for use as template for −RT in qPCR) did not contain any reverse transcriptase or primers. The reaction was incubated for 1 h at 50°C, and then terminated for 5 min at 85°C.

3.2.2.3.5 Quantitative real-time PCR

Each reaction contained 2 µL template in 1X KAPA SYBR FAST Master Mix Universal (Kapa Biosystems), and 0.2 µM of each primer (Table 3.1). The PCR run was performed in a Rotor-Gene 6000 (Corbett Research) with an initial denaturation at 95°C for 3 min followed by either 40 (*rps18*) or 45 (*regA*) PCR cycles (95°C/3 sec; 55°C/30 sec; 72°C/3 sec), and concluded by a melt curve analysis from 72 to 95°C. Two +RT replicates and one −RT for each biological replicate and a no template control (NTC) were included in each run.

3.2.2.3.6 Data analysis

Data was collected with Rotor-Gene 6000 software (Version 1.7.87, Corbett Research) and exported to LinRegPCR (Version 12.17, Ramakers et al. 2003; Ruijter et al. 2009) to calculate average PCR efficiency and threshold cycle (C_T); C_T for technical replicates was averaged. The relative expression of the gene of interest between samples was determined with REST2009 software (Version 2.0.13, Qiagen); the software also determined if differences between the control and treatment group were significant using a randomization test.

3.2.2.4 Cell viability

Cultures were collected on a 30 μm Nitex mesh and resuspended in 1 mL fresh SVM in a microcentrifuge tube. SYTOX Green (Invitrogen) was added at a final concentration of 1 μM and samples were incubated for at least 5 min in the dark (Sato et al. 2004). Spheroids were observed on a glass slide with a Leica DM R upright microscope and Leica DC 500 digital camera using the Leica fluorescence FITC filter. Live and dead cells on one hemisphere of at least 20 spheroids per technical replicate were counted using the Fiji image processing package and the cell counter plug-in. The Effect Test of JMP (Version 10, SAS) was used to determine which independent variable most likely explains the difference in cell viability (variables tested: individual spheroid, technical replicate, biological replicate, light intensity, cell size, and phenotype).

3.2.2.5 Genomic DNA extraction

Genomic DNA (gDNA) was isolated to test for DNA laddering, a general feature of programmed cell death that was previously also observed in *V. carteri* (Nedelcu 2005). About 1.2–2 × 10^7 cells in approx. 3 mL SVM were mixed with 12 mL Buffer A (10 mM Tris-HCl, pH 7.6; 10 mM EDTA; 10 mM NaCl) in a 15 mL screw cap tube and centrifuged for 5 min at 1380 g at room temperature; the supernatant was discarded. Cells were resuspended in 6 mL Buffer A containing freshly added 0.5% SDS and 20 mg/mL Proteinase K, and lysed for 1 h at 50°C. After lysis, 6 mL phenol (equilibrated with 10 mM Tris-HCl, pH 8.0, 1 mM EDTA, Sigma) were added, the sample was mixed on a rotary shaker for 10 min at 200 rpm, and the organic and aqueous phases were separated by centrifugation for 10 min at 1380 g. Nucleic acids in the aqueous phase were further

purified by phenol:chloroform extraction and ethanol:sodium acetate precipitation overnight at 4°C (Sambrook and Russel 2001). The nucleic acid pellet was dissolved in 200 µL TE, pH 8.0, and RNase A (Sigma) was added at a final concentration of 25 µg/mL in a microcentrifuge tube, and the solution was incubated for 15 min at 37°C to remove any RNA contamination. To precipitate polysaccharides, 100 µL of 7 M ammonium acetate were added, the solution was mixed well and centrifuged for 15 min at 13,000 g. DNA in the supernatant was precipitated with ethanol in a fresh microcentrifuge tube and pelleted by centrifugation (Sambrook and Russel 2001). The DNA was resuspended in 20 µL TE with 1X Blue Gel Loading Dye (NEB), and separated on a 1X SB gel (5 mM disodium borate decahydrate, pH adjusted to 8.5 with solid boric acid) containing 2% agarose (Brody and Kern 2004) and 0.5X SYBR Safe (Invitrogen).

3.3 Results

3.3.1 *regA* expression in dmAMN

3.3.1.1 Effect of light exposure following an extended dark period

To test if in addition to being expressed during development, *regA* can also be induced in response to environmental changes, young dmAMN cultures (i.e., newly formed juveniles) were kept in the dark for various lengths of times (16 h, 24 h, 31 h, 35 h) and then exposed to light for several hours (2 h, 4 h, 6 h; Figure 3.4). Under these conditions, cell growth is arrested and cells remain small. As in previous experiments, *regA* was not induced in the dark; however, exposure to light following the dark triggered *regA*

expression. Initial experiments suggested that *regA* transcript levels were dependent on both the length of exposure to light and the length of the preceding dark period. Specifically, relative to the corresponding continuous dark controls, the increase in *regA* transcripts appeared to be the highest after 4 h in the light (Figure 3.4B–D). Also, the highest increase in transcript levels following exposure to 4 h of light was observed after 31 h of darkness (a 23.2-fold increase compared to only a 2.4-fold increase in *regA* transcript levels after 16 h of darkness; Figure 3.4E). Therefore, the 31h darkness followed by a 4 h exposure to light treatment was replicated (Figure 3.4E) and used in subsequent experiments.

To test if the observed *regA* induction is dependent on cell size, cultures were allowed to grow for one day (i.e., one light period) and then placed in the dark for 31 h followed by exposure to light for 2, 4, or 6 h (Figure 3.5A). All treatments resulted in a slight induction of *regA*, but in order to compare *regA* induction in small versus large dmAMN cells, the 4 h time point was chosen for additional experiments run in triplicate. In contrast to what was observed for small dmAMN cells (Figure 3.4C & E), large dmAMN cells exposed to 4 h light following 31 h of darkness showed only a small increase in *regA* transcript levels (Figure 3.5). Specifically, under the same experimental conditions, *regA* expression only increased 2.9-fold in large cells, compared to the 23.2-fold increase observed in small dmAMN cells (Figure 3.4E and 3.5C).

3.3.1.2 Effect of light quality on *regA* expression

To determine if *regA* induction by light in small dmAMN cells is mediated by a photoreceptor, cultures were maintained in the dark for 31 h and then exposed to light of

wavelengths that are in the range of known photoreceptors (i.e., blue, green and red light). The increase in *regA* transcript levels (relative to dark control) ranged from 10.6 (white light) to 14.5-fold (blue light; Figure 3.6B); *regA* induction was independent of the wavelength for the tested light qualities.

3.3.1.3 Effect of light intensity on *regA* expression

To investigate if *regA* transcript levels correlate with light intensities, three light intensities were tested: 20, 70, and standard 260 µmol photons m^{-2} s^{-1}. No difference in the level of *regA* induction in dmAMN was found between cultures exposed to light of different intensities. *regA* transcript levels increased ca. 15-fold (compared to the dark control) regardless of light intensity, suggesting that *regA* induction is either independent of light intensity or was saturated by even the lowest intensity tested (20 µmol photons m^{-2} s^{-1}, Figure 3.7B).

3.3.1.4 Effect of light exposure following extended darkness on cell viability

As *V. carteri* is an obligate photoautotroph, extended dark periods such as those used in the above experiments could affect the viability of dmAMN cells. To address this possibility, cell viability was tested with SYTOX Green, a fluorescent dye that penetrates only dead cells and binds their DNA (Figure 3.8).

Unexpectedly, initial experiments (data not shown) showed that although 31 h of darkness did not have a large effect on cell viability, small dmAMN cells exposed to 4 h of light after 31 h of darkness experienced higher cell death compared to the dark control (i.e. 35 h in dark). To further explore these findings, the percentage of dead cells was assessed as a function of light intensity and cell size (Figure 3.9).

Levels of cell death of small dmAMN cells correlated strongly with light intensity (R^2 = 0.885247, $F_{1,11}$ = 77.1346, DF = 1, $p < 0.0001$) and increased from dark control (M = 7.9%, SE = 0.4%) to the highest intensity at 260 µmol photons m^{-2} s^{-1} (M = 31.5%, SE = 3.3%, Figure 3.9A). So, the conditions associated with light-induction of *regA* in previous experiments appear to be stressful for small dmAMN cells. When compared to dark control, cell death increased non-significantly at 20 µmol photons m^{-2} s^{-1} (Tukey HSD, p = 0.3169), but significantly at 70 or 260 µmol photons m^{-2} s^{-1} (Tukey HSD, p = 0.0019 and $p < 0.0001$ respectively). Effect Tests (JMP 10 Software) were performed to determine which independent variable most likely caused the difference in cell viability data; the tests indicated that the differences in cell death levels observed among treatments are most likely explained by differences in light intensity (Table 3.2A). Preliminary experiments with UTEX1877, the parental *regA*$^-$ strain of dmAMN, showed similar trends (Appendix, Figure 3.14).

To address the possibility that the effect observed is specific to small cells (similar to the observed small size-specific induction of *regA*), cell viability analyses were also done with large dmAMN cells exposed to light (260 µmol photons m^{-2} s^{-1}) following 31 h of dark. The effect was less pronounced in large dmAMN cells; cell death increased significantly (2-sample t-test, $p < 0.0001$) in the light compared to dark control, but cell death levels in large dmAMN cells are about half the levels in small cells, for either treatment (2-sample t-test, $p < 0.0001$, Figure 3.9B). Effect Tests on these data indicated that cell size and light most likely determine the differences in cell death level among treatments (Table 3.2B). In addition, large dmAMN cells showed a range of cell sizes,

and it appeared that the relatively smaller cells were the ones that died while the larger cells survived (personal observations, Figure 3.10).

In stark contrast to cells killed by addition of a fixative (Lugol's solution), which showed a strong signal clearly concentrated in the nucleus, dead cells under the experimental conditions showed a weak and blotchy Sytox Green signal in the whole cell (Figure 3.8). The observed blotchy staining pattern suggested a fragmentation of the nucleus, which could indicate programmed cell death (PCD), a mechanism known to be activated in response to stress in *V. carteri* (Nedelcu 2006). To address the possibility that cell death occurred via PCD, a test for DNA laddering (one hallmark of PCD) was performed. DNA was extracted from small or large dmAMN cells of the dark control or light-treated sample. The DNA laddering pattern indicative of PCD was observed for both small and large cells after light treatment, but was more pronounced in the former (Figure 3.9C), consistent with the increased level of cell death in small cells. Thus, the conditions that induce *regA* expression also activate PCD.

3.3.2 *regA* expression in *V. carteri* wild type strain EVE

3.3.2.1 Effect of light exposure following extended darkness

To test if *regA* can also be induced in EVE under the conditions shown to induce *regA* in dmAMN cells, cultures of early or late EVE juveniles were subjected to various combinations of extended periods of dark (24 h or 31 h) followed by 2, 4, or 6 h of exposure to light (Figure 3.11).

In contrast to the 10–20-fold *regA* light-induction observed in small dmAMN cells (Figure 3.4 and 3.6), light had only a small effect on *regA* expression in early EVE

juveniles under all of the conditions tested (Figure 3.11B–D). Thus, the response to light exposure after extended darkness differs between small dmAMN cells and early EVE juveniles although EVE somatic cells and dmAMN cells are of similar cell size and age.

Late EVE juveniles (i.e. about 2 days old, the same age as large dmAMN cells) responded to light with a 4-fold increase in *regA* expression (the highest increase observed in EVE, Figure 3.11E), which was similar to the increase observed in large dmAMN cells of the same age (Figure 3.5B–C).

3.3.2.2 Effect of light exposure following extended darkness on cell viability

To test if the lower levels of *regA* expression in EVE relative to the dmAMN mutant correlate with higher cell viability in EVE, the number of dead somatic cells was assessed in EVE cultures exposed to 4 h of light following 31 h of dark (Figure 3.12A). To confirm the cell viability data, a DNA laddering assay was also performed (Figure 3.12B).

The cell viability data indicated that a 4-hour exposure to light following 31 h of darkness induced a slight but not significant (2-sample *t*-test, $p = 0.0536$, Table 3.3A) increase in somatic cell death in early EVE juveniles, when compared to the dark control (Figure 3.12A). However, cell death in early EVE juveniles (Figure 3.12A) was almost 40-fold lower than in dmAMN with small cells (Figure 3.9D) under the same conditions (for both the light treatment or the dark control: 2-sample *t*-test, $p < 0.0001$). Thus, exposure to light following extended darkness was less stressful for EVE somatic cells, when compared to dmAMN cells of similar age and size. The presence of light and the phenotype alone most likely explains the response in the level of cell death (Table 3.3B).

In addition to the mitigated effect of light on EVE cell viability, there was also no DNA laddering indicative of PCD (Figure 3.12B); the same conditions that trigger PCD in small dmAMN cells do not do so in early EVE juveniles. Overall, light exposure after an extended darkness increases *regA* expression and cell death in small dmAMN cells more strongly than in somatic cells of early EVE juveniles.

3.4 Discussion

The goal of this study was to find experimental conditions that trigger *regA* expression outside its developmental context as to gain information about the signaling pathway(s) and genetic mechanisms involved in the differential expression of *regA* in *V. carteri*. Specifically, the study was designed to: 1) test whether *regA* can be induced by a combination of extended dark followed by exposure to light; and 2) distinguish between photosynthesis-dependent or -independent light induction. The data presented above indicate that exposure to light after extended darkness can induce *regA* in some circumstances, and that this induction is likely redox-mediated; at the same time these conditions also cause PCD. Below I first argue that a photoreceptor is unlikely to be involved in *regA* induction, and then I discuss the proposed models for the co-option of *regA* (Figure 3.1) in light of the results presented here and of relevant information from literature.

3.4.1 Photoreceptors are likely not involved in *regA* induction

The observed *regA* expression in cells exposed to light raised the question whether induction was mediated by photoreceptors, or by photosynthesis-related activities. Photoreceptors are generally involved in directional movement in response to light.

However, their roles extend to a greater range of cellular activities, including modulating gene expression and protein synthesis, regulating photosynthetic activities, controlling cell division, cell fate and differentiation (Ozawa et al. 2009; Beel et al. 2012; Kianianmomeni and Hallmann 2014). In *V. carteri*, the initiation of cell divisions during embryogenesis and the final steps of cell differentiation are affected by light, and these processes are thought to be mediated by photoreceptors (Kirk and Kirk 1985; Kirk 1998).

A large number of photoreceptors have been described in *C. reinhardtii* and *V. carteri* (Ebnet et al. 1999; Kianianmomeni et al. 2009; Kianianmomeni and Hallmann 2014). In *V. carteri*, several photoreceptors have been characterized, and several more are predicted based on its genome sequence (Prochnik et al. 2010; Kianianmomeni and Hallmann 2014). Known blue light receptors include one phototropin and four cryptochromes (cryptochromes also respond to red light). Interestingly, in *Arabidopsis thaliana* cryptochrome-1 (CRY1) is critical for PCD induction by the ROS $^1O_2$ (Danon, Coll, and Apel 2006). Whether PCD in *V. carteri* is dependent on light quality when induced by extended darkness followed by light is not known; but if a similar pathway were in place it would likely also depend on the production of ROS. Light in the blue–green range is detected by volvoxopsin (VR1) and two channelrhodopsins; green light has been shown to induce phototaxis and regulate translation in *V. carteri* but might also be important for cytodifferentiation after embryogenesis (Schletz 1976; Sakaguchi and Iwasa 1979; Kirk and Kirk 1985). Furthermore, four histidine kinase rhodopsins were predicted but their absorption spectrum has not yet been characterized. The existence of genes encoding a far-red light receptor, e.g. phytochrome, in the genomes of *C. reinhardtii* and *V. carteri* is still a matter of debate (red/far-red reversibility, a characteristic of phytochrome, has not

been demonstrated), but far-red light has been shown to affect expression of some genes in both algae (Grossman, Lohr, and Im 2004; Im et al. 2006; Alizadeh and Cohen 2010; Beel et al. 2012; Kianianmomeni and Hallmann 2014; Kianianmomeni, personal communication).

Interestingly, in *V. carteri*, the distribution and relative abundance of photoreceptors are different between the two cell types, which suggests that they interpret light signals using different signaling pathways. For instance, the animal-type rhodopsin VR1 is expressed only in gonidia, where it might be involved in regulating photosynthetic activities (Ebnet et al. 1999); other photoreceptors are expressed only in somatic cells (Kianianmomeni and Hallmann 2014). Of particular interest is phototropin, which in *C. reinhardtii* not only regulates the expression of channelrhodopsins (light-gated ion channels in the eyespot area) and the eyespot size, but is also involved in cell size regulation (Suzuki et al. 2003; Berthold et al. 2008; Zorin et al. 2009; Kianianmomeni and Hallmann 2014). Because the phototropin gene is highly expressed in somatic cells in *V. carteri*, it has been suggested that a connection between this photoreceptor and the mechanism of cell size regulation during development could exist (Kianianmomeni and Hallmann 2014). Histidine kinase rhodopsins have also been in proposed to regulate development in *V. carteri*. Domains of the histidine kinase rhodopsins are found as part of the two-component signal transduction systems in prokaryotes that are involved in response to stress stimuli and control of cell division and cell growth (Schaller, Shiu, and Armitage 2011). In *V. carteri*, histidine kinase rhodopsins are thought to produce cAMP or cGMP (which are secondary messengers in a variety of cellular processes) in a light-dependent manner and/or as a stress-response, and these cyclic monophosphates then

might activate transcription factors controlling cell cycle regulation and cell differentiation during development (Kianianmomeni and Hallmann 2014).

However, in this study, blue, green and red light induced *regA* in dmAMN to a similar extent, suggesting that *regA* induction is wavelength independent (Figure 3.6B). This action spectrum is not characteristic for any known light receptor, or, for that matter, photosynthesis (i.e. green light would be less efficient in driving photosynthesis), but further analysis of the light filters revealed one caveat: all three filters transmitted far-red light (Figure 3.3B). At this point a red/far-red light receptor that mediates *regA* induction in the dmAMN strain cannot be completely ruled out, but it would have to meet the following requirements: 1) generate a signal only in small dmAMN cells (since *regA* induction was observed in small cells but not in large cells) and 2) be downregulated in EVE somatic cells (since very low *regA* induction was observed in wild-type somatic cells). However, as there is no known receptor for far-red light that meets all of the requirements listed above, the involvement of a photoreceptor in *regA* induction is unlikely.

3.4.2 *regA* is induced by a specific combination of environmental cues, genetic background and cell size

This study showed for the first time the induction of *regA* outside its developmental context. Specifically, *regA* was induced in RegA deficient dmAMN cells exposed to light following extended darkness. Furthermore, *regA* expression was dependent on cell size as well as the length of darkness (Figure 3.4E and 3.9A), being highest in small dmAMN cells exposed to 4 h of light following 31 h of darkness. On the other hand, *regA* was only

slightly induced in EVE somatic cells, and its expression levels were independent of duration of darkness, light exposure or age (Figure 3.11). Since at the end of embryogenesis EVE somatic cells and dmAMN cells are equivalent in size, it is likely that the only difference between the two cell types is related to the status of their *regA* locus; namely, a functional protein is present in EVE but not in the dmAMN mutant. Taken together, these data suggest that *regA* induction requires the following combination of factors: 1) exposure to 4 h of light following 31 h of dark, 2) the absence of a functional RegA protein, and 3) small cell size. Overall, the data reported in this study show that *regA* can be induced in response to environmental changes, suggesting that *regA* has maintained its postulated ancestral environmental regulation (as discussed in the Introduction). However, the data are consistent with both scenarios in Figure 3.1A & B—that is, the developmental and environmental regulation could involve either the same or different signaling pathways.

3.4.3 Conditions that trigger *regA* expression also induce PCD

Interestingly, the conditions that triggered *regA* induction affected cell viability in a manner similar to the *regA* induction pattern, and cell death correlated with the level of *regA* induction. Specifically, exposure to light following extended darkness caused extensive cell death in small dmAMN cells, but less and very little cell death in large dmAMN cells and in EVE somatic cells, respectively (Figure 3.9B and 3.12A; no dead gonidia were observed, data not shown). However, in contrast to *regA* induction, the death of small dmAMN cells was influenced by the intensity of light, with the highest level having the strongest negative effect on cell viability (Figure 3.9A). DNA laddering

in dmAMN indicated that cell death was actually PCD (Figure 3.9C). These findings argue for light inducing a signal that becomes damaging at high levels in small dmAMN cells. On the other hand, in the wild type EVE, the viability of neither gonidia nor somatic cells was strongly affected by the light, suggesting that the absence of a functional RegA protein contributes to the sensitivity of small dmAMN cells to light (however, at the moment it is not known if the RegA protein is actually expressed during extended darkness; see discussion below). Furthermore, the sensitivity of small *regA*$^-$/*gls*$^-$ cells to light and their decrease in cell viability is likely caused by the *regA*$^-$ mutation since the single *regA*$^-$ mutant parental strain UTEX1877 showed similar trends in cell viability under the same experimental conditions (Appendix, Figure 3.14).

Table 3.4 provides a summary of what is known about *regA* induction (both developmentally and environmentally) and PCD in both the wild type strain and the dmAMN mutant. The fact that the viability of both wild type gonidia and the large dmAMN cell populations (both not expressing *regA*) is not, or minimally, affected by light suggests that the light-induced signal is dependent on cell size. On the other hand, the difference in response between the small dmAMN cells and the wild type somatic cells (of a similar cell size) is likely attributed (directly or indirectly) to the absence/presence of a functional RegA protein (Table 3.4). Taken together, these observations suggest that small cells are more susceptible to the damaging effect of light and that a functional RegA protein can confer protection.

Interestingly, RegA might also confer protection against heat shock. Previous work in *V. carteri* EVE has shown that in response to heat shock, gonidia undergo PCD, while somatic cells appear unaffected and continue to provide the colony with motility

(Nedelcu 2006). In this case, as the larger cells appear more sensitive to stress than the smaller cells, it is likely that the differential response can be attributed solely to the presence/absence of the RegA protein.

3.4.4 RegA protein confers stress-resistance

The findings summarized in Table 3.4 suggest that the RegA protein confers resistance to various types of stress, whether mediated by cell size or not. Two possibilities can be envisioned to explain RegA's postulated stress protection: RegA-containing cells either are less sensitive to stress or have a better ability to respond to the effects of stress. Below I discuss these two scenarios and the potential mechanistic basis for the observed differences in response between the wild type and the dmAMN mutant.

In the first scenario, the two strains might differ in their chloroplast protein compositions (due to the presence/absence of RegA), and this difference reflects in their different sensitivity to stress (Figure 3.13A). As discussed in Chapter 1, RegA is thought to act as a transcription factor that directly or indirectly suppresses the transcription of nuclear genes coding for chloroplast proteins, often referred to as "gonidial genes" (Table 3.5; Tam and Kirk 1991a; Choi, Przybylska, and Straus 1996; Meissner et al. 1999). Small cells in *regA*$^{-}$/gonidialess mutants and wild type somatic cells share the same morphology and cell size just after embryogenesis, and both express early somatic genes (Tam and Kirk 1991b). However, a *regA*$^{-}$/gonidialess strain was shown to express at least eight gonidial genes at much higher levels than wild type somatic cells starting on the first day and likely before they encounter light (Tam and Kirk 1991b). Thus, it is possible that the chloroplast composition differs between wild-type somatic cells and

small dmAMN cells at the time when they are exposed to light. These differences can affect differently the overall metabolic/redox state of the two cell lines maintained in dark for extended periods and then exposed to light. Specifically, light might induce a metabolic imbalance in the RegA deficient dmAMN cells, and this imbalance could trigger a signal that induces *regA* expression in an attempt to adjust the chloroplast composition to light. However, in the absence of a functional RegA protein, these cells would be unable to adjust their chloroplast composition, which would maintain the imbalance resulting in the accumulation of ROS and ultimately PCD (Figure 3.13A). Importantly, for this scenario to be true the RegA protein must already be expressed during extended darkness.

Alternatively, if there are no differences in chloroplast composition at the end of the dark period (that is, if RegA did not represses gonidial genes in the dark), light will affect both cell lines in a similar manner (and induce the same signal), but cells with a functional RegA protein might respond differently to that signal (e.g., RegA will repress the expression of gonidial genes; Table 3.5); in this case, the two cell lines differ in their response to the stress-induced signal (Figure 3.13B). In this scenario, the RegA protein is expressed after cells are exposed to light.

In both scenarios, the presence of a functional RegA protein appears to confer stress-resistance to wild type somatic cells, but the role of RegA would be different. In the first scenario, the role of RegA protein is indirect (and "preventative"); its early expression at the end of embryogenesis would affect chloroplast composition in a way that renders cells able to withstand the environmental change. In the second scenario, the RegA protein has a direct (and "responsive") role by activating an acclimation response in

response to the environmental change. In the first scenario, the signal that is triggered by the environmental change would be different between dmAMN and wild type; or, missing altogether in the wild type somatic cells. On the other hand, in the second scenario the same signal will be triggered in both cell types. In wild type cells, this initial signal might trigger a RegA-mediated acclimation response that would alter the chloroplast composition, while in cells lacking the RegA protein, chloroplast composition cannot be adjusted, which might elicit a secondary signal that will induce *regA* expression; ultimately, in the absence of a functional RegA, this signal will, directly or indirectly, induce PCD. In both scenarios, the signal that induces both *regA* expression and PCD is related to the chloroplast status. But what is the nature of the signal?

3.4.5 The environmental induction of *regA* likely involves a chloroplast-related redox signal

The observation that the combination of small cell size and light exposure following extended darkness triggers both *regA* induction and PCD in the dmAMN mutant (similarly, enlarged cells or presence of a functional RegA protein fail to induce both *regA* and PCD) allows for the possibility that a common signaling pathway is involved (directly or indirectly) in triggering *regA* expression and PCD. Reactive oxygen species (ROS) could be involved in this pathway as they are known to act as transduction signals at low levels (e.g. as retrograde signals from the chloroplast regulating nuclear genes) but can also trigger oxidative damage and PCD or even necrosis at higher levels (Reape, Molony, and McCabe 2008; Mullineaux and Baker 2010). In support of this possibility is the observation that light intensity did not influence the level of *regA* induction but

affected the level of PCD. It is likely that up to a specific level and exposure time ROS act as transduction signals, while higher levels of ROS or the accumulation of ROS over time can induce levels of oxidative damage that will correlate with light intensity.

In photosynthetic organisms, ROS can originate in the chloroplast, since environmental stresses affect the redox state of the pETC and stromal electron acceptors (Wykoff et al. 1998; Pfannschmidt et al. 2009; Pfannschmidt and Yang 2012; Suzuki et al. 2012). As discussed in the Introduction, when imbalances lead to excess excitation energy in the pETC and the formation of ROS (such as during phosphate and sulphate deprivation; Wykoff et al. 1998), electrons are redirected via the CEF, which adjusts the ATP:NADPH ratio to metabolic demands. In plants, two CEF pathways are characterized by their sensitivity to antimycin A and by their use of either ferredoxin (Fd) or NADPH as electron donors, and both lead to the reduction of the PQ pool (Figure 3.2; Rumeau, Peltier, and Cournac 2007; Peltier et al. 2010). In *C. reinhardtii,* the antimycin A-insensitive pathway likely uses Nda2, a type II NAD(P)H dehydrogenase for the non-photochemical reduction of PQ (Jans et al. 2008), and the antimycin A-sensitive pathway involves *PGR5* and *PGRL1*. Homologs of the latter have been identified in numerous other algae including *V. carteri* (Peltier et al. 2010). *PGRL1* has recently been identified as a ferredoxin-plastoquinone reductase and forms a heterodimer with *PGR5* (Hertle et al. 2013). The *pgr5* mutant of *A. thaliana* showed less efficient CEF than wild type (Nandha et al. 2007; Joliot and Johnson 2011). A more reduced PQ pool due to CEF might cause more frequent charge recombination events at PSII in the light thus increasing $^1O_2$ evolution involved in retrograde signaling (Krieger-Liszkay, Fufezan, and Trebst 2008).

Alternatively, ROS in form of H_2O_2 may evolve from the non-enzymatic oxidation of PQH_2 (Mubarakshina, Khorobrykh, and Ivanov 2006).

As mentioned above, the RegA protein is thought to repress directly or indirectly gonidial genes which are nuclear-encoded chloroplast protein genes (Table 3.5; Tam and Kirk 1991b; Choi, Przybylska, and Straus 1996; Meissner et al. 1999). Thus, the chloroplast status might differ between wild type and dmAMN cells in the dark. Could the environmental conditions that result in *regA* induction in dmAMN small cells have affected CEF?

The duration of darkness influenced the extent of *regA* induction in small dmAMN cells (Figure 3.4E); in barley, prior dark adaptation of 24 h increased CEF in response to a flash of saturating white light, possibly due to a shift in ATP:ADP and/or $NADPH:NADP^+$ ratios (Golding, Finazzi, and Johnson 2004). In the dark, NADPH (an electron donor for CEF) might be produced by starch metabolism in *C. reinhardtii*, and glycolytic enzymes localized in the chloroplast are considered to cause a more reduced redox poise in comparison to plants (Johnson and Alric 2012). Thus, NADPH produced in the dark might feed into CEF; also the more negative redox poise might favor the formation of the supercomplex involved in CEF.

Another effect of extended darkness might be an increase in stress. In peach, catalase is upregulated as a response to oxidative stress (Bagnoli 2004), and Giannino et al. (2004) showed that 36 h of darkness also induces the upregulation of catalase. Accordingly, it is possible that 31 h of darkness increased oxidative stress in dmAMN, and light exposure further increased stress levels resulting in *regA* induction and ultimately PCD (Figure 3.4 and 3.9).

3.4.6 The potential effects of cell size on CEF and ROS production

In the dmAMN mutant, in addition to the specific combination of dark and light exposure, the size of cells also influences the level of *regA* induction and extent of PCD. If ROS are actually the signal for *regA* induction and PCD, then ROS seem to be produced more readily in small than in large cells. In the light, imbalances in the pETC might also occur if the ratio between membrane-bound electron transport carriers and soluble cofactors is disrupted. Specifically, since most of the cell is occupied by a cup-shaped chloroplast, small cells could experience an excess of pETC molecules that could lead to excess excitation energy and formation of ROS. Relative to large cells, small cells have about 16-fold higher surface to volume (S:V) ratio and accordingly a higher ratio of membrane-bound pETC proteins to electron carriers in the stroma ($NADP^+$, Fd). Thus, small cells are likely more prone to overreduction of the electron acceptors and excess excitation energy in the pETC; the ATP:NADPH ratio might also be affected. It has been proposed that such a redox change exclusive to small cells could be the signal (that is ultimately translated in the form of ROS) inducing *regA* expression in response to light (Nedelcu 2009). Although this is not the case in the somatic cells of the wild type (see Chapter 2), a similar scenario can account for (or contribute to) *regA* induction in small dmAMN cells exposed to light following an extended dark period.

Alternatively, or additionally, the metabolic balance between light and carbon-fixation reactions might be disrupted in small cells since the carbon-fixation reactions are carried out by enzymes in the stroma; in this scenario, NADPH and ATP consumption by the carbon-fixation reactions would be limited, which will lead to excess excitation

energy in the pETC including over-reduction of the PQ pool (Pfannschmidt and Yang 2012).

Lastly, the S:V ratio might affect ferredoxin-$NADP^+$ reductase (FNR). FNR can be found either bound to cyt b_6f (in a supercomplex) or soluble in the stroma (Figure 3.2), and Joliot et al. (2011) proposed that FNR allocation might regulate electron flow between LEF and CEF. The association of cyt b_6f and FNR might be promoted by PGR5 and PGRL1 in *A. thaliana* (DalCorso et al. 2008), though PGR5 was not isolated as part of the supercomplex in *C. reinhardtii* (Iwai et al. 2010). Similar to the *pgr5* mutant of *A. thaliana*, an antisense mutant of tobacco depleted in FNR showed also a reduction of CEF, likely due to less FNR cyt b_6f complexes (Joliot and Johnson 2011). In dmAMN, the S:V ratio characteristic for small or large cells might affect the allocation of FNR (soluble vs. in supercomplex) and thus LEF and CEF distribution and ROS production.

Expanding on the hypothesis that ROS represent the signal for *regA* induction in small dmAMN cells exposed to light, the RegA protein would confer stress resistance in the wild-type somatic cells by affecting the chloroplast composition (either before or right after exposure to light). Interestingly two of the genes thought to be repressed by RegA (Table 3.5) encode FNR and PGR5 whose importance for CEF has been described above, so ultimately RegA might influence the LEF and CEF distribution to abolish ROS production. In small dmAMN cells exposed to light after extended dark, LEF and CEF distribution cannot be regulated and ROS will be produced.

Experiments reported in Chapter 2 indicated that the developmental induction of *regA* is, nevertheless, independent of light in both dmAMN and EVE (Figure 2.7 and 2.9). Thus, if developmental *regA* induction depends on a signal similar to that generated

environmentally (Figure 3.1A), such signal must be independent of light excitation. If ROS is also the signal during the developmental induction of *regA,* the drastic change in cell size and the shift in the S:V ratio might affect the distribution of specific components of the LEF and CEF (including the allocation of FNR) or the ratio between other stromal and membrane-bound proteins in a light-independent manner. Such changes could induce redox imbalances and cause a transient production of a ROS signal in somatic cells. Although the model presented below considers this possibility, further investigations are needed to address this suggestion.

3.4.7 A model for *regA* induction

Previously, *RLS1*—the *regA* homolog in the unicellular *C. reinhardtii*—has been shown to be induced under stressful conditions (Nedelcu 2009). The data presented here show that *regA* in *V. carteri* can also be induced under stress, likely as part of a stress response. These results are consistent with the hypothesis that the *regA* was co-opted from an ancestral stress response gene (Nedelcu 2006, 2009).

Building on the original hypothesis of Nedelcu (2009), I propose the following mechanism for *regA* induction. The drastic changes in cell and chloroplast size at the end of embryogenesis result in imbalances in the ratio of membrane-bound pETC to stromal proteins or a redistribution of LEF and CEF components (including the possible formation of CEF supercomplexes promoted by FNR allocation). These imbalances generate a transient signal that induces *regA* expression as part of an acclimation-like response. In the wild-type strain, the functional RegA counteracts this initial imbalance via down-regulation of genes coding for chloroplast proteins, which changes the

composition of the chloroplast to adjust to the small cell size. As a result, light exposure following extended darkness does not act as a stressor on EVE somatic cells. In contrast, the dmAMN strain is RegA deficient and continues to express gonidial genes, failing to adopt an acclimated-like state in small cells; in this case, light following extended darkness results in an excess formation of ROS that initially induces *regA* expression (in an attempt to trigger an acclimation-like response) but the lack of a functional RegA protein culminates with the accumulation of damaging levels of ROS and the activation of PCD. Under standard growth conditions, cells in the dmAMN mutant are able to grow, which results in the rebalancing of their S:V ratio and the dissipation of the imbalance(s) associated with the initial small cell size.

3.4.8 *regA* evolved to deal with drastic changes in chloroplast size due to multiple fission

Since both *RLS1* and *regA* can be induced environmentally, I argue that the *RLS1*/*regA* ancestral gene was also regulated by the environment. Interestingly, *regA* can be induced only in small cells—either developmentally (at the end of embryogenesis in both EVE and dmAMN mutant) or environmentally (in the dmAMN mutant only). Thus, it is likely that the ancestral *regA* might have initially played a role in dealing with the drastic changes in chloroplast size due to multiple fission and its effect on photosynthesis. Under the selective pressure to increase the number of cells and flagella (which would increase fitness, see Chapter 1) and the constraint of multiple fission, the only available "solution" would have been a decrease in the size of the cells at the end of embryogenesis. However, such a decrease might have affected the redox status of the chloroplast, especially during

the first hours of light. Species that already possessed a good acclimation response might have been available to deal with this initial imbalance due to a decrease S:V ratio (which would later be counteracted by an increase in cell size as cells start to grow) and would have been selected for. With the evolution of terminally differentiated somatic cells in the larger volvocine species, *regA* could have been co-opted into "locking" the smallest cells into a permanent "acclimated" state to prevent them from further growing and reproducing.

3.4.9 *regA* as a cooperation gene

By the virtue of not reproducing, somatic cells in *V. carteri* express an altruistic behavior and *regA* confers this trait. The evolution of altruism is hard to explain as individuals are performing acts that decrease their individual fitness. As with other cooperative traits, selfish mutants that do not pay the cost of cooperation can emerge. The co-option of a vital function for altruistic behavior has been proposed to limit selfishness and promote cooperation (Foster et al. 2004; Nedelcu 2009). That is, cooperation is likely to be more stable if the cooperative gene shows antagonistic pleiotropy, since although mutations in these genes will provide the selfish mutants with immediate advantages in terms of reproduction, they will also have negative effects on other aspects of the cheaters' fitness. Here, I show for the first time antagonistic pleiotropy for *regA*, as although *regA*$^{-}$ mutants gain an advantage in fecundity (since all cells produce offspring), they show decreased viability. These findings provide additional support for the role of antagonistic pleiotropy in stabilizing cooperation, including the establishment of somatic cells in multicellular organisms.

Table 3.1 Gene-specific primer (GSP) for reverse transcription and qPCR primers (F, forward; R, reverse)

Region*	Primer sequences (5' to 3')	
rps18† (+225 to +362 bp)	F	TCGCGCTTACAAGATTCCG
	R	TGGTTGCGGATCTTCTTCAG
regA‡ (+1503 to +1603 bp)	GSP	CGACGCTCCTGTCGAGGC
	F	CAATGGCAGCAAATGGATGTC
	R	GTTCCAAATCAGGCAACACG

all oligonucleotides were provided by Sigma Genosys
*relative to cDNA position
†primers designed with IDT SciTools PrimerQuest program, IDT, Coralville, USA. Retrieved 12 December, 2012. http://www.idtdna.com/Scitools.
‡GSP from Stark et al. (2001); F & R from Nematollahi et al. (2006)

Table 3.2 Light and cell size influence the viability of dmAMN cells (Effect Test for data in Figure 3.9A–B)

Source	DF	F Ratio	Prob > F
(**A**) Effect of light intensity on cell death of small cells			
individual [technical replicate, biological replicate]	202	0.8521	0.9109
technical replicate [biological replicate]	6	0.53	0.7856
biological replicate	2	0.1527	0.8584
light intensity	3	64.1825	< 0.0001
(**B**) Effect of cell size and light on cell death			
individual [technical replicate, biological replicate]	242	0.9768	0.5801
technical replicate [biological replicate]	6	0.6134	0.7197
biological replicate	2	1.1391	0.3208
light	1	236.5805	< 0.0001
cell size	1	6.5005	0.011
light*cell size	1	31.7315	< 0.0001

Table 3.3 Phenotype and light affect viability of *V. carteri* cells

Source	DF	F Ratio	Prob > F
(**A**) Effect of light on cell death of EVE cells (effect test for data in Figure 3.12A)			
individual [technical replicate, biological replicate]	173	1.0685	0.3301
technical replicate [biological replicate]	6	0.0328	0.9998
biological replicate	2	0.0033	0.9967
light	1	3.7757	0.0536
(**B**) Effect of light and phenotype on cell death (effect test for data of small dmAMN cells and EVE in Figure 3.9B and 3.12A)			
individual [technical replicate, biological replicate]	194	1.0833	0.2419
technical replicate [biological replicate]	6	0.4671	0.8328
biological replicate	2	0.3563	0.7005
light	1	129.926	< 0.0001
phenotype	1	26.4331	< 0.0001
light*cell phenotype	1	120.9234	< 0.0001

Table 3.4 Summary of conditions for *regA* expression and PCD

Differences between wild type and *regA*$^-$/gonidialess are in red. Summary of results from (**A**) Chapter 2, Figure 2.6 and 2.8, and Kirk (1999), (**B**) Figure 3.4, 3.5 and 3.11, (**C**) Figure 3.9 and 3.12, and (**D**) Nedelcu (2006).

	wild type		***regA*$^-$/gonidialess**	
(**A**) Developmental cue				
cell size	small	large	small	
RegA protein	no	no	no	
regA expression	yes	no	yes	
(**B**) Environmental cue				
cell size	small	large	small	large
RegA protein	yes?	no	no	no
regA expression	no	no	yes	no
(**C**) PCD environmental cue				
cell size	small	large	small	large
RegA protein	yes?	no	no	no
PCD	no	no	yes	no*
(**D**) PCD heat shock				
cell size	small	large	small	large
RegA protein	yes	no	ND	ND
PCD	no	yes	ND	ND

*the cells counted as dead in the "large cell treatment" (Figure 3.9) are in fact small cells (Figure 3.10)

Table 3.5 Gonidial genes and putative targets of *regA* regulation (Tam and Kirk 1991a; Choi, Przybylska, and Straus 1996; Meissner et al. 1999)

cDNA clone	*C. reinhardtii* homolog	Protein encoded
G36	*LHCSR3*	in *C. reinhardtii* a low-CO2 inducible protein regulated by CCM1
G14*	*PSBO*	oxygen-evolving enhancer protein 1 (OEE1); subunit of oxygen evolving complex of photosystem II
G5*	*PSBQ*	oxygen evolving enhancer protein 3 (OEE3); subunit of oxygen evolving complex of photosystem II
G21	*PETO*	Cytochrome b_6f complex subunit V
G37*	*PETN*	Cytochrome b_6f complex subunit VIII
G9	*PETC*	Cytochrome b_6f complex Rieske iron-sulfur subunit (RISP)
G32	*PGR5*	in *C. reinhardtii* inducible by high light and likely a thylakoid membrane protein involved in cyclic electron flow, possibly as part of a ferredoxin-dependent quinone reduction pathway; a mutant of the homologue in *Arabidopsis thaliana* is deficient in NPQ, cyclic electron transport, and shows increased PSI photoinhibition; interacts with PGRL1
G8*	*LHCA4*	ortholog in *C. reinhardtii* shows synteny
G18*	*LHCA8*	
G12*	*LHCA9*	ortholog in *C. reinhardtii* shows synteny
G46*	*PSAN*	Photosystem I reaction centre subunit N, no known function, localized in the thylakoid lumen, extrinsic subunit at the lumen side, likely involved in the docking of plastocyanin
G40*	*PETH*	ferredoxin-$NADP^+$ reductase (FNR), involved in photosynthetic linear and cyclic, electron flow
G34	*ATPG*	ATPase CF_0-II, a subunit of the ATPase proton channel
G45	*ATPD*	ATPase CF_1-δ, a subunit of the stalk connecting CF_1 and CF_0
G23	*PGK*	phosphoglycerate kinase (PGK), enzyme of the Calvin cycle
G15	*RB60*	Protein disulfide isomerase (PDI) (Class: PDI-L2), the ortholog in *C. reinhardtii* is localized in the chloroplast and the endoplasmic reticulum, might regulate RuBisCO activity, might be involved in ROS signaling, is part of a complex involved in the control of *psbA* mRNA translation by light (encodes D1 protein of PSII), is potential thioredoxin target,
G30	*LCIC*	in *C. reinhardtii*, a low-CO2 inducible protein regulated by CCM1, predicted to be located in the chloroplast, part of CO_2 concentration mechanism, associated with pyrenoid
G1		unknown (thioredoxin?)

*confirmed gonidial genes expressed by a gonidialess/*regA*$^-$ mutant; remaining genes have not been determined (Tam and Kirk 1991b)

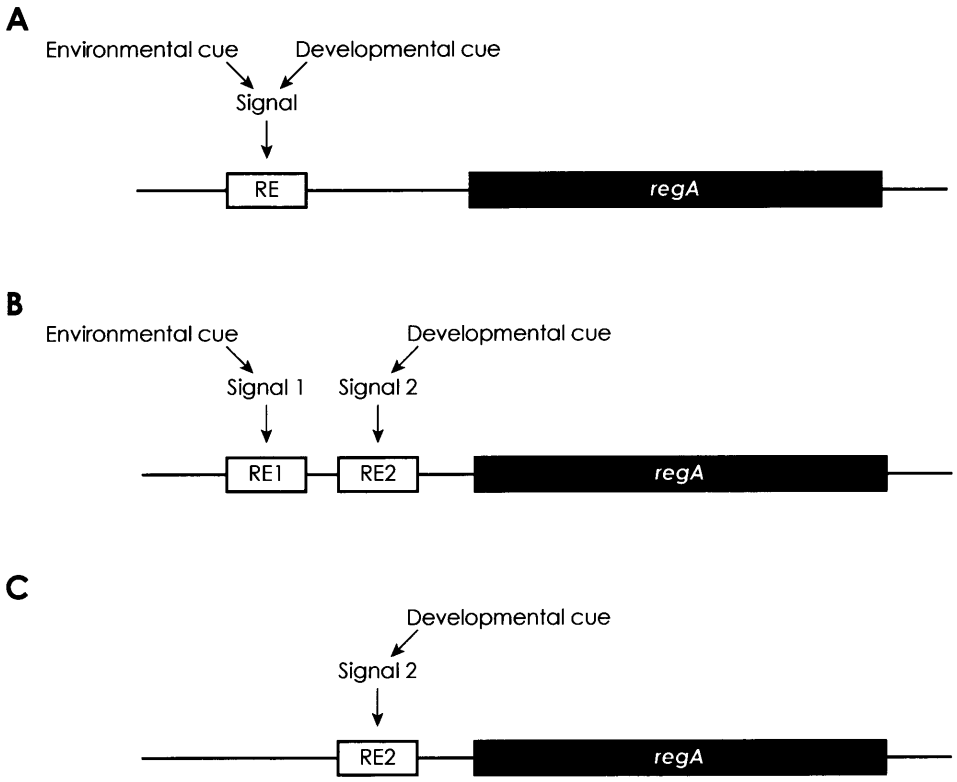

Figure 3.1 Different models for the evolution of *regA* regulation.

Three different models (and their predictions) for the evolution of *regA* via changes in the regulation of an ancestral environmentally-induced *RLS1*/*regA*-like gene. (**A**) Model: no new regulatory elements evolved; rather, the same ancestral environmentally-induced signaling pathway was also induced during development in multicellular volvocine algae (prediction: *regA* can be induced both environmentally and developmentally by the same signal). (**B**) Model: In addition to the environmentally-induced regulation, a new layer of regulation evolved as part of a new (developmentally-induced) signaling pathway (prediction: both environmental and developmental cues can induce *regA* expression acting via distinct signaling pathways and REs). (**C**) Model: New regulatory elements evolved and the ancestral regulation was replaced or lost. Prediction: *regA* can only be induced by a developmental cue via a signaling pathway and regulatory element unrelated to the ancestral environmental regulation.

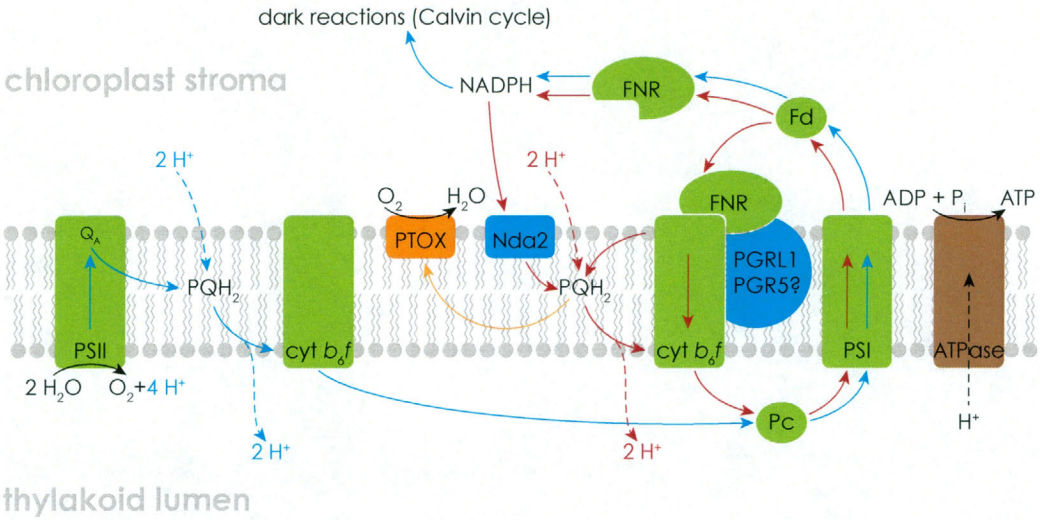

Figure 3.2 Linear electron flow (LEF, blue solid arrows) and cyclic electron flow (CEF, red solid arrows) in the photosynthetic electron transport chain and chlororespiration (orange solid arrow); adapted from Joliot and Johnson (2011), and Peltier et al. (2010).

Protons transferred during the LEF are in blue (dashed blue arrows); protons transferred as part of the CEF are in red (dashed red arrows). PS, photosystem; cyt *b6f*: cytochrome *b6f* complex; Pc, plastocyanin; Fd, ferredoxin; FNR, ferredoxin $NADP^+$ reductase; PQH_2, plastoquinol; PTOX, plastid terminal oxidase; Nda2, type II NAD(P)H dehydrogenase.

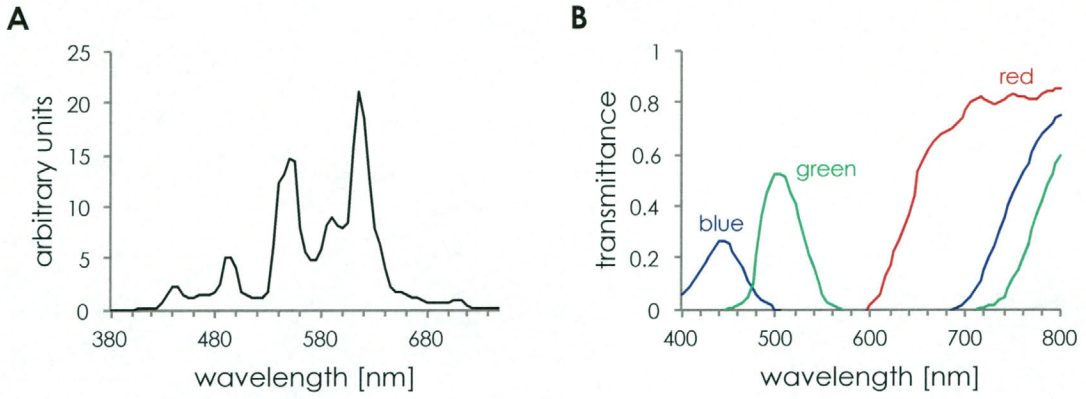

Figure 3.3 (A) Cool white light spectrum and (B) transmittance of red, green or blue filter (#027, 735, and 071 respectively, LEE Filters).

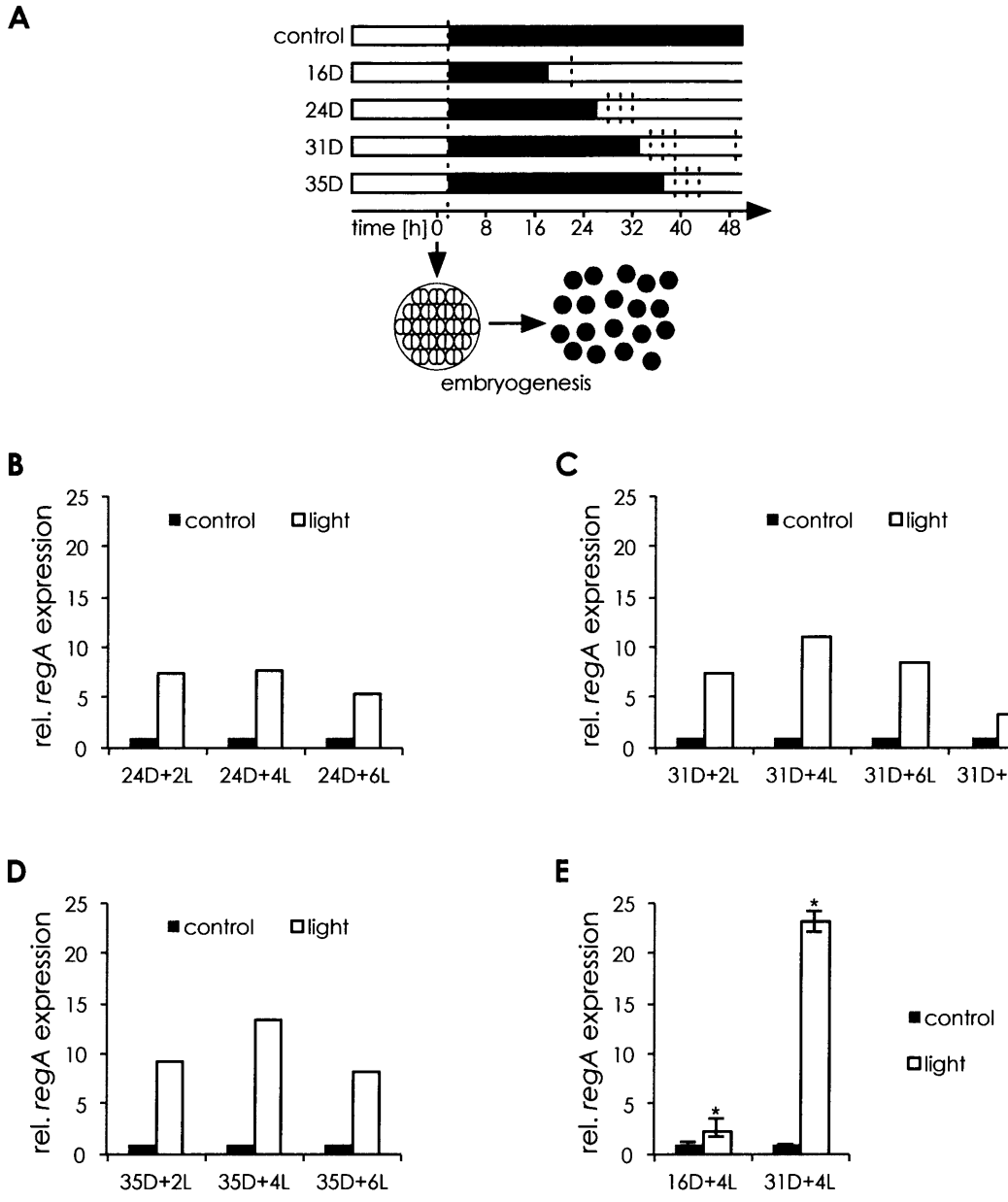

Figure 3.4 In small dmAMN cells, *regA* expression is induced by light after extended periods of darkness.

(**A**) dmAMN cultures were first grown in a standard 16L:8D light regime. After the onset of embryogenesis (time point 0 h) and at the end of the first light period (time point 2 h, red dashed line), cultures were switched to continuous darkness (control), or kept for 16, 24, 31 or 35 h in darkness and then treated with light. White bars, light periods; black bars, dark periods; black dashed lines, time points of collecting samples for RNA extraction; red dashed line, time point 2 h; D, hours of dark; L, hours of light. (**B–E**) *regA* transcript levels of light-treated samples measured by RT-qPCR. Levels are given relative to dark control samples from the same time point (dark control level = 1). (**B–D**) Three independent initial experiments ($n = 1$) show the relative *regA* transcript levels after 2, 4, 6, or 16 h of light after (**B**) 24, (**C**) 31, or (**D**) 35 h of darkness. (**E**) Comparison of 4 h light treatment after 16 or 31 h of darkness ($n = 3$, bars indicate SE; randomization test, $*p < 0.05$). Note: differences in relative expression levels for the same treatment among different experiments are simply due to expected biological variation among experiments; nevertheless, the trends are always consistent.

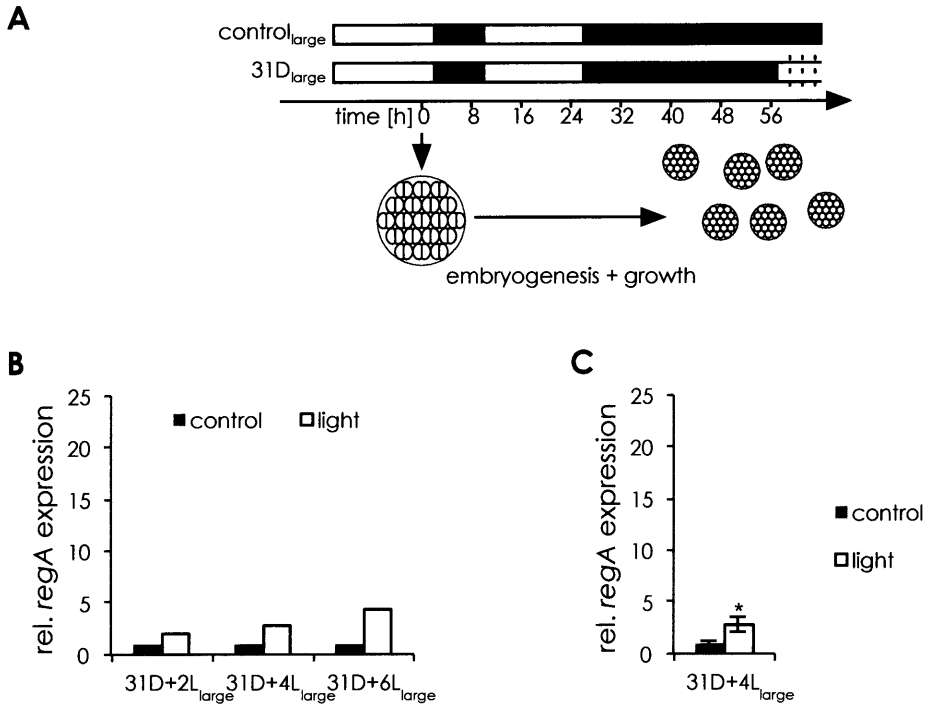

Figure 3.5 In large dmAMN cells, light only weakly induces *regA* expression.

(**A**) dmAMN cultures were first grown in the standard 16L:8D light regime until the end of the first light period after embryogenesis (time point 26 h); during this time cells grew from ca. 4 µm to ca. 8 µm. Cultures were then switched to continuous darkness ($control_{large}$) or kept for 31 h in darkness followed by light treatment ($31D_{large}$). White bars, light periods; black bars, dark periods; dashed lines, time points of samples; D, hours of dark; L, hours of light. (**B–C**) *regA* transcript levels (measured by RT-qPCR) of light-treated samples relative to dark control of the same time point (dark control level = 1). (**B**) In an initial experiment ($n = 1$), cultures were treated for 2, 4, or 6 h with light after 31 h of darkness. (**C**) Follow-up experiment in triplicates; samples treated with light for 4 h after 31 h of darkness ($n = 3$, bars indicate SE; randomization test, $*p < 0.05$).

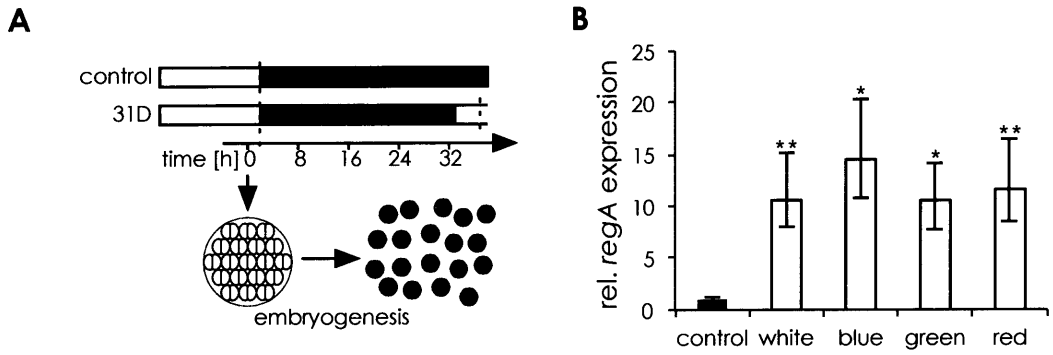

Figure 3.6 Light quality does not affect the level of *regA* induction in dmAMN.

(**A**) dmAMN cultures were first grown in a standard 16L:8D light regime. After the onset of embryogenesis (time point 0 h) and at the end of the current light period (time point 2 h, red dashed vertical line), cultures were switched to continuous darkness (control), or kept for 31 h in darkness and then treated with 4 h of light (31D). White bars, light periods; black bars, dark periods; black dashed line, time point of samples; red dashed line, time point 2 h; D, hours of dark; L, hours of light. (**B**) *regA* transcript levels measured in RT-qPCR of light-treated samples relative to dark control of the same time point (dark control level = 1, $n = 3$, bars indicate SE; randomization test, $*p < 0.05$; $**p < 0.01$) using different light qualities (red, green or blue light at 5 µmol photons m^{-2} s^{-1} or standard white light at 260 µmol photons m^{-2} s^{-1}).

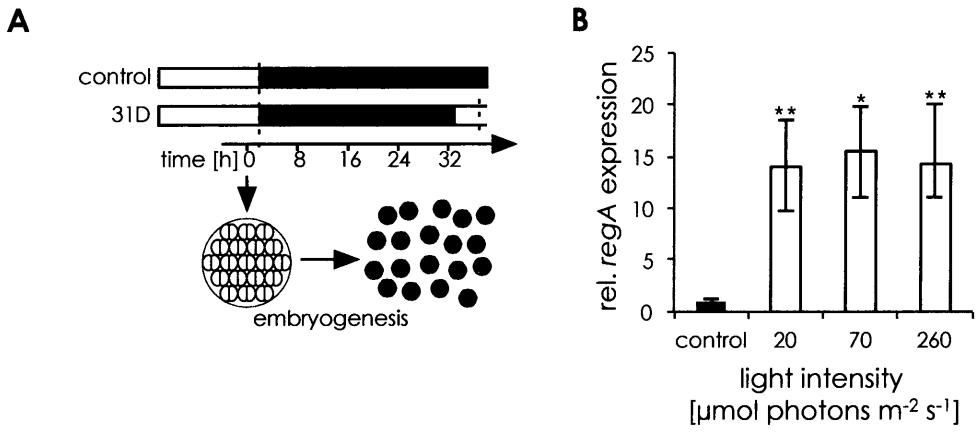

Figure 3.7 Light intensity does not influence *regA* expression levels.

(**A**) dmAMN cultures were first grown in a standard 16L:8D light regime. After the onset of embryogenesis (time point 0 h) and at the end of the current light period (time point 2 h, red dashed line), cultures were switched to continuous darkness (control), or kept for 31 h in darkness and then treated with 4 h of light (31D). White bars, light periods; black bars, dark periods; black dashed line, time point of samples; D, hours of dark; L, hours of light. (**B**) *regA* transcript levels measured in RT-qPCR of light-treated samples relative to dark control of the same time point (dark control level = 1, $n = 3$, bars indicate SE; randomization test, $*p < 0.05$; $**p < 0.01$) using different light intensities (white light of 20, 70, or standard 260 µmol photons m^{-2} s^{-1} intensity).

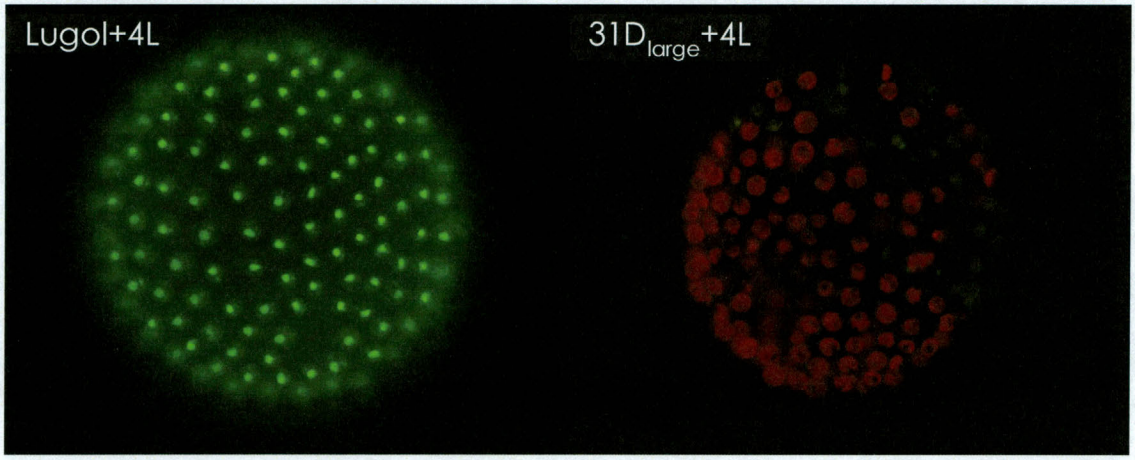

Figure 3.8 SYTOX Green staining of large dmAMN cells.

dmAMN cultures were first grown in the standard 16L:8D light regime up to and including the first light period after embryogenesis, and exposed to 4 h of light after cells were either killed with Lugol's solution (as a positive control; **Lugol+4L**), or kept in darkness for 31 h (**$31D_{large}$+4L**). Green, dead cells stained with SYTOX Green (binds nucleic acids); red, living cells (chlorophyll fluorescence).

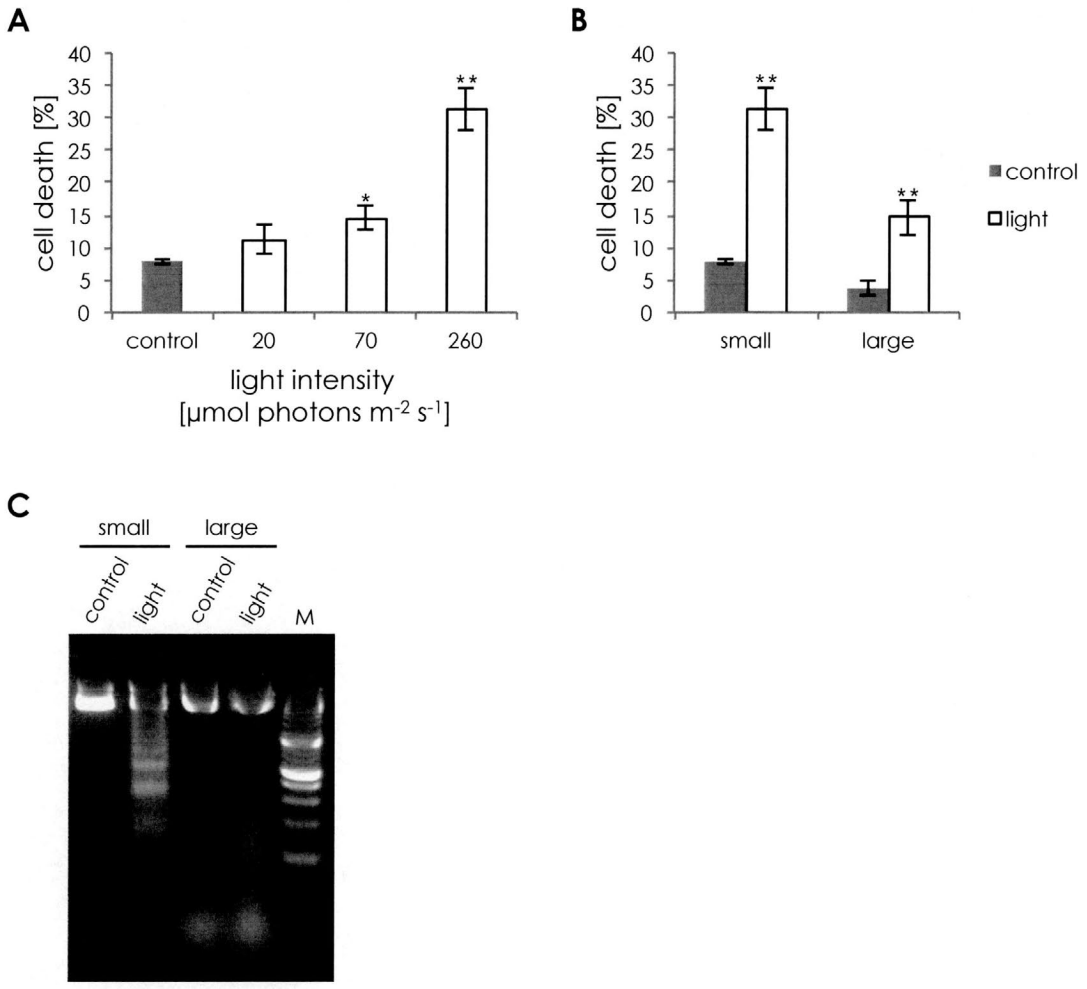

Figure 3.9 After 31 h of darkness, light causes higher levels of PCD in small than in large dmAMN cells.

After the onset of embryogenesis, dmAMN cultures were either switched to continuous darkness at the end of the first light period (small cells), or first grown until the end of the second daylight period (large cells) before being placed in continuous darkness or 31 h of darkness followed by 4 h of light. (**A–B**) Samples were treated with SYTOX Green to stain dead cells. Live and dead cells of one hemisphere of each individual were counted and percent cell death per individual calculated ($n = 3$; 3 technical replicates with ≥ 20 individuals each; bars indicate SE). (**A**) Small cells were exposed to 20, 70, or 260 µmol photons m^{-2} s^{-1} light intensity (Tukey HSD, $*p < 0.01$; $**p < 0.001$); (**B**) Comparison of small and large cells exposed to 260 µmol photons m^{-2} s^{-1} light intensity (2-sample *t*-test, $**p < 0.001$). (**C**) gDNA was isolated from samples of one biological replicate of (**B**). small = small cells; large = large cells; control = dark control; light = light-treated; M = DNA marker.

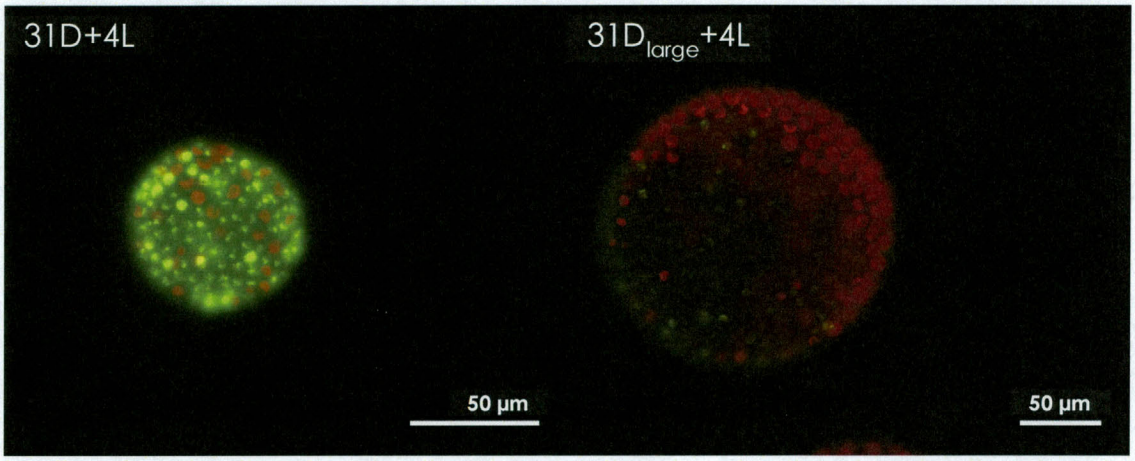

Figure 3.10 Only small cells enter PCD after 31 h of darkness followed by 4 h of light.

After the onset of embryogenesis, dmAMN cultures were either switched to continuous darkness at the end of the first light period (small cells, **31D+4L**), or first grown until the end of the second daylight period (large cells, **31D$_{large}$+4L**) before being placed in continuous darkness or 31 h of darkness followed 4 h (light intensity of 260 µmol photons m^{-2} s^{-1}). Samples were treated with SYTOX Green to stain dead cells. Green, dead cells stained with SYTOX Green (binds nucleic acids); red, living cells (chlorophyll fluorescence).

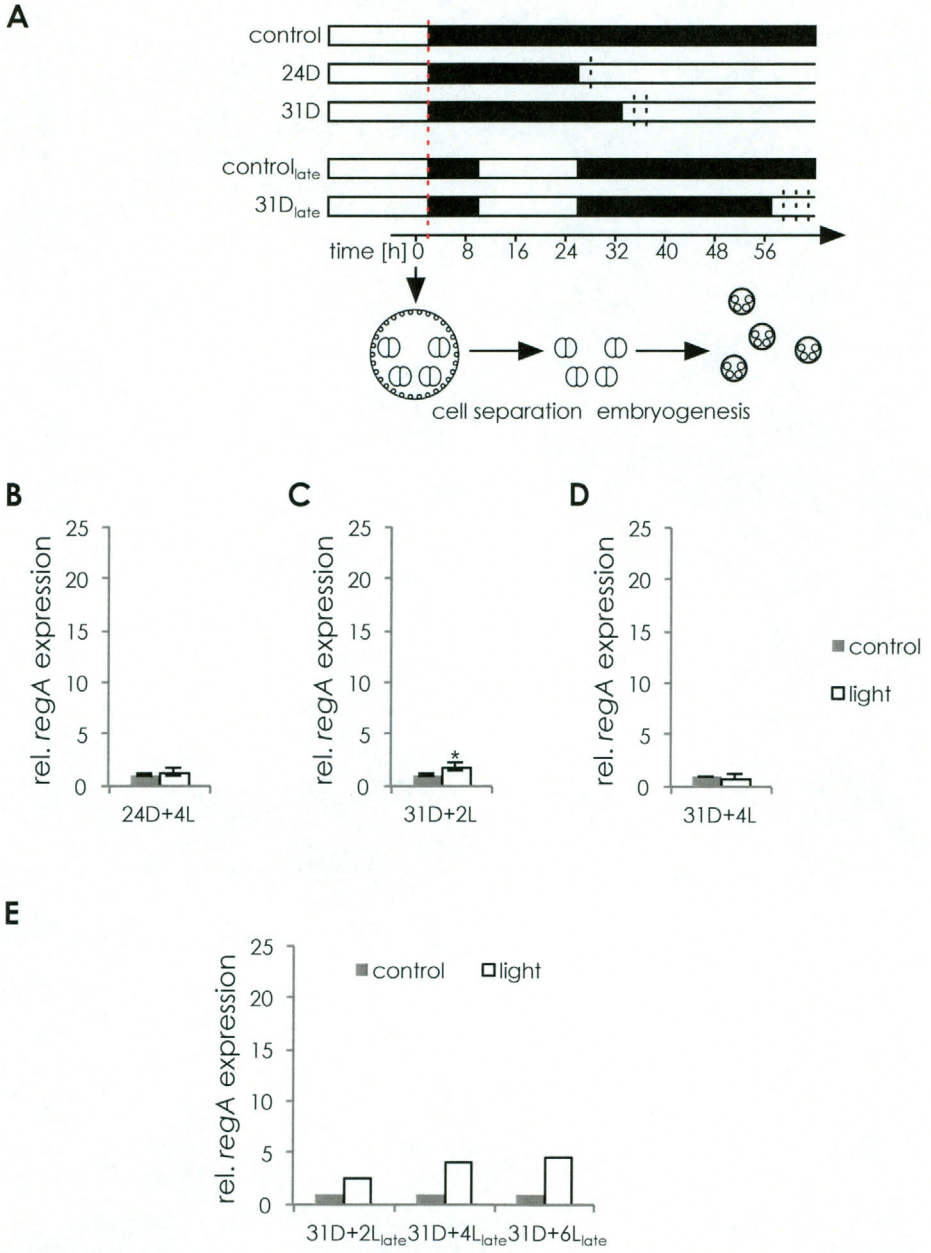

Figure 3.11 In EVE, *regA* is only slightly induced by light after extended period of darkness.

(**A**) EVE was first grown in a standard 16L:8D light regime. After the onset of embryogenesis (time point 0 h), parental somatic cells were removed and embryos were switched to continuous darkness at the end of either the first light period (time point 2 h, control, for early juveniles) or the second light period (time point 26 h, control$_{late}$, for late juveniles); after 24–31 h in darkness, cultures were then exposed to 2–6 h of light. White bars, light periods; black bars, dark periods; dashed vertical lines, time points of samples; D, hours of dark; L, hours of light. (**B**–**E**) *regA* transcript levels (measured using RT-qPCR) of light-treated samples relative to dark control of the same time point (dark control level = 1; **B**–**D**, $n = 3$, bars indicate SE; randomization test, $*p < 0.05$; **E**, $n = 1$); (**B**) light induction for 4 h after 24h of dark; (**C**) light induction for 2 h after 31 h of dark; (**D**) light induction for 4 h after 31 h of dark; (**E**) late juveniles exposed to 2–6 h of light after 31 h of darkness.

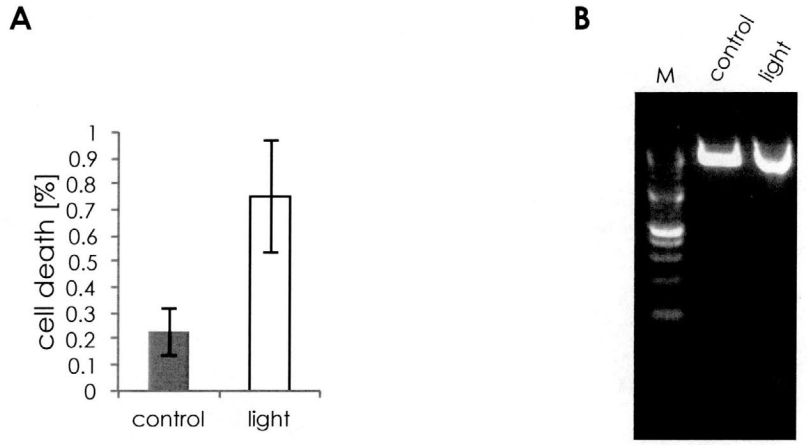

Figure 3.12 Light after extended darkness does not cause detectable levels of PCD in EVE.

EVE cultures were first grown in a standard 16L:8D light regime. After the onset of embryogenesis (time point 0 h) and at the end of the current light period (time point 2 h), cultures of isolated embryos were switched to continuous darkness as dark control or after 31 h of darkness exposed to 4 h of light. (**A**) Samples were treated with SYTOX Green to stain dead cells. Life and dead somatic cells of one hemisphere of each individual were counted ($n = 3$; 3 technical replicates with ≥ 20 individuals each; bars indicate SE). (**B**) gDNA isolated from one biological replicate of (**A**). control = dark control; light = light-treated; M = DNA marker.

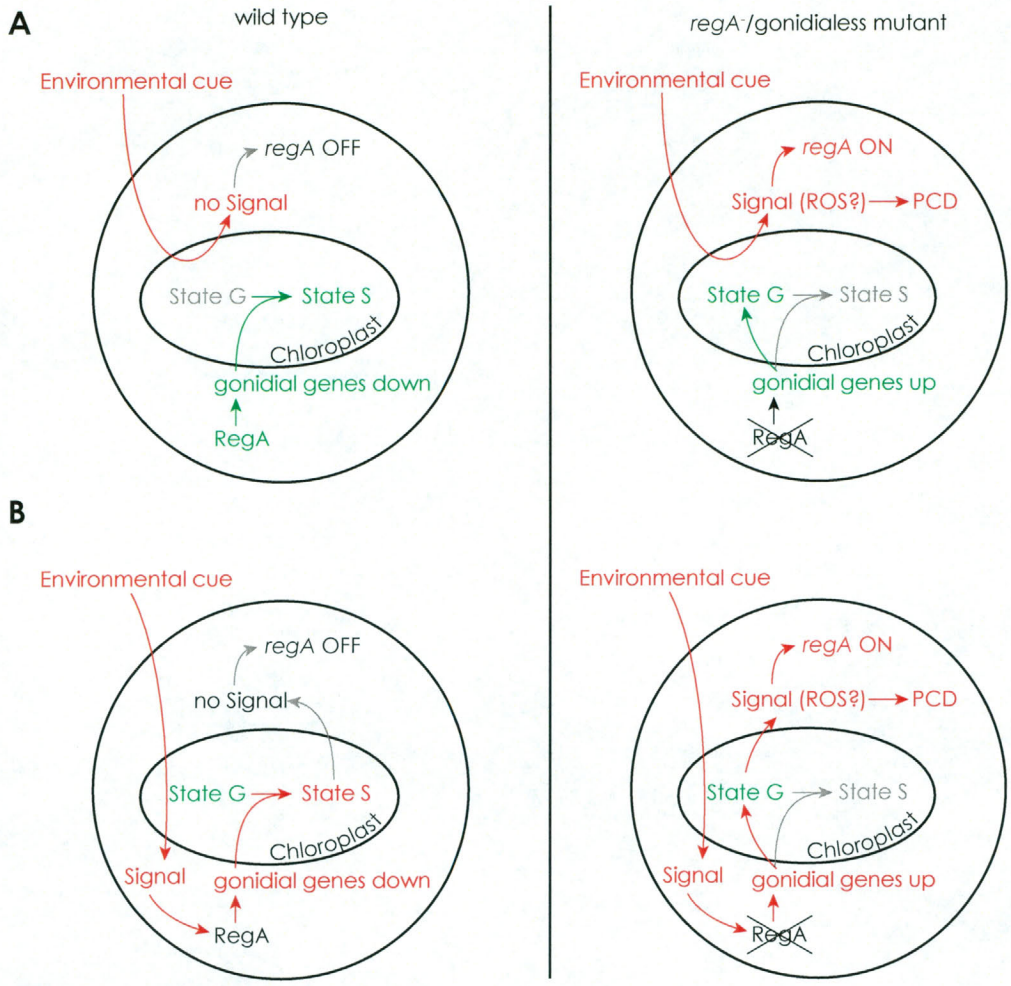

Figure 3.13 Two different models for the role of RegA in stress resistance, with RegA either in a (A) preventative or (B) responsive role.

(**A**) During extended darkness in wild type somatic cells, the RegA protein represses gonidial genes, which encode chloroplast proteins. As a result, the chloroplast composition changes from the inherited state (from the parental gonidium, State G) to a state specific to somatic cells (State S). In contrast, dmAMN does not contain a functional RegA protein, and the chloroplast is maintained in State G. The environmental cue does only elicit a signal in the dmAMN chloroplast, which results in *regA* induction and ultimately PCD; in the wild type, the preventive action of RegA averts the induction of such signal. (**B**) In wild type, the environmental cue activates RegA (maybe by post-transcriptional or post-translational regulation) and initiates the change of the chloroplast to State S. In contrast, in dmAMN no functional RegA is present, the chloroplast remains in State G and a secondary signal is triggered initiating *regA* induction and ultimately PCD. State G, chloroplast in gonidial state; State S, chloroplast in somatic state. (See main text for further information.)

3.5 References

Adams CR, Stamer KA, Miller JK, McNally JG, Kirk MM, Kirk DL. 1990. Patterns of organellar and nuclear inheritance among progeny of two geographically isolated strains of *Volvox carteri*. Curr Genet 18:141–153.

Alizadeh D, Cohen A. 2010. Red light and calmodulin regulate the expression of the *psbA* binding protein genes in *Chlamydomonas reinhardtii*. Plant Cell Physiol 51:312–322.

Alric J. 2010. Cyclic electron flow around photosystem I in unicellular green algae. Photosyn Res 106:47–56.

Bagnoli F, Danti S, Magherini V, Cozza R, Innocenti AM, Racchi ML. 2004. Molecular cloning, characterisation and expression of two catalase genes from peach. Functional Plant Biol. 31:349.

Beel B, Prager K, Spexard M, Sasso S, Weiss D, Müller N, Heinnickel M, Dewez D, Ikoma D, Grossman AR, et al. 2012. A flavin binding cryptochrome photoreceptor responds to both blue and red light in *Chlamydomonas reinhardtii*. Plant Cell 24:2992–3008.

Berthold P, Tsunoda SP, Ernst OP, Mages W, Gradmann D, Hegemann P. 2008. Channelrhodopsin-1 initiates phototaxis and photophobic responses in *Chlamydomonas* by immediate light-induced depolarization. Plant Cell 20:1665–1677.

Bottomley MJ, Collard MW, Huggenvik JI, Liu Z, Gibson TJ, Sattler M. 2001. The SAND domain structure defines a novel DNA-binding fold in transcriptional regulation. Nat Struct Biol 8:626–633.

Brody JR, Kern SE. 2004. Sodium boric acid: a Tris-free, cooler conductive medium for DNA electrophoresis. BioTechniques 36:214–216.

Carles CC, Fletcher JC. 2010. Missing links between histones and RNA Pol II arising from SAND? Epigenetics 5:381–385.

Carroll SB. 2000. Endless forms: the evolution of gene regulation and morphological diversity. Cell 101:577–580.

Carroll SB. 2008. Evo-devo and an expanding evolutionary synthesis: a genetic theory of morphological evolution. Cell 134:25–36.

Chen RE, Thorner J. 2007. Function and regulation in MAPK signaling pathways: lessons learned from the yeast *Saccharomyces cerevisiae*. Biochim Biophys Acta 1773:1311–1340.

Choi G, Przybylska M, Straus D. 1996. Three abundant germ line-specific transcripts in *Volvox carteri* encode photosynthetic proteins. Curr Genet 30:347–355.

Cinalli RM, Rangan P, Lehmann R. 2008. Germ cells are forever. Cell 132:559–562.

Coleman AW, Maguire MJ. 1982. A microspectrofluorometric analysis of nuclear and chloroplast DNA in *Volvox*. Dev Biol 94:441–450.

DalCorso G, Pesaresi P, Masiero S, Aseeva E, Schünemann D, Finazzi G, Joliot P, Barbato R, Leister D. 2008. A complex containing PGRL1 and PGR5 is involved in the switch between linear and cyclic electron flow in *Arabidopsis*. Cell 132:273–285.

Danon A, Coll NS, Apel K. 2006. Cryptochrome-1-dependent execution of programmed cell death induced by singlet oxygen in *Arabidopsis thaliana*. PNAS 103:17036–17041.

Duncan L, Nishii I, Harryman A, Buckley S, Howard A, Friedman NR, Miller SM. 2007. The *VARL* gene family and the evolutionary origins of the master cell-type regulatory gene, *regA*, in *Volvox carteri*. J Mol Evol 65:1–11.

Duncan L, Nishii I, Howard A, Kirk DL, Miller SM. 2006. Orthologs and paralogs of *regA*, a master cell-type regulatory gene in *Volvox carteri*. Curr Genet 50:61–72.

Ebnet E, Fischer M, Deininger W, Hegemann P. 1999. Volvoxrhodopsin, a light-regulated sensory photoreceptor of the spheroidal green alga *Volvox carteri*. Plant Cell 11:1473–1484.

Feng X, Zilberman D, Dickinson H. 2013. A Conversation across Generations: Soma-Germ Cell Crosstalk in Plants. Developmental Cell 24:215–225.

Forti G, Furia A, Bombelli P, Finazzi G. 2003. In vivo changes of the oxidation-reduction state of NADP and of the ATP/ADP cellular ratio linked to the photosynthetic activity in *Chlamydomonas reinhardtii*. Plant Physiol 132:1464–1474.

Foster KR, Shaulsky G, Strassmann JE, Queller DC, Thompson CRL. 2004. Pleiotropy as a mechanism to stabilize cooperation. Nature 431:693–696.

Giannino D, Condello E, Bruno L, Testone G, Tartarini A, Cozza R, Innocenti AM, Bitonti MB, Mariotti D. 2004. The gene geranylgeranyl reductase of peach (*Prunus persica* [L.] Batsch) is regulated during leaf development and responds differentially to distinct stress factors. J Exp Bot 55:2063–2073.

Goda SK, Minton NP. 1995. A simple procedure for gel electrophoresis and northern blotting of RNA. Nucleic Acids Res 23:3357–3358.

Golding AJ, Finazzi G, Johnson GN. 2004. Reduction of the thylakoid electron transport chain by stromal reductants—evidence for activation of cyclic electron transport upon dark adaptation or under drought. Planta 220:356–363.

Grossman AR, Lohr M, Im CS. 2004. *Chlamydomonas reinhardtii* in the landscape of pigments. Annu Rev Genet 38:119–173.

Hanschen ER, Ferris PJ, Michod RE. 2014. Early evolution of the genetic basis for soma in the Volvocaceae. Evolution.

Hertle AP, Blunder T, Wunder T, Pesaresi P, Pribil M, Armbruster U, Leister D. 2013. PGRL1 is the elusive ferredoxin-plastoquinone reductase in photosynthetic cyclic electron flow. Mol Cell 49:511–523.

Hoekstra HE, Coyne JA. 2007. The locus of evolution: evo devo and the genetics of adaptation. Evolution 61:995–1016.

Houille-Vernes L, Rappaport F, Wollman F-A, Alric J, Johnson X. 2011. Plastid terminal oxidase 2 (PTOX2) is the major oxidase involved in chlororespiration in *Chlamydomonas*. PNAS 108:20820–20825.

Im CS, Eberhard S, Huang K, Beck CF, Grossman AR. 2006. Phototropin involvement in the expression of genes encoding chlorophyll and carotenoid biosynthesis enzymes and LHC apoproteins in *Chlamydomonas reinhardtii*. Plant J 48:1–16.

Iwai M, Takizawa K, Tokutsu R, Okamuro A, Takahashi Y, Minagawa J. 2010. Isolation of the elusive supercomplex that drives cyclic electron flow in photosynthesis. Nature 464:1210–1213.

Jain N, Iyer KV, Kumar A, Shivashankar GV. 2013. Cell geometric constraints induce modular gene-expression patterns via redistribution of HDAC3 regulated by actomyosin contractility. PNAS 110:11349–11354.

Jans F, Mignolet E, Houyoux P-A, Cardol P, Ghysels B, Cuiné S, Cournac L, Peltier G, Remacle C, Franck F. 2008. A type II NAD(P)H dehydrogenase mediates light-independent plastoquinone reduction in the chloroplast of *Chlamydomonas*. PNAS 105:20546–20551.

Johnson X, Alric J. 2012. Interaction between starch breakdown, acetate assimilation, and photosynthetic cyclic electron flow in *Chlamydomonas reinhardtii*. J Biol Chem 287:26445–26452.

Joliot P, Johnson GN. 2011. Regulation of cyclic and linear electron flow in higher plants. PNAS 108:13317–13322.

Jorgensen P, Edgington NP, Schneider BL, Rupes I, Tyers M, Futcher B. 2007. The size of the nucleus increases as yeast cells grow. Mol Biol Cell 18:3523–3532.

Kianianmomeni A, Hallmann A. 2014. Algal photoreceptors: *in vivo* functions and potential applications. Planta 239:1–26.

Kianianmomeni A, Stehfest K, Nematollahi G, Hegemann P, Hallmann A. 2009. Channelrhodopsins of *Volvox carteri* Are Photochromic Proteins That Are Specifically Expressed in Somatic Cells under Control of Light, Temperature, and the Sex Inducer. Plant Physiol 151:347–366.

Kirk DL, Harper JF. 1986. Genetic, biochemical, and molecular approaches to *Volvox* development and evolution. Int. Rev. Cytol. 99:217–293.

Kirk DL, Kirk MM. 1983. Protein synthetic patterns during the asexual life cycle of *Volvox carteri*. Dev Biol 96:493–506.

Kirk DL. 1998. *Volvox*: the molecular genetic origins of multicellularity and cellular differentiation. Cambridge.

Kirk MM, Kirk DL. 1985. Translational regulation of protein synthesis, in response to light, at a critical stage of *Volvox* development. Cell 41:419–428.

Kirk MM, Stark K, Miller SM, Müller W, Taillon BE, Gruber H, Schmitt R, Kirk DL. 1999. *regA*, a *Volvox* gene that plays a central role in germ-soma differentiation, encodes a novel regulatory protein. Development 126:639–647.

Krieger-Liszkay A, Fufezan C, Trebst A. 2008. Singlet oxygen production in photosystem II and related protection mechanism. Photosyn Res 98:551–564.

Marguerat S, Bähler J. 2012. Coordinating genome expression with cell size. Trends Genet 28:560–565.

Meissner M, Stark K, Cresnar B, Kirk DL, Schmitt R. 1999. *Volvox* germline-specific genes that are putative targets of RegA repression encode chloroplast proteins. Curr Genet 36:363–370.

Mubarakshina M, Khorobrykh S, Ivanov B. 2006. Oxygen reduction in chloroplast thylakoids results in production of hydrogen peroxide inside the membrane. Biochim Biophys Acta 1757:1496–1503.

Mullineaux PM, Baker NR. 2010. Oxidative stress: antagonistic signaling for acclimation or cell death? Plant Physiol 154:521–525.

Nandha B, Finazzi G, Joliot P, Hald S, Johnson GN. 2007. The role of PGR5 in the redox poising of photosynthetic electron transport. Biochim Biophys Acta 1767:1252–1259.

Nedelcu AM, Michod RE. 2006. The evolutionary origin of an altruistic gene. Mol Biol Evol 23:1460–1464.

Nedelcu AM. 2005. Sex as a response to oxidative stress: stress genes co-opted for sex. Proc Biol Sci 272:1935–1940.

Nedelcu AM. 2006. Evidence for p53-like-mediated stress responses in green algae. FEBS Lett 580:3013–3017.

Nedelcu AM. 2009. Environmentally induced responses co-opted for reproductive altruism. Biol. Lett. 5:805–808.

Nematollahi G, Kianianmomeni A, Hallmann A. 2006. Quantitative analysis of cell-type specific gene expression in the green alga *Volvox carteri*. BMC Genomics 7:321.

Neumann FR, Nurse P. 2007. Nuclear size control in fission yeast. J Cell Biol 179:593–600.

Ohta T. 2003. Evolution by gene duplication revisited: differentiation of regulatory elements versus proteins. Genetica 118:209–216.

Ozawa S-I, Nield J, Terao A, Stauber EJ, Hippler M, Koike H, Rochaix J-D, Takahashi Y. 2009. Biochemical and structural studies of the large Ycf4-photosystem I assembly complex of the green alga *Chlamydomonas reinhardtii*. Plant Cell 21:2424–2442.

Peltier G, Tolleter D, Billon E, Cournac L. 2010. Auxiliary electron transport pathways in chloroplasts of microalgae. Photosyn Res 106:19–31.

Pfannschmidt T, Brautigam K, Wagner R, Dietzel L, Schroter Y, Steiner S, Nykytenko A. 2009. Potential regulation of gene expression in photosynthetic cells by redox and energy state: approaches towards better understanding. Ann. Bot. 103:599–607.

Pfannschmidt T, Yang C. 2012. The hidden function of photosynthesis: a sensing system for environmental conditions that regulates plant acclimation responses. Protoplasma 249 Suppl 2:S125–36.

Prochnik SE, Umen JG, Nedelcu AM, Hallmann A, Miller SM, Nishii I, Ferris P, Kuo A, Mitros T, Fritz-Laylin LK, et al. 2010. Genomic analysis of organismal complexity in the multicellular green alga *Volvox carteri*. Science 329:223–226.

Ramakers C, Ruijter JM, Lekanne Deprez RH, Moorman AFM. 2003. Assumption-free analysis of quantitative real-time polymerase chain reaction (PCR) data. Neurosci Lett 339:62–66.

Reape TJ, Molony EM, McCabe PF. 2008. Programmed cell death in plants: distinguishing between different modes. J Exp Bot 59:435–444.

Ríos-Barrera LD, Riesgo-Escovar JR. 2013. Regulating cell morphogenesis: the *Drosophila* Jun N-terminal kinase pathway. Genesis 51:147–162.

Ruijter JM, Ramakers C, Hoogaars WMH, Karlen Y, Bakker O, van den Hoff MJB, Moorman AFM. 2009. Amplification efficiency: linking baseline and bias in the analysis of quantitative PCR data. Nucleic Acids Res 37:e45.

Rumeau D, Peltier G, Cournac L. 2007. Chlororespiration and cyclic electron flow around PSI during photosynthesis and plant stress response. Plant Cell Environ 30:1041–1051.

Saito H. 2010. Regulation of cross-talk in yeast MAPK signaling pathways. Curr Opin Microbiol 13:677–683.

Sakaguchi H, Iwasa K. 1979. 2 Photophobic Responses in *Volvox carteri*. Plant Cell Physiol 20:909–916.

Sambrook J, Russel DW. 2001. Molecular cloning: A laboratory manual. 3rd ed.

Sato M, Murata Y, Mizusawa M, Iwahashi H, Oka S. 2004. A simple and rapid dual-fluorescence viability assay for microalgae. Microbiol Cult Coll 20:53–59.

Schaller GE, Shiu S-H, Armitage JP. 2011. Two-component systems and their co-option for eukaryotic signal transduction. Curr Biol 21:R320–30.

Scheibe R, Backhausen JE, Emmerlich V, Holtgrefe S. 2005. Strategies to maintain redox homeostasis during photosynthesis under changing conditions. J Exp Bot 56:1481–1489.

Schletz K. 1976. Phototaxis bei *Volvox*. Pigmentsysteme der Lichtrichtungsperzeption. Z Pflanzenphysiol 77:189–211.

Stapley J, Reger J, Feulner PGD, Smadja C, Galindo J, Ekblom R, Bennison C, Ball AD, Beckerman AP, Slate J. 2010. Adaptation genomics: the next generation. Trends Ecol. Evol. (Amst.) 25:705–712.

Stark K, Kirk DL, Schmitt R. 2001. Two enhancers and one silencer located in the introns of *regA* control somatic cell differentiation in *Volvox carteri*. Genes Dev 15:1449–1460.

Suzuki N, Koussevitzky S, Mittler R, Miller G. 2012. ROS and redox signalling in the response of plants to abiotic stress. Plant Cell Environ 35:259–270.

Suzuki T, Yamasaki K, Fujita S, Oda K, Iseki M, Yoshida K, Watanabe M, Daiyasu H, Toh H, Asamizu E, et al. 2003. Archaeal-type rhodopsins in *Chlamydomonas*: model structure and intracellular localization. Biochem Biophys Res Commun 301:711–717.

Takahashi H, Clowez S, Wollman F-A, Vallon O, Rappaport F. 2013. Cyclic electron flow is redox-controlled but independent of state transition. Nat Commun 4:1954.

Tam L-W, Kirk DL. 1991a. Identification of cell-type-specific genes of *Volvox carteri* and characterization of their expression during the asexual life cycle. Dev Biol 145:51–66.

Tam L-W, Kirk DL. 1991b. The program for cellular differentiation in *Volvox carteri* as revealed by molecular analysis of development in a gonidialess/somatic regenerator mutant. Development 112:571–580.

True JR, Carroll SB. 2002. Gene co-option in physiological and morphological evolution. Annu Rev Cell Dev Biol 18:53–80.

Umen JG. 2005. The elusive sizer. Curr Opin Cell Biol 17:435–441.

Voronina E, Seydoux G, Sassone-Corsi P, Nagamori I. 2011. RNA granules in germ cells. Cold Spring Harb Perspect Biol 3.

Wittkopp PJ, Kalay G. 2012. *Cis*-regulatory elements: molecular mechanisms and evolutionary processes underlying divergence. Nat Rev Genet 13:59–69.

Wu C-Y, Rolfe PA, Gifford DK, Fink GR. 2010. Control of transcription by cell size. PLoS Biol 8:e1000523.

Wykoff DD, Davies JP, Melis A, Grossman AR. 1998. The regulation of photosynthetic electron transport during nutrient deprivation in *Chlamydomonas reinhardtii*. Plant Physiol 117:129–139.

Yang W-C, Shi D-Q, Chen Y-H. 2010. Female gametophyte development in flowering plants. Annu Rev Plant Biol 61:89–108.

Zorin B, Lu Y, Sizova I, Hegemann P. 2009. Nuclear gene targeting in *Chlamydomonas* as exemplified by disruption of the PHOT gene. Gene 432:91–96.

3.6 Appendix

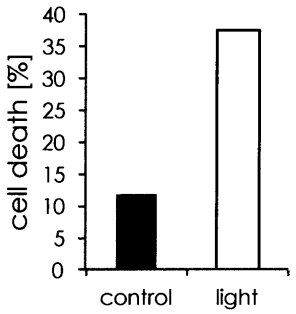

Figure 3.14 Light after extended darkness causes cell death in UTEX1877 at levels similar to dmAMN.

UTEX1877 cultures were first grown in a standard 16L:8D light regime. After the onset of embryogenesis (time point 0 h) and at the end of the current light period (time point 2 h), cultures of isolated embryos were switched to continuous darkness as dark control or after 31 h of darkness exposed to 4 h of light. Samples were treated with SYTOX Green to stain dead cells. Life and dead somatic cells of one hemisphere of each individual were counted (initial experiment, $n = 1$; 1 technical replicate with 20 individuals).

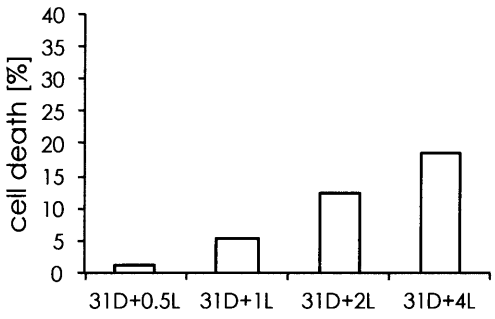

Figure 3.15 After 31 h of darkness, light causes increasing levels of cell death in dmAMN over time.

After the onset of embryogenesis, dmAMN was switched to continuous darkness at the end of the current light period; after 31 h of darkness cultures were exposed to 0.5, 1, 2 or 4 h of light (260 µmol photons m^{-2} s^{-1} light intensity). Dead cells were stained with SYTOX Green. Life and dead cells of one hemisphere of each individual were counted and percent cell death per individual calculated (preliminary experiment, $n = 1$; 1 technical replicate with ≥ 20 individuals).

Chapter 4 Yeast one-hybrid screens to identify *trans*-acting factors binding to *cis*-regulatory elements in *regA*'s introns

4.1 Introduction

Volvox carteri is a spherical multicellular alga and consists of about 2000 mortal somatic cells and ca. 16 potentially immortal reproductive cells called gonidia (Kirk 1998). Cell fate is dependent on cell size and determined during embryogenesis when mature gonidia enter a series of symmetric and asymmetric divisions forming large and small cells that differentiate into gonidia and somatic cells, respectively (Kirk et al. 1993). Somatic cells are not able to grow and their terminal differentiation involves the expression of *regA*, which is restricted to somatic cells (*regA* transcripts are never detected in gonidia; Kirk et al. 1999). The cell type-specific expression is likely controlled at the level of transcription (Kirk et al. 1999; Stark, Kirk, and Schmitt 2001). Mutations in *regA* show the regenerator phenotype, in which somatic cells start growing during the second day, take on the morphology of gonidia, and after 72 h undergo embryogenesis and form new spheroids. The mechanisms responsible for the differential expression of *regA* are unknown.

4.1.1 Brief overview of gene regulation

Transcriptional regulation in eukaryotes generally involves both non-coding DNA sequences called *cis*-regulatory elements and transcription factors binding them (known as *trans*-acting factors; Bassett 2007). There are three types of *cis*-regulatory elements (Riethoven 2010). 1) Promoter sequences are located upstream of the regulated gene. The

core promoter is the binding site of the RNA polymerase and the location of transcription initiation. Promoter sequences are also bound by transcription factors that either stimulate or repress gene transcription. 2) Enhancers and silencers can be hundreds of base pairs long and located up to 100 kb away from the gene they control; depending on whether the sequences (and their corresponding transcription factors) stimulate or repress transcription they are known as enhancers or silencers, respectively. 3) Insulators either delimit the DNA regions influenced by enhancers, or prevent the spread of heterochromatin that would otherwise result in the chromatin-mediated inactivation of genes.

The activity/binding of transcription factors is regulated by one or a combination of the following mechanisms: 1) *de novo* synthesis or degradation of the transcription factor; 2) control of nuclear localization; 3) covalent modification (e.g. phosphorylation); and 4) binding of ligands or other proteins (often transcription factors themselves).

4.1.2 Differential *regA* expression involves intronic elements

The *regA* gene contains 8 exons and 7 introns with 4 of the introns contained in the 5'UTR (Figure 4.1; Kirk et al. 1999). Surprisingly, the minimal promoter consists of only 42 bp upstream of the transcription start site and contains a potential TATA box (TAATTGA), and an initiator element (CACTCAT), but no regulatory elements were detected (Stark, Kirk, and Schmitt 2001). Subsequently, it has been shown that introns 3, 5 and 7 influence *regA* expression in a position independent and promoter specific manner within the gene, thus indicating that they contain sequences acting as *cis*-regulatory elements (Stark, Kirk, and Schmitt 2001). *regA* constructs with intronic

rearrangements of intron 5 or 7 showed that the function of these introns is position independent (Stark, Kirk, and Schmitt 2001).

Different deletion constructs of the *regA* gene missing introns or parts of the promoter were transformed into a regenerator mutant and tested for their ability to restore the wild-type phenotype (Stark, Kirk, and Schmitt 2001). Deletion constructs missing either intron 3 or part of intron 5 (between two *Eco*RV sites) did not rescue the regenerator phenotype; i.e. intron 3 and 5 were both necessary for the expression of *regA* (Stark, Kirk, and Schmitt 2001). Deletion of intron 7 caused a new mutant phenotype called *fruitless*; although this deletion construct restored the wild-type phenotype in somatic cells, gonidia grew and reproduced only slowly, and died out after 2 or 3 generations (Stark, Kirk, and Schmitt 2001). The same *fruitless* phenotype was also observed for a *regA* construct in which a constitutive promoter replaced the wild-type promoter leading to *regA* mRNA expression in both gonidia and somatic cells; thus, the deletion of intron 7 likely also led to the expression of *regA* in gonidia causing the phenotype (Stark, Kirk, and Schmitt 2001). Two unusual features of intron 7 include a non-canonical GC donor splice site (instead of GT) and the fact that it encodes an open reading frame (ORF) that is in frame with the flanking exons. It was not tested if this ORF is expressed independently, but, interestingly, some *regA* transcripts still contain the unspliced intron 7 sequence in *V. carteri* f. *nagariensis*, and in the closely related strain *V. carteri* f. *kawasakiensis* the sequence homologous to intron 7 is never spliced (Stark, Kirk, and Schmitt 2001; Duncan et al. 2006). These findings suggested that either the RNA or the protein encoded by the ORF located in intron 7 actually has regulatory function for *regA* expression (i.e. by acting as a *trans*-acting factor). However, none of these postulated

roles could be demonstrated by either preventing splicing of intron 7 (by mutating the donor splice site to CC) or expressing intron 7 from a constitutive promoter (Stark, Kirk, and Schmitt 2001).

4.1.3 Hypothesis and objectives of this study

How the 3 introns actually influence the expression of *regA* is not known. Stark et al. (2001) proposed that introns 3 and 5 contain enhancers while intron 7 contains a silencer. Intronic enhancers and silencers have been described, for example, in the closely related single-celled alga *Chlamydomonas reinhardtii* as well as in the land plant, *Arabidopsis thaliana* (Sieburth and Meyerowitz 1997; Kang and Mitchell 1998; Lumbreras, Stevens, and Purton 1998; Deyholos and Sieburth 2000). The hypothetical *trans*-acting factors binding to introns 3 or 5 would be present in both cell types and promote *regA* expression, but the factor binding to intron 7 would be specifically active in gonidia, preventing *regA* expression (Stark, Kirk, and Schmitt 2001; Figure 4.2). So far, no potential *trans*-acting factors binding to intron 3, 5 or 7 are known and there has been no published attempts to identify these postulated transcription factors and the *cis*-regulatory elements they bind to.

The objectives of this study were (i) to establish for the first time the use of the yeast one-hybrid (Y1H) assay in *V. carteri,* and (ii) identify *trans*-acting factors binding to intron 3, 5 and 7 using 1 of 2 approaches—either 1) a Y1H screen of each intron against a cDNA library of *V. carteri*, or 2) identification of potential binding sites in the 3 introns using bioinformatics tools and then testing the corresponding predicted *trans*-acting factors for interaction with the respective introns in a Y1H assay.

The yeast one-hybrid assay (Vidal and Legrain 1999) is a system to test DNA-protein interactions *in vivo* using yeast as a "host". The system can be used to either test for a specific interaction between a known DNA sequence (the so-called bait sequence) and a protein suspected to bind to the bait, or to screen a cDNA library to identify which protein binds specifically to the bait (Vidal and Legrain 1999). The bait sequence—usually a characterized binding site present as a tandem repeat—is cloned in front of a reporter gene (commonly *HIS3*) on the so-called bait plasmid; larger gDNA fragments up to 1.7 kb have also been successfully used as bait, especially when the exact binding sequence is not known (Hameister et al. 2007). Either a single specific protein or a population of proteins encoded by a cDNA library are fused to the GAL4 activation domain (GAL4 AD) forming the so-called prey, which is encoded on the prey plasmid. Both bait and prey plasmids are transformed into yeast. Because non-specific interactions between the bait and endogenous yeast transcription factors might lead to the background expression of HIS3, 3-Amino-1,2,4-triazole (3AT) is added to the medium at a concentration that suppresses HIS3 action from background expression. If the prey interacts with the bait sequence present in front of the reporter gene *HIS3*, the GAL4 AD is in close proximity of the *HIS3* promoter, which stimulates HIS3 expression above background levels; consequently, yeast strains auxotrophic for histidine are able to grow on selective medium without histidine and at higher 3AT concentrations (Figure 4.3).

4.2 Material and Methods

4.2.1 *Volvox carteri* strain and culturing conditions

The wild type strain of *Volvox carteri* f. *nagariensis* (Vcn) known as EVE (Adams et al. 1990) was grown in standard *Volvox* medium (SVM; Kirk and Kirk 1983). The culture was kept asynchronous by being maintained in continuous light, so various developmental stages were present at any given time. Photosynthetically active radiation of 260 μmol photons $m^{-2}s^{-1}$ (Kirk and Kirk 1985)—measured with a Laboratory Quantum Scalar Irradiance Meter QSL-100 (Biospherical Instruments Inc.)—was provided by cool white fluorescent light bulbs. The culture was diluted every day with fresh SVM to ca. 5 spheroid/mL and density never exceeded 50 spheroids/mL. Spheroids were concentrated on a 30 μm Nitex filter and flash-frozen drop-wise in liquid nitrogen forming frozen pellets.

4.2.2 Molecular Cloning

4.2.2.1 *Escherichia coli* strains and growth conditions

The *ccd*B Survival-T1^R strain was used for cloning and propagation of plasmids containing the negative marker *ccd*B; for the propagation of other plasmids, the OmniMax 2-T1^R strain was used (Table 4.1). Both strains were grown at 37°C in either lysogeny broth (LB) (1% tryptone, 0.5% yeast extract, 1% NaCl) or on LB plates (containing 1.5% agar) with appropriate antibiotics for plasmid selection (50 μg/mL for kanamycin, 15 μg/mL for chloramphenicol); liquid cultures were placed on a rotary shaker at 250 rpm.

4.2.2.2 Transformation of *E. coli* by electroporation

To prepare electrocompetent cells, 10 mL LB were inoculated with a single *E. coli* colony and incubated overnight. All of the overnight culture was added to 500 mL fresh LB and the culture incubated until its OD_{600} reached 0.5–0.6. The culture was transferred to pre-cooled 250 mL centrifuge bottles, chilled on ice for 10 min, centrifuged for 15 min at 1000 g at 4°C, and the supernatant discarded. The cells were washed once with 200 mL and once with 50 mL ice-cold 10% glycerol (i.e. resuspended in glycerol, centrifuged for 20 min at 1000 g at 4°C, then the supernatant was discarded). Cells were finally resuspended in 5 mL ice-cold 10% glycerol, 40 µL-aliquots flash-frozen in liquid nitrogen, and stored at −80°C.

For transformation, 40 µL of electrocompetent *E. coli* were thawed on ice and the 1–2 µL DNA added (e.g. ligation mix, recombination mix, or plasmid prep from yeast); the cells were transferred to a pre-chilled electroporation cuvette with a 2 mm gap (Molecular BioProducts) and transformed by electroporation at 2.2 kV, 25 µF capacitance, and 200 Ω in a Electroporator 2510 (Eppendorf). After electroporation, cells were immediately mixed with 450 µL SOC medium (2% tryptone, 0.5% yeast extract, 10 mM NaCl, 2.5 mM KCl, 10 mM $MgCl_2$, 10 mM $MgSO_4$, 20 mM glucose), transferred to a microcentrifuge tube, and recovered for 1 h at 37°C at 250 rpm on a rotary shaker. 50–200 µL of the cells were plated on LB plates with appropriate antibiotics.

4.2.3 Yeast one-hybrid assays

4.2.3.1 *Saccharomyces cerevisiae* strains and culturing conditions

Yeast liquid cultures were grown at 30°C, on a rotary shaker (at 200 rpm). YPDA medium (1% yeast extract, 2% bacto peptone, 2% dextrose and 0.003% adenine sulfate) was used for non-selective growth of yeast. Strain Y187 and Y1HGold are both auxotrophic for tryptophan, leucine and histidine (Table 4.2). For selective growth, synthetically defined (SD) medium (0.67% yeast nitrogen base w/o AA, 2% glucose) with amino acids provided by the appropriate dropout supplement (Clontech) was used: without tryptophan (−T) to select for nutritional marker *TRP1* (i.e. bait plasmid); without leucine (−L) to select for marker *LEU2* (i.e. prey plasmid); and without histidine (−H) to select for expression of reporter gene *HIS3* (i.e. prey and bait interaction). Solid media for plates contained 2% agar. 3-Amino-1,2,4-triazole (3AT) was added to suppress HIS3 activity from background expression of *HIS3* on the bait plasmid; the necessary 3AT concentration was determined empirically by titration.

4.2.3.2 Construction of bait plasmids

The DNA sequences used as bait were *regA* intron 3, part of intron 5, and intron 7. The Gateway system (Invitrogen) was used for cloning; first, the bait plasmid pHIS2.1 was converted to a Gateway plasmid and then the *regA* introns were cloned by recombination in front of *HIS3* on the plasmid. In addition, one predicted protein-binding site in intron 3 (AE box 2, see below) was cloned by restriction digest and ligation into the bait plasmid pHIS2.1 (Clontech) in front of reporter gene *HIS3*. The Geneious 6.0 software (Biomatters) was used to plan construction of all plasmids (Table 4.3) and for sequencing

data analysis. Sequencing was performed on a 3730xl DNA Analyzer (Applied Biosystems) at McGill University and Génome Québec Innovation Centre.

4.2.3.2.1 Conventional cloning of a bait sequence containing the AE box 2 into pHIS2.1

A bioinformatics approach was used to identify potential protein binding sites in *regA* intron 3. Specifically, I determined conserved regions among 4 *V. carteri* formas: *nagariensis* (GenBank AF106963), *kawasakiensis* (GenBank DQ247963), *weismannia* (sequence was kindly provided by Richard Michod, University of Arizona; Hanschen, Ferris, and Michod 2014), and *wangii* (intron 3–exon 5 was amplified and sequenced as in Table 4.4; primers bound to well conserved areas known from the 3 other formas). Intronic sequences were aligned with ClustalW (Thompson, Higgins, and Gibson 1994) as part of Geneious 6.0 (Biomatters). NSITEH (Softberry) detected a conserved AE box 2 in *regA* intron 3 among all 4 formas. To test if the predicted AE box 2 acts as a binding site in the Y1H assay, two oligonucleotides were annealed to form an adapter containing a 3-tandem repeat of AE box 2 flanked by an upstream *Sac*I and a downstream *Spe*I cohesive end (Figure 4.4); the adapter was cloned between *Sac*I and *Spe*I upstream of *HIS3* on bait plasmid pHIS2.1 and the correct sequence was confirmed by sequencing.

4.2.3.2.2 Gateway cloning of bait sequences

4.2.3.2.2.1 Conversion of pHIS2.1 to Gateway bait plasmid pDEST-HIS2.1

To use the Gateway system for cloning of bait sequences, pHIS2.1 was converted to a Gateway plasmid (similar to Deplancke et al. 2004) by cloning the *att*R gateway

cassette—containing both chloramphenicol resistance gene and *ccd*B gene flanked by recombination sites *att*R1 and *att*R2—into the multiple cloning site of pHIS2.1. First, the *att*R Gateway cassette of pDEST22 was PCR-amplified with the forward primer containing a 5' *Sac*I and the reverse primer a 5' *Spe*I site (Table 4.4). The PCR product of the gateway cassette was cloned between *Sac*I and *Spe*I sites of pHIS2.1 upstream of reporter gene *HIS3* forming the Gateway bait plasmid pDEST-HIS2.1 (Table 4.3). Plasmid identity was confirmed by the restriction pattern analysis with *Sac*I and *Spe*I or with *Hind*III and *Nco*I, and by full-length sequencing of the *att*R gateway cassette.

4.2.3.2.2.2 Gateway cloning of *regA* introns into Gateway bait plasmid pDEST-HIS2.1

In the first step of Gateway cloning, *Vcn_regA* intron 3, part of intron 5, and intron 7 were PCR amplified with a forward primer containing a 5' *att*B1 and a reverse primer containing a 5' *att*B2 recombination site necessary for Gateway cloning (Table 4.4). The PCR products were cloned by recombination into pDONR221 with the Gateway BP Clonase II Enzyme Mix (Invitrogen) forming pENTR221 constructs (Table 4.3) and the correct DNA sequence of the insert was confirmed by sequencing.

To prevent recovery of pENTR221 constructs and their pDONR221 derivatives after transformation, 1 μg of each pENTR221 construct was first linearized by digestion with *Pvu*I, purified by phenol:chloroform extraction and ethanol:sodium acetate precipitation (Sambrook and Russel 2001), and dissolved in 10 μL TE, pH 8.0. The DNA bait sequence was shuttled by recombination from pENTR221 constructs to the bait plasmid pDEST-HIS2.1 using the Gateway LR Clonase II Enzyme Mix (Invitrogen) and forming

the final pEXP-HIS2.1 constructs containing the bait sequence upstream of reporter gene *HIS3* (Table 4.3). Clones were confirmed by restriction fragment pattern analysis with *Nde*I and *Sal*I.

4.2.3.3 Preparation of prey cDNA

cDNA of a single gene (e.g., coding for the transcription factors DofA and B3TF) or a cDNA library of *V. carteri* f. *nagariensis* was prepared to be used as prey and test for interaction with the bait sequence in a Y1H assay. The final cDNA contained an upstream SMART III and downstream CDS III sequence necessary for cloning into the prey plasmid pGADT7-Rec2 (Table 4.5).

4.2.3.3.1 Total RNA extraction for cDNA synthesis

Frozen pellets of an asynchronous *V. carteri* EVE culture were ground in a mortar with liquid nitrogen; 2 g of ground material were transferred to a 13 mL screw cap tube, resuspended in 10 mL TRIzol (38% phenol, 0.8 M guanidine thiocyanate, 0.4 M ammonium thiocyanate, 0.1 M sodium acetate, pH 5, 5% glycerol) by shaking, and incubated for 5 min at room temperature (Chomczynski and Sacchi 1987). The sample was centrifuged for 10 min at 12,000 *g* at 4°C, then the supernatant combined with 2 mL chloroform in a new 13 mL screw cap tube and mixed by shaking for 15 s. After incubation for 3 min at room temperature and centrifugation for 15 min at 12,000 *g* at 4°C, approx. 8 mL of the top aqueous phase were transferred to a new 13 mL screw cap tube and mixed with 5 mL isopropanol. RNA was precipitated for 10 min at room temperature and pelleted for 10 min at 12,000 *g* at 4°C. The RNA pellet was washed with 10 mL of ice-cold 75% ethanol, centrifuged for 10 min at 12,000 *g* at 4°C, and the

supernatant discarded. After the wash step was repeated once, the RNA was blow-dried and then resuspended in 62.5 µL DEPC-treated ddH_2O.

4.2.3.3.2 Isolation of mRNA and library cDNA preparation

mRNA was purified from 100 µg of total RNA with the Oligotex Mini Kit (Qiagen) according to the manufacturer's protocol, and eluted in 200 µL OEB buffer. mRNA was mixed with 0.1 volumes 3 M sodium acetate, pH 5.3 and 3 volumes 95% ethanol, and precipitated at −20°C overnight. After centrifugation for 30 min at 20,800 *g* at 4°C, the mRNA pellet was washed with 1 mL of ice-cold 75% ethanol, centrifuged again, and the supernatant discarded. The mRNA was air-dried for 10 min at room temperature, and dissolved in 3 µL DEPC-treated ddH_2O. All of the RNA was used for first-strand cDNA synthesis using either the CDS III oligo(dT) primer (for oligo(dT) libraries) or CDS III/6 random primer (for random hexamer libraries), then the cDNA was amplified in a long distance PCR (using 26–28 cycles), and purified by size exclusion chromatography according to the protocol of the Matchmaker One-Hybrid Library Construction & Screening Kit (Clontech).

4.2.3.3.3 *Vcn_dofA* cDNA synthesis

The TESS software (Schug 2008) predicted a potential DNA-binding site for the Dof family of transcription factors in *Vcn_regA* intron 3, and one DofA gene was identified in the genome of *V. carteri* (*dofA*, JGI Protein ID 107971). The predicted coding sequence of *Vcn_dofA* was amplified using RT-PCR. To obtain the DNA binding domain of *Vcn_dofA* (a zinc finger motif, AA93–152), 1.5 µg total RNA were first treated with 2 U Amplification Grade DNaseI (Invitrogen) in 1X DNase I Reaction Buffer in a total

volume of 20 µl for 10 min at room temperature. The reaction was stopped by adding 2 µl 25 mM EDTA, followed by incubation for 10 min at 65°C, and then kept on ice. The reverse transcription reaction contained 600 ng DNase-treated RNA and oligo$(dT)_{20}$ primer, and the resulting cDNA was PCR amplified (Table 4.6). To obtain full-length *Vcn_dofA*, cDNA was synthesized from 5 µg total RNA (untreated with DNase) with a gene-specific primer and PCR-amplified (Table 4.6). All forward PCR primers contained the SMART III and the reverse PCR primers the CDS III sequence. PCR products were concentrated by ethanol:sodium acetate precipitation (Sambrook and Russel 2001) and purified by gel-electrophoresis and gel-extraction.

4.2.3.3.4 cDNA of B3TF factor DNA binding domain

In *Arabidopsis thaliana*, AEF (AE box-binding factor) binds to the AE box 2 DNA sequence (Roy et al. 2012), a potential binding site identified in *regA* intron 3 (see above). AEF belongs to the B3 domain transcription factors (B3TF), and only one B3TF is predicted in the genome of *V. carteri*. The cDNA sequence encoding the DNA-binding domain (AA4–114) of the predicted *Vcn*_B3TF (JGI Protein ID 116438) was codon-optimized for *S. cerevisiae*, synthesized *de novo* flanked by an upstream SMART III and a downstream CDS III sequence, and cloned into the *Eco*RV site of pBS_II_SK(+) (Biomatik). The SMART III-B3TF-CDS III sequence was then amplified in a PCR reaction (Table 4.6); the PCR product was purified by gel-electrophoresis and gel-extraction.

4.2.3.4 Y1H screen

For the Y1H screen, yeast was transformed with the bait plasmid, linearized prey plasmid pGADT7-Rec2, and cDNA. pGADT7-Rec2 and cDNA contained the SMART III and CDS III sequences; using these sequences, the cDNA was cloned into pGADT7-Rec2 by homologous *in vivo* recombination facilitated by endogenous recombinases in yeast creating a circular plasmid; if no cDNA was transformed into a particular cell the linearized pGADT7-Rec2 cannot be replicated and the selection marker on it is lost, i.e. the cell cannot grow on SD medium without leucine. The cDNA was expressed as a fusion to the GAL4 activation domain encoded by pGADT7-Rec2.

4.2.3.4.1 cDNA library screens

The Matchmaker One-Hybrid Library Construction & Screening Kit (Clontech) was used for large-scale transformations of yeast strain Y1HGold for library screens using 5.7 µg bait plasmid pEXP-HIS2.1_regA_Intron_5 or 5.9 µg bait plasmid pEXP-HIS2.1_regA_Intron_7 (Table 4.7). Alternatively, a modified protocol for high-efficiency transformations (Woods and Gietz 2001) was used for library screens of pEXP-HIS2.1_regA_Intron_3. A culture of Y187 carrying the bait plasmid pEXP-HIS2.1_regA_Intron_3 was grown in 25 mL SD_{-T} medium overnight at 30°C at 200 rpm. The overnight culture was used to inoculate 60 mL 2X YPDA (2% yeast extract, 4% bacto peptone, 4% glucose and 0.01% adenine hemisulfate) at starting density of 5×10^6 cells/mL; the culture was grown for 4–5 h to a density of about 2×10^7 cells/mL, then was centrifuged at 1100 *g* for 5 min at room temperature, and the supernatant discarded. Cells were washed twice with 30 mL sterile ddH_2O, collected by

centrifugation and the supernatant discarded. The cell pellet was resuspended in 4320 µL transformation mix (2880 µL 50% PEG 3350, 432 µL 1 M LiAc, 120 µL of 10 µg/µL denatured Carrier DNA, 3 µg pGADT7-Rec2 (*Sma*I-linearized), 20 µL cDNA, and 862 µL of sterile ddH_2O), and incubated for 45 min at 42°C; during incubation, cells were mixed every 5 min. Cells were centrifuged at 1100 *g* for 5 min at room temperature, supernatant was discarded and the cells were finally resuspended in sterile ddH_2O and plated on SD_{-TLH} plates (∅100 mm) with appropriate concentration of 3AT. Plates were incubated for 5 days–2 weeks. The prey cDNA insert of positives forming colonies was amplified in a colony PCR (Table 4.6) and the PCR product sequenced.

4.2.3.4.2 Single gene screens

To screen a single gene for interaction with a bait sequence, 125 ng cDNA of the gene of interest, 250 ng pGADT7-Rec2 (*Sma*I-linearized), and 250 ng bait plasmid were transformed into Y1HGold with the Matchmaker One-Hybrid Library Construction & Screening Kit (Clontech) and plated on SD_{-TLH} selection plates containing 0–100 mM 3AT (Table 4.8). Negative controls did not contain cDNA and pGADT7-Rec2, and were plated on SD_{-TH} plates containing 0–100 mM 3AT. The correct inserts of prey plasmids formed by *in vivo* recombination (Table 4.5) were confirmed by colony PCR (Table 4.6) and sequencing.

4.2.3.4.3 Plasmid rescue from *S. cerevisiae*

For propagation, prey plasmids were extracted from yeast and transformed into *E. coli*. One yeast colony was resuspended in 2 mL of SD_{-TL} and grown overnight at 30°C on a shaker at 200 rpm. 1.5 mL culture were transferred to a microcentrifuge tube and

centrifuged at 20,800 g for 20 s. The supernatant was discarded, the cell pellet resuspended in the remaining liquid, and 0.2 mL Triton SDS lysis buffer (2% Triton X-100, 1% SDS, 100 mM NaCl, 1 mM EDTA), 0.2 mL PCIA (50% phenol, 48% chloroform, 2% isoamyl alcohol) and 0.3 g acid washed glass beads (0.45–0.5 mm) were added (Amberg, Burke, and Strathern 2006); the sample was vortexed for 2 min and centrifuged at 20,800 g for 20 s. The DNA in the aqueous phase was further purified by phenol:chloroform extraction, and then—after the NaCl concentration was adjusted to 200 mM—ethanol precipitated (Sambrook and Russel 2001). Finally, the DNA pellet was dissolved in 10 µL TE, pH 8.0, and 1 µL of the DNA solution was transformed into OmniMax 2-T1^R by electroporation and plated on LB plates with the appropriate antibiotics. Prey plasmids were used for sequencing or for retransformation into yeast to confirm bait-prey interaction.

4.3 Results

4.3.1 Y1H assays for specific interactions between *cis*-regulatory elements predicted by bioinformatics approaches and their *trans*-acting factors

To identify potential binding sites and transcription factors binding to them I first used bioinformatic approaches; the interactions between the identified *cis*-regulatory elements and their postulated *trans*-acting factor were then tested in a Y1H assay. Various algorithms and software have been developed to predict *cis*-regulatory elements based on the sequences of known motifs and/or on the high degree of sequence conservation of such sequences between related species. TESS (www.cbil.upenn.edu/tess) identifies sequences that share specific motifs with known *cis*-regulatory elements in other species (Schug

2008). A binding site for Dof (DNA-binding with one finger) domain proteins—a family of plant-specific transcription factors with an important role in plant-specific processes related to light, phytohormone and defense responses, seed development and germination (Yanagisawa 2002)—was predicted in *regA* intron 3 (Figure 4.5). A gene (*dofA*) encoding a Dof domain was found in both *V. carteri* and *C. reinhardtii* genomes. In addition, light had been shown to induce *regA* expression (see Chapter 3), adding credibility to the predicted binding site, and providing the opportunity to test for a potential interaction. The DNA binding domain alone of DofA (DofA DBD, AA93-152) and the full-length protein (DofA FL) were each fused to the Gal4 AD domain forming the prey, and then tested against *regA* intron 3 as bait in an Y1H assay. A crude negative control in form of a 3x tandem repeat of the p53 binding site instead (which should not interact with the Dof domain) was included. However, it turned out that this negative control was not suitable as it conferred a higher 3AT tolerance than *regA* intron 3 (10 mM vs. 1 mM 3AT, Table 4.9), confounding any comparisons between these two bait sequences in their interaction with the prey.

Yeast transformed with DofA DBD and intron 3 demonstrated a higher 3AT tolerance (10 mM vs.1 mM) than yeast transformed with the bait alone, suggesting that DofA DBD interacted with intron 3 and lead to HIS3 expression above background levels (Table 4.9). In conflict with these results were experiments with DofA FL and intron 3, as the transformed yeast did not show an increased 3AT tolerance, suggesting no interaction with *regA* intron 3 (Table 4.9). Because of the conflicting results using DofA DBD vs. FL and the lack of a suitable negative control further testing of this interaction was not

pursued; furthermore, the lack of interaction between the DofA FL and intron 3 and additional bioinformatics analyses (see below) deemed this interaction rather unlikely.

The NSITEH software (http://linux1.softberry.com/berry.phtml?topic=nsiteh&group=programs&subgroup=promoter) identifies regions that contain known transcription factor binding sites but are also conserved among closely related species. Intronic sequences are usually non-functional apart from the sequences required for splicing (donor site, branch site, and acceptor site), but any *cis*-regulatory elements contained within introns are functional and should also be under selection. For this reason, I compared the sequences of four closely related strains (i.e. formas) of *V. carteri—nagariensis*, *kawasakiensis*, *weismannia* and *wagii*—and used the NSITEH software to identify conserved regions that contain known transcription factor binding sites (Figure 4.5). Only two potential binding sites were detected: the CCA1 motif and the AE box 2. Interestingly, the Dof binding site has not been predicted by NSITEH, consistent with the fact that the site identified previously is not fully conserved in one of the 4 formas.

In *A. thaliana, CCA1* (Circadian Clock-Associated 1) is a master clock control gene involved in the regulation of circadian genes; such genes show a 24 h-periodicity in their expression pattern under regular light:dark conditions that is still maintained when switched to conditions without any light cues (e.g. in continuous darkness). Because the *regA* expression did not show a circadian pattern either in 16L:8D (Chapter 2, Figure 2.8) or a free-running rhythm in continuous darkness (i.e. in the absence of light cues gene expression would still show 24 h-periodicity; Chapter 2, Figure 2.9), it is likely that a CCA1 homolog in *V. carteri* is not involved in *regA* regulation; thus, the putative CCA1 binding site in *regA* intron 3 is was not further investigated.

In *A. thaliana*, AE (activation element) box 2 confers light responsiveness to *GAPB* and the DNA polymerase λ genes (Park, Kwon, and Shih 1996); a 52 kDA protein called AE box-binding factor (AEF) is known to bind the AE box 2 (AEF; AT4G31615; Roy et al. 2012). AEF belongs to the superfamily of plant transcription factors that share the B3 domain for DNA binding, and a B3 domain transcription factor (B3TF) has been identified in the *V. carteri* genome (Romanel et al. 2009). Since in the *regA*$^{-}$/gonidialess mutant dmAMN *regA* is induced by light after 31 h of darkness (see Chapter 3), this light responsiveness might involve the AE box 2 in *regA* intron 3 and its binding by a B3TF in *V. carteri*.

The DNA binding domain of B3TF (B3TF DBD) was tested for interaction with the *regA* intron 3 or with a 3-tandem repeat of AE box 2 in a Y1H assay (Table 4.10). Yeast transformed with intron 3 as bait and B3TF DBD as prey did not show an increase in 3AT tolerance, i.e. there was no interaction between B3TF DBD and intron 3 detected (Table 4.10). B3TF DBD also did not interact with the AE box 2 3-tandem used as bait (Table 4.10).

4.3.2 Y1H screen of *regA* intron 3

More than 1.2 million unique clones of a *V. carteri* cDNA library were screened for positive interactions with *regA* intron 3 in 5 independent screens (4 oligo(dT) and one random hexamer library, Table 4.11). Five screens were necessary to screen at least 1 million unique clones ensuring complete coverage of the *V. carteri* transcriptome. Because no positive colonies were observed when *regA* intron 3 was screened on SD$_{-TLH}$ plates with 3 mM 3AT (Table 4.11), the stringency was reduced to 1 mM 3AT. The

reduction in stringency resulted in a large amount of background colonies (i.e. > 500 positives). Assuming that true bait-prey interactions would be stronger than nonspecific interactions and thus result in a higher HIS3 expression, faster cell growth, and larger colonies, positives were selected based on their colony size of at least 2 mm. The number of SD_{-TLH} plates was reduced from 100 to 20 because it simplified the handling during the experiment and the denser plating of the yeast cells did not appear to increase the number of background colonies (data not shown; too dense plating of yeast cells can lead to scavenging of limiting nutrients from dying cells leading to false positives). The inserts of positives were amplified by colony PCR and sequenced if they were at least 300 bp long; inserts below 300 bp were excluded especially in the case of oligo(dT) generated cDNAs as they mostly or only encoded the 3'UTR of the respective gene (data not shown).

A total of 22 positive clones were sequenced. These 22 sequenced clones either mapped to 3'UTRs only, were out of frame, encoded only short proteins (< 20 AA, too small to encode any known DNA binding domains), mapped to genes coding for proteins not known to bind DNA (i.e. ribosomal protein S8E represented twice in screen and phosphoribulokinase), mapped to predicted intronic sequences, or a combination of these (Table 4.12). InterProScan analysis (http://www.ebi.ac.uk/interpro/; Jones et al. 2014) analysis of any predicted amino acids sequence encoded by the insert of at least 30 AA did not reveal any potential DNA binding domains for any of the positives. No true *trans*-acting factors binding to *regA* intron 3 were identified.

4.3.3 Intron 7

Three cDNA libraries were screened in yeast strain Y1HGold against bait plasmid pEXP-HIS2.1-regA_Intron_7 on SD_{-TLH} selection plates containing 100 mM 3AT. Switching to the transformation protocol of the Clontech kit increased transformation efficiency to 80–100% of target efficiency for oligo(dT) cDNA libraries, and a total of 2 million unique clones were screened among 3 library screens (Table 4.13). An initial screen of an oligo(dT) library on 20 selection plates resulted in > 400 positives (i.e. background) and only the 124 colonies of at least 2 mm diameter were further analyzed. In following screens, an increase to 100 selection plates (instead of 20) reduced the amount of inoculum per plate, removed background colonies, and decreased the number of positives to 17 for the screen of an random hexamer cDNA library and 105 positives for an additional oligo(dT) cDNA library (Table 4.13). A total of 71 positives contained inserts larger than 300 bp and were sequenced (Table 4.14): 13 mapped to 3'UTR; 15 were out of frame; 1 mapped to an intron only; 4 were cloned in anti-sense orientation; 9 coded for short proteins; 2 contained the 5'UTR resulting in a premature stop codons; 4 coded for proteins not known to bind DNA (i.e. C-terminal domain of 1-Cys peroxiredoxin; Chlorophyll A-B binding protein; G protein beta subunit-like protein; unknown protein containing a thioredoxin domain); and 4 were low complexity sequences. Ribosomal proteins were overrepresented (31 out of 71, i.e. 44%) and are common false positives in yeast hybrid screens (MacDonald 2001). Nonetheless, because of the high representation of the small ribosomal protein S8 (*rps8*) in the screens (17 out of 71 positives), I tested *rps8* again for interaction with *regA* intron 7 by retransformation; no colonies were observed at 100 mM 3AT stringency, i.e. retransformation did not confirm the interaction

(data not shown). Taken together, likely none of the 71 positives actually interacts with *regA* intron 7.

4.3.4 Intron 5

One oligo(dT) cDNA library was transformed into yeast strain Y1HGold together with bait plasmid pEXP-HIS2.1-regA_Intron_5 using the Clontech kit and plated on 100 SD_{-TLH} selection plates with 50 mM 3AT. A total of 540,000 unique clones were screened, but because the number of positive colonies obtained was high (estimated > 1000, i.e. a lot of background colonies), and picking positives by size had not been successful for screens with intron 3 or 7 previously, none of the background colonies were further analyzed.

4.4 Discussion

To learn more about the signaling pathway(s) resulting in differential *regA* expression, I attempted to identify the last component of the pathway(s) (i.e. *trans*-acting factors binding to *regA* introns 3, 5 or 7) by using Y1H assays. However, I was not able to identify any *trans*-acting factors involved in *regA* regulation. Below, I discuss reasons for these unsuccessful outcomes and suggest that cooperative binding of *trans*-acting factors or their covalent modification might be the main reason.

4.4.1 Technical difficulties of Y1H screens

The Y1H screens showed a bias towards short insert sizes, i.e. cDNAs covering mostly the 3'-end and therefore the C-terminus of the encoded proteins; only 2 out of 93 sequenced positives encoded for proteins longer than 100 AA (Table 4.12 and 4.14). Due

to this bias any *trans*-acting factor with its DBD in the N-terminus of the protein would not have been represented in the Y1H screens. The short length of inserts cannot be explained by the RNA quality used for cDNA synthesis or the efficiency of cDNA synthesis; integrity of total RNA (prior to mRNA isolation) was confirmed on agarose gels and cDNA after LD-PCR contained molecules up to 3000 bp (data not shown). For Y1H screens of *regA* intron 3, a bias toward small insert sizes might have been caused by a low transformation efficiency (only 20% of target efficiency); in general, large DNA molecules are transformed into yeast with less efficiency than small ones (Connelly et al. 1991) which might have created a bias towards shorter inserts.

4.4.2 Testing of specific *trans*-acting factors for interaction with *regA* intron 3

Because bioinformatics approaches predicted the presence of putative binding motifs for two plant-specific transcription factors (DofA and B3TF), Y1H assay was used to test for the postulated interactions. Although yeast transformed with the DofA DBD as prey acquired increased 3AT tolerance, the lack of interaction when the full-length protein was used as well as the lack of conservation of the predicted DofA binding site among the four *V. carteri* formas argue against DofA being involved in *regA* regulation. Nevertheless, the Dof domain—like other zinc finger domains—is known to have a dual role, interacting with both DNA and other proteins (Yanagisawa 2004). In maize, binding of Dof1 to the high-mobility-group protein 1 has been shown to increase DNA binding of Dof1 (Yanagisawa 1997). If an additional protein were necessary for DofA binding in *V. carteri*, it would not have been present in the Y1H assay. In addition, phosphorylation and dephosphorylation might regulate Dof activity in maize (Yanagisawa 2002) and if

DofA needs to be activated in *V. carteri*, the necessary regulatory proteins would be absent in the Y1H assay. It is also possible that only DofA FL needs to be activated for DNA binding but the DofA DBD alone in absence of regulatory domains on the protein can bind DNA even without activation; this would explain why DofA DBD showed interaction with intron 3 in the Y1H assay, while DofA DBD did not (Table 4.9). So, in conclusion, either 1) DofA does not bind to the predicted Dof binding site in the *regA* intron 3 of *V. carteri*, 2) additional factors might be required to facilitate DofA binding to its DNA target, or 3) DofA may need to be activated to bind to DNA.

B3TF also did not show any interaction with either the *regA* intron 3 or the 3-tandem repeat of AE box 2. B3TF belongs to the B3 DNA binding superfamily that is divided into five families based on the general domain structure of the protein and the similarities of the B3 domain; the five B3 families are the ABI3/VP1, HSI, RAV, ARF and REM family (Romanel et al. 2009). The DNA binding specificity of the B3 domain was characterized for the ABI3, RAV and ARF families, and B3TF in *V. carteri* belongs to the ABI3 family (Romanel et al. 2009). In contrast, the transcription factor AEF (which binds to the AE box 2 in *A. thaliana*) belongs to the REM family and it remains to be determined if members of this family share DNA binding specificity of their B3 domain (Romanel et al. 2009). Thus, since B3TF in *V. carteri* and AEF in *A. thaliana* are not in the same B3 family, they are unlikely to share the same DNA binding specificity, and B3TF might not bind AE box 2 (the target of AEF); this would explain why there was no interaction between B3TF and AE box 2 in a Y1H assay. If the conserved AE box 2 in *regA* intron 3 is actually involved in *regA* regulation, it is not mediated by B3TF.

4.4.3 *trans*-acting factors might bind to *regA* introns cooperatively or they might be covalently modified

The Y1H screen of cDNA libraries of *V. carteri* against *regA* intron 3 or 7 did not identify any likely *trans*-acting factors. A limitation of Y1H assays is that only a single library protein is tested for interaction with the DNA bait. Some *trans*-acting factors show cooperative binding, i.e. their binding to DNA is stabilized by protein-protein interactions among two or more different *trans*-acting factors (Spitz and Furlong 2012). Since only one single protein is screened in Y1H, other proteins necessary for cooperative binding would be absent. If *regA* regulation involves cooperative binding of *trans*-acting factors an Y1H screen would not be able to identify these factors due to the inherent limitation of the assay.

In addition, the activity or binding of transcription factors can be regulated by covalent modification. For example members of the bZIP family of transcription factors form homo- or heterodimers and their dimerization is important for DNA binding and influenced by phosphorylation executed by kinases in the region of the leucine zipper (Llorca 2014). Such transcription factors would not be identified in a yeast one-hybrid assay as the necessary enzymes executing the covalent modification would be absent and thus the transcription factor would not be binding to the bait sequence.

Table 4.1 *E. coli* strains used in this study

*ccd*B Survival-T1^{R} (Invitrogen)	F^{-} *mcr*A Δ(*mrr-hsd*RMS-*mcr*BC) Φ80*lac*ZΔM15 Δ*lac*X74 *rec*A1 *ara*Δ139 Δ(*ara-leu*)7697 *gal*U *gal*K *rps*L (Str^{R}) *end*A1 *nup*G *tonA*::P*trc-ccd*A
OmniMax 2-T1^{R} (Invitrogen)	F′ {*pro*AB^{+} *lac*I^{q} *lac*ZΔM15 *Tn*10(Tet^{R}) Δ(*ccd*AB)} *mcr*A Δ(*mrr-hsd*RMS-*mcr*BC) Φ80(*lac*Z)ΔM15 Δ(*lac*ZYA-*arg*F) U169 *end*A1 *rec*A1 *sup*E44 *thi*-1 *gyr*A96 *rel*A1 *ton*A *pan*D

Table 4.2 *S. cerevisiae* strains used in this study

Y1HGold (Clontech)	*MATα, ura3-52, his3-200, ade2-101, trp1-901, leu2-3, 112, gal4Δ, gal80Δ, met⁻, MEL1*
Y187 (Harper et al. 1993)	*MATα, ura3-52, his3-200, ade2-101, trp1-901, leu2-3, 112, gal4Δ, gal80Δ, met⁻, URA3 : : GAL1$_{UAS}$-GAL1$_{TATA}$-LacZ, MEL1*

Table 4.3 Bait plasmids (and other plasmids used for their construction) used in this study

Plasmid name (and size)	Features
pDEST22 (8923 bp, Invitrogen)	The *att*R Gateway cassette (*att*R1, *ccd*B, Cam^R, *att*R2) of this plasmid was PCR-amplified for cloning into pHIS2.1; pDEST22 also contains Amp^R, pUC ori, f1 intergenic region, *TRP1*, and *CEN6/ARS4*
pHIS2.1 (7190 bp, Clontech)	Bait plasmid for the Y1H system; the bait sequence is cloned into the multiple cloning site upstream of reporter gene *HIS3*; the plasmid also contains Kan^R, ColE1 ori, *TRP1*, and *CEN6/ARS4*
pHIS2.1-AE-box_2 (7202 bp)	A 3-tandem repeat of AE box 2 was cloned as bait sequence between *Sac*I and *Spe*I of pHIS2.1 upstream of reporter gene *HIS3*
pDEST-HIS2.1 (9024 bp)	pHIS2.1 converted to a gateway plasmid: *att*R Gateway cassette (*att*R1, *ccd*B, Cam^R, *att*R2) was cloned between *Sac*I and *Spe*I of pHIS2.1 upstream of reporter gene *HIS3*
pDONR221 (4762 bp, Invitrogen)	PCR products flanked by *att*B recombination sites are initially cloned into pDONR221; the plasmid contains a *att*P Gateway cassette (*att*P1, *ccd*B, Cam^R, *att*P2), Kan^R, and pUC ori
PCR product of an *Vcn_regA* intron was cloned by BP recombination reaction into pDONR221 (target construct in red with intron sequence between *att*L sites): *att*B1-regA_Intron_X-*att*B2 × pDONR221-*ccd*B ➔ pENTR221-regA_Intron_X × *att*R1-ccdB-*att*R2	
pENTR221-regA_Intron_3 (3216 bp)	intron 3: +1,229 to +1,900
pENTR221-regA_Intron_5 (3490 bp)	part of intron 5: +2,885 to +3,830
pENTR221-regA_Intron_7 (3804 bp)	intron 7: +7,280 to +8,539
regA intron sequence was then shuttled from pENTR221 to pDEST-HIS2.1 by LR recombination reaction (final prey plasmid in red; intron between *att*B sites acts as bait sequence upstream of reporter gene *HIS3*): pENTR221-regA_Intron_X × pDEST-HIS2.1-*ccd*B ➔ pEXP-HIS2.1-regA_Intron_X × pDONR221-*ccd*B	
pEXP-HIS2.1-regA_Intron_3 (7900 bp) pEXP-HIS2.1-regA_Intron_5 (8174 bp) pEXP-HIS2.1-regA_Intron_7 (8488 bp)	

Table 4.4 PCRs used for construction of bait plasmids

All PCRs were run in a RoboCycler Gradient 96 (Stratagene) except when noted otherwise; additional primers used for sequencing of PCR products are also listed; F, forward primer; R, reverse primer; SP, sequencing primer.

regA region*	Primer sequences (5' to 3', artificial sequences are in red) and conditions
regA Intron 3–Exon 5† (+1158 to +2361 bp)	F CGTTATGGCAAAGCCCTCT R AGCACGCTCTCACCTCCAT 50 µL PCR mix: 0.2 µM each Primer, Platinum PCR SuperMix High Fidelity PCR program: 95°C/2 min—[94°C/0.5 min; 50°C/0.5 min; 68°C/80 sec]×40—68°C/10 min (in Bio-Rad C1000 Touch Thermal Cycler)
attR Gateway cassette (4663 to 6508 bp)	F MluI SacI ACGCGTGAGCTCACAAGTTTGTACAAAAAAGCTG R MluI SpeI ACGCGTACTAGTACCACTTTGTACAAGAAAGCTG 50 µL PCR mix: 0.2 µM each Primer, 2.5 U *Taq*, 1X AB, 0.5X ES, 1.5 mM $MgSO_4$, 0.2 mM each dNTPs PCR Program: 94°C/2 min—[94°C/0.5 min; 55°C/1 min; 68°C/2 min]×35—68°C/10 min SP CAGTCAGTTGCTCAATGTACC SP CTGAGATCAGCCACTTCTTCC
regA Intron 3 (+1229 to +1900 bp)	F attB1 GGGGACAAGTTTGTACAAAAAAGCAGGCTGTAAGCCTGTTCCGCTTCC R attB2 GGGGACCACTTTGTACAAGAAAGCTGGGTCTGCAGACAATGCAAAAAGC 50 µL PCR mix: 0.2 µM each Primer, 1 U *Taq*, 1X HB, 2 mM $MgSO_4$, 0.2 mM each dNTPs PCR program: 94°C/2 min—[94°C/0.5 min; 50°C/1 min; 68°C/2 min]×35—68°C/10 min
Part of *regA* Intron 5 (+2885 to +3830 bp)	F attB1 GGGGACAAGTTTGTACAAAAAAGCAGGCTCATTGATATCAGATGTAAC R attB2 GGGGACCACTTTGTACAAGAAAGCTGGGTGGATATCCGATTGAGGCAGG 50 µL PCR mix: 0.2 µM each Primer, 1 U *Taq*, 1X HB, 2 mM $MgSO_4$, 0.2 mM each dNTPs PCR program: 94°C/2 min—[94°C/0.5 min; 50°C/1 min; 68°C/2 min]×35—68°C/10 min
regA Intron 7 (+7280 to + 8539 bp)	F attB1 GGGGACAAGTTTGTACAAAAAAGCAGGCTGGCGGCTCTTCCGGCAGTG R attB2 GGGGACCACTTTGTACAAGAAAGCTGGGTTGCGGAACCTGCGACGGTG 50 µL PCR mix: 0.2 µM each Primer, 2.5 U *Taq*, 1X AB, 1X ES, 1.5 mM $MgSO_4$, 0.2 mM each dNTPs PCR program: 94°C/2 min—[94°C/0.5 min; 55°C/1 min; 68°C/2 min]×35—68°C/10 min SP CTCCTGCAACAGCACCAACG SP CCTGAAGGTCAAGGTGAAGC

Taq, Platinum *Taq* DNA Polymerase High Fidelity; HB, High Fidelity PCR Buffer; AB, PCRx Amplification Buffer; ES, PCRx Enhancer Solution (all reagents Invitrogen); all oligonucleotides were provided by Sigma Genosys

*for *regA* relative to gDNA; for *attR* Gateway cassette relative to plasmid pDEST22

†designed by Aurora M. Nedelcu

Table 4.5 Prey plasmids and other plasmids used in this study

Plasmid name (and size)	Plasmid features
pBSIISK(+)B3TF_DBD (3351 bp, Biomatik)	The cDNA sequence encoding amino acids 4–114 of the predicted B3TF (B3 domain transcription factor) of *V. carteri* f. *nagariensis* was codon-optimized for *S. cerevisiae*, synthesized *de novo* with flanking *in vivo* recombination sites SMART III upstream and CDS III downstream, and cloned into the *Eco*RV site of pBSIISK(+); also contains Amp^R, pUC ori, and f1 intergenic region
pGADT7-Rec2 (7588 bp, Clontech)	Prey plasmid of the Y1H system; prey is under the control of a ADH1 promoter and contains sequences encoding SV40 NLS followed by GAL4AD, hemagglutinin epitope tag, and SMART III and CDS III used for homologous recombination in yeast. The linearized plasmid is closed *in vivo* in yeast by recombination; endogenous recombinases integrate cDNA containing SMART III and CDS III sequences into the plasmid, and as a result the expressed cDNA is fused to GAL4 activation domain; the plasmid also contains Amp^R, pUC ori, *LEU2*, and *CEN6/ARS4*
pGADT7-Rec2 derivatives formed by *in vivo* recombination in yeast	
pGADT7-Rec2-dofA_DBD (7744 bp)	The cDNA encoding the DNA binding domain (AA93–152) of the predicted *Vcn_dofA* protein was cloned between SMART III and CDS III of pGADT7-Rec2 in frame with the GAL4 activation domain
pGADT7-Rec2-dofA_FL (9604 bp)	The cDNA of the predicted full-length *Vcn_dofA* protein was cloned between SMART III and CDS III of pGADT7-Rec2 in frame with the GAL4 activation domain
pGADT7-Rec2-B3TF_DBD (7876 bp)	cDNA sequence encoding amino acids 4–114 of the predicted B3TF of *V. carteri* f. *nagariensis* was cloned between SMART III and CDS III of pGADT7-Rec2 in frame with the GAL4 activation domain

Table 4.6 RT-PCR and PCR for prey

All PCRs were run in a RoboCycler Gradient 96 (Stratagene) except where noted otherwise; GSP, gene specific primer for reverse transcription; F, forward primer; R, reverse primer; SP, sequencing primer.

Region	Primer sequences (5' to 3', artificial sequences are in red) and conditions
dofA, full length (+1 to +2040 bp)*	CDS III GSP ATCGATGCCCACCCTCTAGAGGCCGAGGCGGCCGACTTACCTACCACCCGAGTATGC 20 µL RT mix: 0.1 µM GSP, 200 U SSIII, 40 U RnaseOut, 1X FSB, 5 mM DTT, 0.5 mM each dNTPs RT program: 50°C/1 h—85°C/5 min—on ice SMART III F GAATTCCACCCAAGCAGTGGTATCAACGCAGAGTGGATGGAGGGCGCCTCGCGAG CDS III R ATCGATGCCCACCCTCTAGAGGCCGAGGCGGCCGACTTACCTACCACCCGAGTATGC 50 µL PCR mix: 0.2 µM each Primer, 2.5 U *Taq*, 1X AB, 1X ES, 1.5 mM $MgSO_4$, 0.2 mM each dNTPs PCR program: 94°C/2 min—[94°C/0.5 min; 60°C/1 min; 68°C/2.5 min]×45—68°C/10 min
dofA, DNA-binding domain (+277 to +456 bp)*	20 µL RT mix: 2.5 µM oligo$(dT)_{20}$, 15 U TS and 40 U RnaseOut, 1X SB, 5 mM DTT, 1 mM each dNTPs RT program: 50°C/1 h—85°C/5 min—on ice SMART III F GAATTCCACCCAAGCAGTGGTATCAACGCAGAGTGGCGGCCCGAGAAAAAGGAAACG CDS III R ATCGATGCCCACCCTCTAGAGGCCGAGGCGGCCGACGCTCTTGCTCTTGCGGCGACC 50 µL PCR mix: 0.2 µM each Primer, 1 U *Taq*, 1X HB, 2 mM $MgSO_4$, 0.2 mM each dNTPs PCR program: 94°C/2 min—[94°C/0.5 min; 57°C/1 min; 68°C/2.5 min]×45—68°C/10 min
B3TF, DNA-binding domain (701 to 1084 bp)†	SMART III F GAATTCCACCCAAGCAGTGG CDS III R ATCGATGCCCACCCTCTAG 50 µL PCR mix: 0.2 µM each Primer, Platinum PCR SuperMix High Fidelity PCR program: 95°C/2 min—[94°C/0.5 min; 50°C/0.5 min; 68°C/0.5 min]×30—68°C/10 min (in Bio-Rad C1000 Touch Thermal Cycler)
Colony PCR for prey cDNA in (Clontech)	F CTATTCGATGATGAAGATACCCCACCAAACCC R GTGAACTTGCGGGGTTTTTCAGTATCTACGAT 50 µL PCR mix: 0.2 µM each Primer, 1 U *Taq*, 1X HB, 2 mM $MgSO_4$, 0.2 mM each dNTPs or 0.4 µM each Primer, Platinum PCR SuperMix High Fidelity or 0.2 µM each Primer, 1X A2P, 1X A2B, 0.2 mM each dNTPs with PCR program: 94°C/5 min—[94°C/0.5 min; 68°C/3 min]×35—68°C/10 min alternatively: 50 µL PCR mix: 0.2 µM each Primer, 2.5 U *Taq* (Sigma), 1X Sigma Buffer, 0.2 mM each dNTPs with PCR program: 94°C/5 min—[94°C/0.5 min; 68°C/0.5 min; 72°C/3 min]×35—68°C/10 min

SSIII, SuperScriptIII Reverse Transcriptase; TS, ThermoScript Reverse Transcriptase; SB, cDNA Synthesis Buffer; FSB, First-Strand Buffer; *Taq*, Platinum *Taq* DNA Polymerase High Fidelity; HB, High Fidelity PCR Buffer; AB, PCRx Amplification Buffer; ES, PCRx Enhancer Solution (all reagents Invitrogen); A2P, Advantage 2 Polymerase; A2B, Advantage 2 PCR Buffer (both Clontech)

*relative to cDNA

†relative to plasmid pBS_II_SK(+)-B3TF_DBD (Biomatik)

Table 4.7 Summary of cDNA library screens of *regA* introns

Either oligo(dT) cDNA libraries (generated with CDS III oligo(dT) primer) or RH libraries (generated with CDS III/6 random hexamer primer) were screened on the number of SD_{-TLH} selection plates and concentration of 3AT indicated. Either the Woods (2001) or Clontech (Matchmaker One-Hybrid Library Construction & Screening Kit) transformation protocol was used.

Yeast strain	Bait plasmid	cDNA library	cDNA [µg]	Transformation protocol	SD_{-TLH} plates 3AT [mM]	# selection plates
Y187	pEXP-HIS2.1-regA_Intron_3	oligo(dT)	ND	Woods	3	100
Y187	pEXP-HIS2.1-regA_Intron_3	oligo(dT)	ND	Woods	1	100
Y187	pEXP-HIS2.1-regA_Intron_3	RH	ND	Woods	1	100
Y187	pEXP-HIS2.1-regA_Intron_3	oligo(dT)	5.8	Woods	1	20
Y187	pEXP-HIS2.1-regA_Intron_3	oligo(dT)	5.8	Woods	1	20
Y1HGold	pEXP-HIS2.1-regA_Intron_5	oligo(dT)	4.7	Clontech	50	100
Y1HGold	pEXP-HIS2.1-regA_Intron_7	oligo(dT)	5.6	Clontech	100	20
Y1HGold	pEXP-HIS2.1-regA_Intron_7	RH	4	Clontech	100	100
Y1HGold	pEXP-HIS2.1-regA_Intron_7	oligo(dT)	5.6	Clontech	100	100

Table 4.8 Single gene screens

Bait plasmid	cDNA
pEXP-HIS2.1-regA_Intron_3	***dofA*, DNA-binding domain**
pEXP-HIS2.1-regA_Intron_3	*dofA*, full length
pEXP-HIS2.1-regA_Intron_3	**B3TF, DNA binding domain**
pHIS2.1-AE-box_2	B3TF, DNA binding domain

Table 4.9 Interaction of prey protein DofA with bait sequence *regA* intron 3.

The yeast strain Y1HGold was transformed with either both a bait plasmid and a prey plasmid or with a bait plasmid alone. The bait plasmid contained either the *regA* intron 3 sequence (pEXP-HIS2.1-regA_Intron_3) or a 3-tandem repeat of the murine p53 binding site (p53HIS2, Clontech) used as a negative control. The prey plasmid (formed by *in vivo* recombination) encoded a fusion protein of the GAL4 AD and either the DNA binding domain of DofA (DofA DBD, AA93-152, pGADT7-Rec2-dofA_DBD) or the full length protein (DofA FL, pGADT7-Rec2-dofA_FL). The transformed yeast cells were plated on selective media (SD_{-TLH} for bait and prey plasmid, or SD_{-TH} for bait plasmid alone) containing varying amount of 3AT to test for interaction between bait and prey (if co-transformed with both plasmids) and to determine background expression of the reporter gene *HIS3* on the bait plasmid (if transformed with bait plasmid only). In addition, cells were also plated on SD_{-T} or SD_{-TL} to confirm successful transformation (data not shown). After 5 d plates were scored for the absence (-) or presence (+) of colonies.

		Colonies on selection plates (either SD_{-TLH} or SD_{-TH}) with 3AT [mM]				
Bait Sequence	**Prey Protein**	0	1	3	10	50
***regA* intron 3**	**DofA DBD**	+	+	+	+	-
regA intron 3	DofA FL	+	-	-	-	-
***regA* intron 3**	***no prey***	+	+	-	-	-
p53 binding site	DofA DBD	+	+	+	+	-
p53 binding site	***no prey***	+	+	+	+	-

Table 4.10 interaction of B3TF DBD with *regA* intron 3 or AE box 2.

A bait plasmid alone or together with a prey plasmid (formed by *in vivo* recombination) encoding a fusion protein of the GAL4 AD and the DNA binding domain of B3TF (B3TF DBD; AA4–114; on plasmid pGADT7-Rec2-B3TF_DBD) were transformed into the yeast strain Y1HGold. The bait plasmid contained either the *regA* intron 3 sequence (pEXP-HIS2.1-regA_Intron_3) or a 3-tandem repeat of AE box 2 (pHIS2.1-AE-box_2). The transformed yeast cells were plated on selective media (SD_{-TLH} for bait and prey plasmid, or SD_{-TH} for bait plasmid alone) containing varying amount of 3AT to test for interaction between bait and prey (if co-transformed with both plasmids) and to determine background expression of the reporter gene *HIS3* on the bait plasmid (if transformed with bait plasmid only). In addition, cells were also plated on SD_{-T} or SD_{-TL} to confirm successful transformation (data not shown). After 5 d plates were scored for the absence (-) or presence (+) of colonies.

		Colonies on selection plates (either SD_{-TLH} or SD_{-TH}) with 3AT [mM]		
Bait Sequence	**Prey Protein**	0	50	100
regA intron 3	B3TF DBD	+	-	-
regA intron 3	*no prey*	+	-	-
AE box 2	B3TF DBD	+	+	-
AE box 2	*no prey*	+	+	-

Table 4.11 Summary of Y1H screens of *regA* intron 3

Either oligo(dT) or random hexamer (RH) cDNA libraries were transformed into yeast strain Y187 containing bait plasmid pEXP-HIS2.1-regA_Intron_3 using the Woods and Grietz (2001) protocol and plated on the number of SD_{-TLH} selection plates and concentration of 3AT indicated. Because the number of positive colonies was too large, positives were picked based on size (≥ 2 mm) and their cDNA insert was amplified by colony PCR. The insert was sequenced if it was at least 300 bp in size.

cDNA library (amount [µg])	SD_{-TLH} plates 3AT [mM]	SD_{-TLH} selection plates	Background? (> 400 colonies)	unique clones [$x10^5$]	# positives (colony size ≥ 2 mm)	Inserts sequenced
oligo(dT) (ND)	3	100	–	2.94	–	–
oligo(dT) (ND)	1	100	+	2.19	11	5
oligo(dT) (5.8)	1	20	+	2.06	19	7
oligo(dT) (5.8)	1	20	+	4.46	21	7
RH (ND)	1	100	+	0.7	4	3

Table 4.12 Sequenced positives of Y1H screen of *regA* intron 3.

Gene (JGI Protein ID)	Comments (predicted length of encoded protein)
phosphoribulokinase (104265)	**maps to last exon (113 AA)**
ribosomal protein S8E (72506)	maps to part of the last intron and to last exon (exon is in frame), represented twice in screen (74 AA)
unknown protein (N/A)	**(18 AA)**
unknown protein (95859)	includes intron of predicted gene, cloned in antisense orientation (part of sequence missing, length unknown)
Cytochrome b5 (80369)	**3'UTR, cloned in antisense orientation (30 AA)**
homolog of *C. reinhardtii* RubisCO activase (105291)	3'UTR (29 AA)
oxygen-evolving enhancer protein 1, *OEE1* (83003)	**3'UTR (53 AA)**
homolog of *C. reinhardtii* Photosystem II reaction center W protein, *PSBW* (106616)	3'UTR (10 AA)
Selenoprotein (121242)	**3'UTR (38 AA)**
glutaredoxin 6, CGFS type (109678)	3'UTR (55 AA)
RNA polymerase II general transcription factor, BTF3 (104715)	**3'UTR (14 AA)**
subunit SRm300 of Splicing coactivator SRm160/300, (103023)	3'UTR (10 AA)
Unnamed Protein (118141)	**maps to predicted intron (5 AA)**
Predicted E3 ubiquitin ligase (117815)	maps to intron (6 AA)
unknown protein (104504)	**maps to predicted intron (6 AA)**
unknown protein (108619)	maps to predicted intron (19 AA)
unknown protein (103002)	**maps to predicted intron, cloned in antisense orientation (86 AA)**
ribosomal protein S2 (109242)	out of frame (77 AA)
NaCl-inducible protein, *nipA* (83314)	**out of frame (17 AA)**
unknown protein (N/A)	either out of frame or only contains 3'UTR (131 AA)
spermidine synthase (76291)	**out of frame (54 AA)**

Table 4.13 Summary of Y1H screens of *regA* intron 7

Either a oligo(dT) or random hexamer (RH) cDNA library was transformed into yeast strain Y1HGold together with bait plasmid pEXP-HIS2.1-regA_Intron_7 using the Clontech kit and plated on the number of SD_{-TLH} selection plates indicated containing 100 mM 3AT. If the number of positive colonies received was too large, positives were picked based size (≥ 2 mm) and their cDNA insert was amplified by colony PCR. The insert was sequenced if it was at least 300 bp in size.

cDNA library (amount [µg])	SD_{-TLH} selection plates	Background? (> 400 colonies)	unique clones [$x10^5$]	# positives	Inserts sequenced
RH (4)	100	–	2.14	17	10
oligo(dT) (5.6)	100	–	>10	105	42
oligo(dT) (5.6)	20	> 400	8.18	124 (selected based on colony size)	19

Table 4.14 Sequenced positives of Y1H screen of *regA* intron 7.

Gene (JGI Protein ID)	Comments
unknown (N/A)	low complexity sequence; no predicted DBD (32 AA)
unknown (N/A)	low complexity sequence; no predicted DBD (51 AA)
unknown (N/A)	low complexity sequence; no predicted DBD (37 AA)
unknown (N/A)	low complexity sequence; no predicted DBD (38 AA)
unknown (N/A)	overlap with EST; predicted thioredoxin-like fold (45 AA)
ribosomal protein L7, *rpl7* (81255)	maps to exon 3 up to 3'UTR; contains point mutation V131A (131 AA)
ribosomal protein L35A, *rpl35A* (103447)	maps from exon 1 to 3'UTR (74 AA)
ribosomal protein S8, *rps8* (72506)	maps to complete last exon and 3'UTR, represented 17 times in screens (73 AA)
G protein beta subunit-like protein (78914)	maps to exon 4 and 5, encodes WD40 repeat-like domain involved in protein-protein interactions (67 AA)
gon18, ortholog of *C. reinhardtii LHCA8* (108852)	gonidial gene; maps to last exon and 3'UTR; chlorophyll A-B binding domain (35 AA)
unknown protein (73821)	Chlorophyll A-B binding protein (53 AA)
unknown protein (121640)	maps to 5'UTR, complete ORF and 3'UTR, 5'UTR encodes premature stop codon (23 AA derived from 5'UTR)
polyubiquitin, *ubqC* (83910)	maps to 5'UTR, complete ORF and 3'UTR; 5'UTR encodes premature stop codon (5 AA derived from 5'UTR)
Oxygen-evolving enhancer protein 2, *oeeB* (121519)	maps to last exon and 3'UTR (10 AA)
protein likely involved in thiamine biosynthesis (74899)	maps to last exon and 3'UTR (9 AA)
ribosomal protein S30, *rps30* (78308)	maps to part of last exon and 3'UTR (6 AA)
unknown (N/A)	overlap with EST (5 AA)
unknown (N/A)	overlap with EST (1 AA)
unknown (N/A)	overlap with EST (5 AA)
unknown (N/A)	overlap with EST (16 AA)
unknown (N/A)	(18 AA)
unknown (N/A)	(7 AA)
ribosomal protein L27A, *rpl27A* (77145)	cloned in antisense orientation (some sequence missing, ORF unknown)
ortholog of *C. reinhardtii PSBX* (106026)	cloned in antisense orientation (some sequence missing, ORF unknown)
light-harvesting protein of photosystem I, *lhcaE* (106964)	cloned in antisense orientation (10 AA)
unknown protein (78555)	cloned in antisense orientation (5 AA)
dehydrogenase (121544)	maps to predicted intron (9 AA)
predicted RNA-binding protein (105597)	predicted 3'UTR, no predicted DNA binding domain (40 AA)
unknown protein (104025)	predicted 3'UTR, no predicted DNA binding domain (98 AA)
RNA polymerase II general transcription factor BTF3 and related protein (104715)	3'UTR (13 AA)
L-ascorbate peroxidase, *apx1* (82395)	3'UTR (14 AA)
elongation factor 2, *efg2* (109649)	3'UTR (11 AA)
manganese superoxide dismutase, *msd1* (108150)	3'UTR (17 AA)
transketolase (75893)	3'UTR (7 AA)
unknown protein (105818)	3'UTR (16 AA)
unknown protein (85029)	3'UTR (9 AA)
ribulose-bisphosphate carboxylase small subunit *rbcS* (83349)	3'UTR (28 AA)
ribosomal protein S26, *rpl26* (76074)	3'UTR (3 AA)
NADH:ubiquinone oxidoreductase (complex I) B22 subunit, *nuoB22* (99267)	3'UTR (9 AA)
manganese superoxide dismutase *msd3* (72831)	3'UTR (4 AA)
ribosomal protein L6, *rpl6* (83175)	out of frame (55 AA)
gon18, ortholog of C. reinhardtii *LHCA8* (108852)	out of frame (8 AA); gonidial gene
transcription factor *MBF1* (110064)	out of frame (27 AA)
60S acidic ribosomal protein P0 (84328)	out of frame (37 AA)
ribosomal protein S27, *rps27* (85510)	out of frame (6 AA)
ribosomal protein L31, *rpl31* (103828)	out of frame (10 AA)
ribosomal protein L40, *rpl40* (64049)	out of frame (15 AA)
ATP binding protein (74289)	out of frame (33 AA)
gon34, ortholog of C. reinhardtii *ATPG* (83961)	out of frame (38 AA)
ribosomal protein L6, *rpl6* (83175)	out of frame (55 AA)
ribosomal protein S25, rps25 (82071)	out of frame (6 AA)
ribulose-bisphosphate carboxylase small subunit rbcS (121519)	out of frame (44 AA)
ribosomal protein L17, rpl17 (85333)	out of frame (40 AA)
photosystem I reaction center subunit psaK (109536)	out of frame (18 AA)
ribosomal protein L29, rpl29 (85396)	out of frame (6 AA)

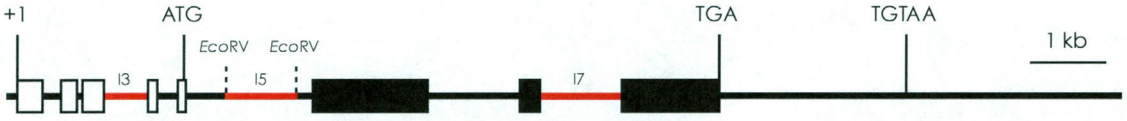

Figure 4.1 *regA* gene structure (adapted from Stark, Kirk, and Schmitt 2001).

The *regA* gene contains 8 exons and 7 introns. Three of the introns (indicated in red) are important for *regA* regulation; intron 3 and a fragment of intron 5 (between 2 *Eco*RV sites) are necessary for *regA* expression independent of cell type while intron 7 is important for *regA* repression in gonidia. Transcription start site (+1), translation start site (ATG), translation stop site (TGA) and polyadenylation site (TGTAA) are indicated. Open boxes show noncoding exons, closed boxes designate coding exons, and lines between exons indicate introns.

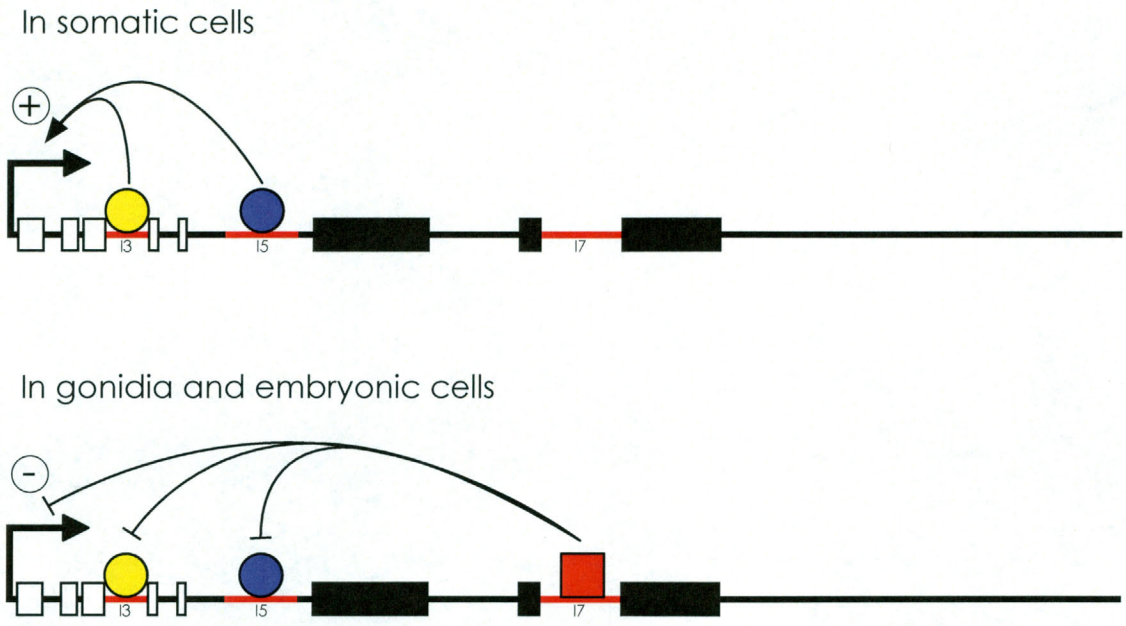

Figure 4.2 Model for *regA* regulation (based on Stark, Kirk, and Schmitt 2001).

In both somatic cells and gonidia, the enhancers postulated to be present in intron 3 and 5 (I3 and I5) are bound by transcription factors (circles). In somatic cells these transcription factors cooperatively stimulate *regA* expression maybe by stabilizing each other's binding to their respective *cis*-regulatory element. In gonidia and embryonic cells (but not in somatic cells), a third transcription factor (square) is active and binds to a silencer in intron 7 (I7); this factor represses *regA* transcription, even overriding the *trans*-acting factors bound to the enhancers.

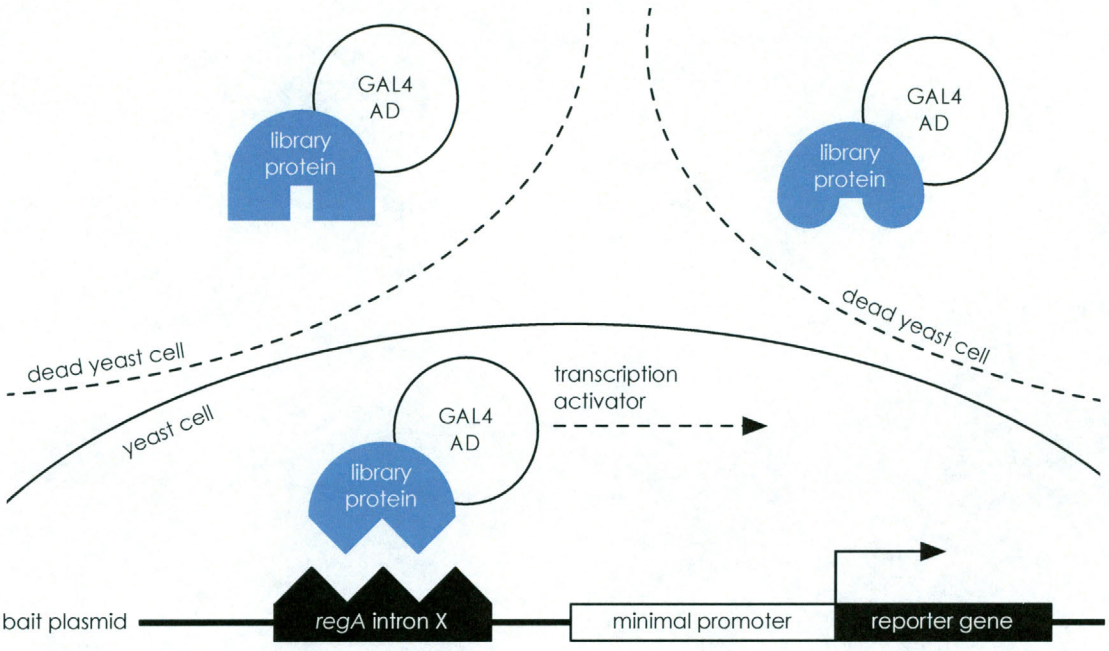

Figure 4.3 The principle of the yeast one-hybrid assay.

To identify *trans*-acting factors binding to a specific *regA* intron, the intron was cloned as bait sequence in front of the reporter gene *HIS3* on the bait plasmid. A cDNA library was cloned into a second plasmid (called the prey plasmid) and fused to the GAL4 activation domain (GAL4 AD) forming the prey. Bait plasmid and prey plasmid were transformed into yeast. If the prey protein interacts with the intron used as bait, then the close proximity of the GAL4 AD to the minimal promoter stimulates HIS3 expression and the respective yeast cell can survive on selective medium lacking histidine; in the absence of the interaction, the yeast cell dies The prey plasmid insert of surviving cells is then sequenced to identify the library protein that interacts with the bait.

```
   SacI          3XAE-box 2          SpeI
    5'-C AGAATCTT AGAATCTT AGAATCTT A-3'
3'-TCGAG TCTTAGAA TCTTAGAA TCTTAGAA TGATC-5'
```

Figure 4.4 AE box 2 adapter

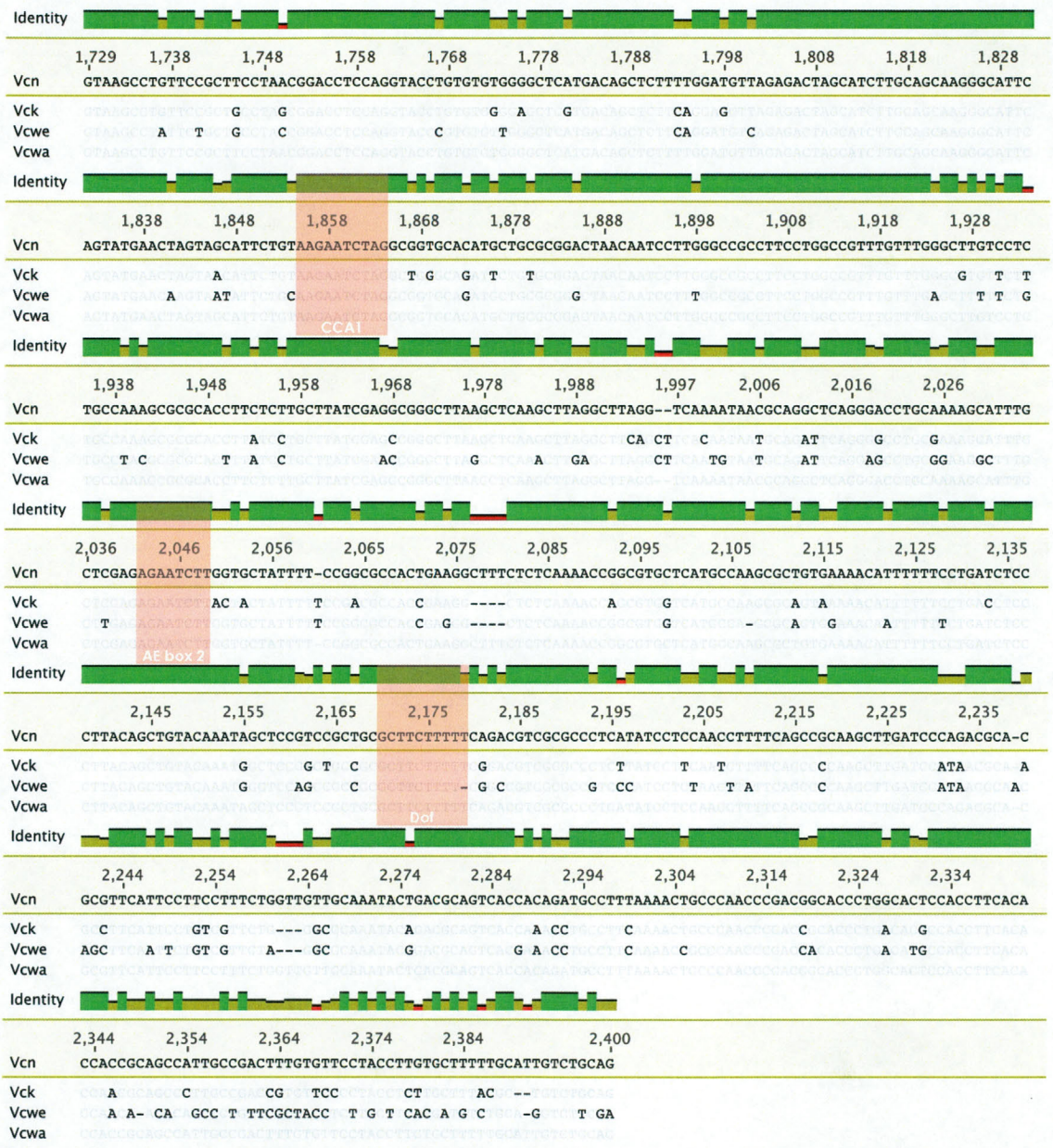

Figure 4.5 Potential binding sites (red boxes) of transcription factors in *regA* intron 3.

regA intron 3 sequences from 4 *Volvox carteri* formas—*nagariensis* (Vcn), *kawasakiensis* (Vck), *weismannia* (Vcw), and *wagii* (Vcwa)—were aligned using ClustalW (Thompson, Higgins, and Gibson 1994). TESS predicted a potential Dof binding site for Vcn only. NSITEH predicted a CCA1 motif and AE box 2 as binding sites conserved among all 4 formas.

4.5 References

Adams CR, Stamer KA, Miller JK, McNally JG, Kirk MM, Kirk DL. 1990. Patterns of organellar and nuclear inheritance among progeny of two geographically isolated strains of *Volvox carteri*. Curr Genet 18:141–153.

Amberg DC, Burke DJ, Strathern JN. 2006. Isolation of plasmid DNA from yeast cells: a ten-minute preparation. CSH Protoc 2006.

Bassett CL. 2007. Regulation of gene expression in plants. Springer Verlag.

Chomczynski P, Sacchi N. 1987. Single-step method of RNA isolation by acid guanidinium thiocyanate-phenol-chloroform extraction. Anal Biochem 162:156–159.

Connelly C, McCormick MK, Shero J, Hieter P. 1991. Polyamines eliminate an extreme size bias against transformation of large yeast artificial chromosome DNA. Genomics 10:10–16.

Deplancke B, Dupuy D, Vidal M, Walhout AJM. 2004. A gateway-compatible yeast one-hybrid system. Genome Res. 14:2093–2101.

Deyholos MK, Sieburth LE. 2000. Separable whorl-specific expression and negative regulation by enhancer elements within the AGAMOUS second intron. Plant Cell 12:1799–1810.

Duncan L, Nishii I, Howard A, Kirk DL, Miller SM. 2006. Orthologs and paralogs of *regA*, a master cell-type regulatory gene in *Volvox carteri*. Curr Genet 50:61–72.

Hameister S, Becker B, Holtgrefe S, Strodtkötter I, Linke V, Backhausen JE, Scheibe R. 2007. Transcriptional regulation of NADP-dependent malate dehydrogenase: comparative genetics and identification of DNA-binding proteins. J Mol Evol 65:437–455.

Hanschen ER, Ferris PJ, Michod RE. 2014. Early evolution of the genetic basis for soma in the Volvocaceae. Evolution.

Harper JW, Adami GR, Wei N, Keyomarsi K, Elledge SJ. 1993. The p21 Cdk-interacting protein Cip1 is a potent inhibitor of G1 cyclin-dependent kinases. Cell 75:805–816.

Jones P, Binns D, Chang H-Y, Fraser M, Li W, McAnulla C, McWilliam H, Maslen J, Mitchell A, Nuka G, et al. 2014. InterProScan 5: genome-scale protein function classification. Bioinformatics.

Kang Y, Mitchell DR. 1998. An intronic enhancer is required for deflagellation-induced transcriptional regulation of a *Chlamydomonas reinhardtii* dynein gene. Mol Biol Cell 9:3085–3094.

Kirk DL, Kirk MM. 1983. Protein synthetic patterns during the asexual life cycle of *Volvox carteri*. Dev Biol 96:493–506.

Kirk DL. 1998. *Volvox*: the molecular genetic origins of multicellularity and cellular differentiation. Cambridge.

Kirk MM, Kirk DL. 1985. Translational regulation of protein synthesis, in response to light, at a critical stage of *Volvox* development. Cell 41:419–428.

Kirk MM, Ransick A, McRae SE, Kirk DL. 1993. The relationship between cell size and cell fate in *Volvox carteri*. J Cell Biol 123:191–208.

Kirk MM, Stark K, Miller SM, Müller W, Taillon BE, Gruber H, Schmitt R, Kirk DL. 1999. *regA*, a *Volvox* gene that plays a central role in germ-soma differentiation, encodes a novel regulatory protein. Development 126:639–647.

Llorca CM, Potschin M, Zentgraf U. 2014. bZIPs and WRKYs: two large transcription factor families executing two different functional strategies. Frontiers in Plant Science 5:169.

Lumbreras V, Stevens D, Purton S. 1998. Efficient foreign gene expression in *Chlamydomonas reinhardtii* mediated by an endogenous intron. Plant J 14:441–447.

MacDonald PN. 2001. Two-hybrid systems. Humana Pr Inc.

Park SC, Kwon HB, Shih MC. 1996. *Cis*-acting elements essential for light regulation of the nuclear gene encoding the A subunit of chloroplast glyceraldehyde 3-phosphate dehydrogenase in *Arabidopsis thaliana*. Plant Physiol 112:1563–1571.

Riethoven J-JM. 2010. Regulatory regions in DNA: promoters, enhancers, silencers, and insulators. Methods Mol Biol 674:33–42.

Romanel EAC, Schrago CG, Couñago RM, Russo CAM, Alves-Ferreira M. 2009. Evolution of the B3 DNA binding superfamily: new insights into REM family gene diversification. PLoS ONE 4:e5791.

Roy S, Choudhury SR, Singh SK, Das KP. 2012. Functional analysis of light-regulated promoter region of AtPolλ gene. Planta 235:411–432.

Sambrook J, Russel DW. 2001. Molecular cloning: A laboratory manual. 3rd ed.

Schug J. 2008. Using TESS to predict transcription factor binding sites in DNA sequence. Curr Protoc Bioinformatics Chapter 2:Unit 2.6.

Sieburth LE, Meyerowitz EM. 1997. Molecular dissection of the *AGAMOUS* control region shows that *cis* elements for spatial regulation are located intragenically. Plant Cell 9:355–365.

Spitz F, Furlong EEM. 2012. Transcription factors: from enhancer binding to developmental control. Nat Rev Genet 13:613–626.

Stark K, Kirk DL, Schmitt R. 2001. Two enhancers and one silencer located in the introns of *regA* control somatic cell differentiation in *Volvox carteri*. Genes Dev 15:1449–1460.

Thompson JD, Higgins DG, Gibson TJ. 1994. CLUSTAL W: improving the sensitivity of progressive multiple sequence alignment through sequence weighting, position-specific gap penalties and weight matrix choice. Nucleic Acids Res 22:4673–4680.

Vidal M, Legrain P. 1999. Yeast forward and reverse "n"-hybrid systems. Nucleic Acids Res 27:919–929.

Woods RA, Gietz RD. 2001. High-efficiency transformation of plasmid DNA into yeast. Methods Mol Biol 177:85–97.

Yanagisawa S. 1997. Dof DNA-binding domains of plant transcription factors contribute to multiple protein-protein interactions. Eur J Biochem 250:403–410.

Yanagisawa S. 2002. The Dof family of plant transcription factors. Trends Plant Sci 7:555–560.

Yanagisawa S. 2004. Dof domain proteins: plant-specific transcription factors associated with diverse phenomena unique to plants. Plant Cell Physiol 45:386–391.

Chapter 5 Conclusions

The evolution of cell differentiation is responsible for the increase in complexity and diversity observed among the extant multicellular lineages. Nevertheless, little is known about the early steps in the transition to multicellular forms with different cell types, especially with respect to the separation of vegetative and reproductive cells between a somatic and a germ line. *Volvox carteri* is a simple multicellular alga that consists of only two cell types (somatic and reproductive) whose cell fate is established early during development through the differential expression of *regA* (a master regulatory gene specifically induced in somatic cells). Its low level of morphological complexity and its simple genotype-phenotype map make this alga an ideal system with which to address the mechanistic and evolutionary basis for the evolution of germ-soma separation. The goal of this work was to investigate the regulation of *regA* using both mechanistic and evolutionary approaches. In this context, the specific objectives of this study were: 1) to explore *regA* expression patterns under various conditions, and 2) to identify transcription factors controlling *regA* expression. A deeper understanding of *regA* regulation will provide insight into the evolution of multicellularity/cell differentiation as well as cooperation, and will reveal how genes are co-opted during these processes. Below, I discuss how my findings relate to these general and important topics in evolutionary biology. In the last section I present some future directions emerging from my work.

5.1 Evolution of multicellularity and cell differentiation

The evolution of life is marked by striking changes in complexity levels that involve groups of individuals becoming integrated into a larger whole; such events are known as

major transitions in individuality. These transitions involve the reorganization of fitness as individuals within the group incur a fitness cost while at the same time increase the fitness of the higher level individual that possesses traits on which natural selection can act (Michod 2007). One such major transition is the evolution of multicellularity, which requires the separation of reproductive and survival function between germ and soma (Michod 2007); the somatic cells forgo their own reproduction (i.e. decrease their direct fitness) to increase the survival of the multicellular individual.

The transition to multicellularity is thought to occur in incremental steps, each associated with an increase in fitness. The first step might be the formation of cell groups, and these cells increasingly cooperate among themselves to the point where a division of labor involving cell specialization emerges (Michod 2007). The volvocine algae represent a great model system with which to study the transition to multicellularity as its members represent different steps towards complex multicellularity, and have been used to demonstrate the benefit of increased group size and germ-soma differentiation (e.g. for nutrient scavenging and maintaining mobility; Koufopanou and Bell 1993; Koufopanou 1994; Solari et al. 2006; Solari, Kessler, and Michod 2006).

Although the separation of germ and soma during development is fairly well understood in animals (Cinalli, Rangan, and Lehmann 2008), it remains to be elucidated in other lineages. With only two cell types, *V. carteri* is the simplest possible model system to study cell differentiation into soma or germ. Cell fate is determined by cell size at the end of embryogenesis; cells above the threshold size of 8 μm differentiate as germ cells, whereas cells below the threshold will enter a somatic cell fate (Kirk et al. 1993). Furthermore, the terminal differentiation of somatic cells involves the expression of

regA—a gene that is only expressed in presumptive somatic cells (Kirk et al. 1999). The correlation between cell size and *regA* expression suggests that *regA* induction depends on cell size, but this correlation has never been demonstrated before. As well, the signaling pathway involved in the cell size-dependent differential regulation of *regA* is not known.

Using a newly isolated *regA* and gonidialess mutant in which all cells start as somatic-like but then differentiate as gonidia (Chapter 2), I was able to demonstrate for the first time that *regA* can be induced not only developmentally, but also in response to environmental stimuli, and that this induction is also strictly dependent on cell size; that is, the environmental induction of *regA* was observed in small but not in large cells (Chapter 3). This argues for *V. carteri* (in addition to being an exciting model system to study cell differentiation) as a great system to study the connection between cell size and gene regulation, a newly burgeoning field whose importance has long been recognized but woefully neglected (Umen 2005; Wu et al. 2010; Marguerat and Bähler 2012; Jain et al. 2013). Furthermore, since *RLS1*—the closest homolog of *regA* in *C. reinhardtii*—is also expressed in response to environmental stress, the findings reported in this study provide support to the hypothesis that the evolution of somatic cells involved a change in the regulation of an ancestral life history trade-off genes (which increase survival with a cost to reproduction), from a temporal/environmental context into a spatial/developmental context (Nedelcu and Michod 2006; Nedelcu 2009).

The finding that *regA* could also be induced by environmental stress argues that *regA*'s proposed ancestral environmental regulation has been conserved and is still present in *V. carteri* (Chapter 3). It remains to be seen if the developmental and

environmental regulation of *regA* involve the same (or different) signals and regulatory elements. The data presented here suggest that the environmental signal might involve (directly or indirectly) a change in the cellular/chloroplast redox status. Nevertheless, other signaling pathways could be involved and further studies are needed to elucidate the exact mechanism that converts environmental signals into *regA* expression. Identifying the environmentally-induced signal will allow the direct testing of the models proposed here; that is, if the developmental and environmental regulation are both based on the same signaling pathway, interfering with components of the environmentally-induced pathway (e.g. by altering redox status, inhibiting kinases) should also affect the developmental differentiation of somatic cells.

Understanding how an environmentally-induced *RLS1*-like gene was co-opted into a developmental gene will help us understand how major morphological innovations can evolve. The evolution of new morphological traits is thought to often involve gene co-option most likely via changes in gene regulation (Carroll 2000; True and Carroll 2002; Ohta 2003; Carroll 2008; Wittkopp and Kalay 2012), but the exact mechanisms remain elusive. The system I developed in this work can provide a great opportunity to address such questions.

5.2 Evolution of cooperation

The evolution of multicellularity also involves the evolution of cooperation as typified by the division of labor between soma and germ. It has been proposed that cooperation is more stable, and cheaters can be prevented from taking over a population of cooperators, if the cooperative behavior is linked to a gene that also affects one or more traits

important for individual fitness. In this way, a mutation in such a cooperation gene might enable a cell to "cheat" but will, at the same time, be detrimental as another trait is negatively affected (antagonistic pleiotropy; Foster et al. 2004). For example, upon starvation the social amoeba *Dictyostelium discoideum* aggregates into a multicellular migratory slug, which then develops into a sterile stalk and a fruiting body with reproductive spores (Strassmann, Zhu, and Queller 2000; Kessin 2009). The differentiation into terminally differentiated sterile prestalk cells is triggered by the signaling molecule DIF-1 and involves the gene *dimA* (a basic-leucine zipper transcription factor; Thompson et al. 2004). *dimA*$^-$ mutants do not respond to DIF-1 and evade the prestalk cell fate, and in a chimera of wild type and *dimA*$^-$ cells they should be overrepresented in the spores. However, experiments showed that they are actually outcompeted and excluded from spores, suggesting that *dimA* must also be important for spore formation by an unknown mechanism (Foster et al. 2004).

In *V. carteri*, *regA* is a gene that ensures cooperation among cells by repressing the reproductive abilities of the somatic cell line. As the somatic cells decrease their reproductive potential to increase the fitness of the multicellular organism, they can be seen as altruistic cells and *regA* as an altruism gene (Nedelcu and Michod 2006). In this context, *regA* mutant somatic cells are cheaters as they regain their reproductive potential, i.e. they redifferentiate as gonidia; this behavior results in their losing the flagella, which negatively affects the motility, and likely the fitness of the whole organism (Solari, Kessler, and Michod 2006). In this study, I showed for the first time that *regA* has antagonistic pleiotropic effects at the cell level. Indeed, although *regA*$^-$ cells might regain their reproductive functions, at the same time they are more susceptible

to stress (and undergo programmed cell death) under certain environmental conditions (Chapter 3).

5.3 Future directions

Although this study uncovered unexpected aspects of the regulation of *regA* and provided experimental evidence for proposed scenarios regarding the evolution of somatic cell differentiation in *V. carteri* and of cooperation in general, the precise pathway and mechanism responsible for the differential expression of *regA* is still not known. A number of directions can be pursued to add more pieces to this puzzle that has fascinated *Volvox* researchers for decades.

For instance, follow up experiments to characterize the environmental signal responsible for *regA* induction should use inhibitors of photosynthetic electron flow or of components of other potential signaling pathways (e.g. kinases). *regA* induction might be related to the distribution between linear and cyclic electron flow and/or the redox state of the plastoquinone pool. If *regA* induction depends on cyclic electron flow then it should be sensitive to methyl viologen, a ferredoxin electron acceptor that abolishes cyclic electron flow (P. Joliot and A. Joliot 2006). The redox state of plastoquinone can also be manipulated; DCMU leads to an oxidized PQ pool (Wilson, Krol, and Hüner 2003) while a lower temperature (at the same light intensity) leads to the overreduction of the plastoquinone pool (Maxwell, Falk, and Huner 1995; Wilson, Krol, and Hüner 2003). If developmental and environmental regulation of *regA* involves the same signal, then an inhibitor that affects environmental induction of *regA* should also affect developmental regulation, i.e. somatic cells would show the regenerator phenotype. To identify *cis*-

regulatory elements in the *regA* introns, DNase I footprinting should be attempted (Hampshire et al. 2007) and their sequences might point to potential transcription factors involved in *regA* regulation. Alternative methods for isolating transcription factors binding to regulatory elements are available (e.g., DNA affinity chromatography; Gadgil, Jurado, and Jarrett 2001).

5.4 References

Carroll SB. 2000. Endless forms: the evolution of gene regulation and morphological diversity. Cell 101:577–580.

Carroll SB. 2008. Evo-devo and an expanding evolutionary synthesis: a genetic theory of morphological evolution. Cell 134:25–36.

Cinalli RM, Rangan P, Lehmann R. 2008. Germ cells are forever. Cell 132:559–562.

Foster KR, Shaulsky G, Strassmann JE, Queller DC, Thompson CRL. 2004. Pleiotropy as a mechanism to stabilize cooperation. Nature 431:693–696.

Gadgil H, Jurado LA, Jarrett HW. 2001. DNA affinity chromatography of transcription factors. Anal Biochem 290:147–178.

Hampshire AJ, Rusling DA, Broughton-Head VJ, Fox KR. 2007. Footprinting: a method for determining the sequence selectivity, affinity and kinetics of DNA-binding ligands. Methods 42:128–140.

Herron MD, Hackett JD, Aylward FO, Michod RE. 2009. Triassic origin and early radiation of multicellular volvocine algae. PNAS 106:3254–3258.

Jain N, Iyer KV, Kumar A, Shivashankar GV. 2013. Cell geometric constraints induce modular gene-expression patterns via redistribution of HDAC3 regulated by actomyosin contractility. PNAS 110:11349–11354.

Joliot P, Joliot A. 2006. Cyclic electron flow in C3 plants. Biochim Biophys Acta 1757:362–368.

Kessin RH. 2009. *Dictyostelium*. Cambridge: Cambridge University Press.

Kirk DL. 1998. *Volvox*: the molecular genetic origins of multicellularity and cellular differentiation. Cambridge.

Kirk MM, Ransick A, McRae SE, Kirk DL. 1993. The relationship between cell size and cell fate in *Volvox carteri*. J Cell Biol 123:191–208.

Kirk MM, Stark K, Miller SM, Müller W, Taillon BE, Gruber H, Schmitt R, Kirk DL. 1999. *regA*, a *Volvox* gene that plays a central role in germ-soma differentiation, encodes a novel regulatory protein. Development 126:639–647.

Koufopanou V, Bell G. 1993. Soma and germ: an experimental approach using *Volvox*. Proc Biol Sci 254:107–113.

Koufopanou V. 1994. The evolution of soma in the Volvocales. Am Nat 143:907–931.

Marguerat S, Bähler J. 2012. Coordinating genome expression with cell size. Trends Genet 28:560–565.

Maxwell DP, Falk S, Huner N. 1995. Photosystem II Excitation Pressure and Development of Resistance to Photoinhibition. Plant Physiol 107:687–694.

Michod RE. 2007. Evolution of individuality during the transition from unicellular to multicellular life. PNAS 104 Suppl 1:8613–8618.

Nedelcu AM, Michod RE. 2006. The evolutionary origin of an altruistic gene. Mol Biol Evol 23:1460–1464.

Nedelcu AM. 2009. Environmentally induced responses co-opted for reproductive altruism. Biol. Lett. 5:805–808.

Ohta T. 2003. Evolution by gene duplication revisited: differentiation of regulatory elements versus proteins. Genetica 118:209–216.

Prochnik SE, Umen JG, Nedelcu AM, Hallmann A, Miller SM, Nishii I, Ferris P, Kuo A, Mitros T, Fritz-Laylin LK, et al. 2010. Genomic analysis of organismal complexity in the multicellular green alga *Volvox carteri*. Science 329:223–226.

Solari CA, Ganguly S, Kessler JO, Michod RE, Goldstein RE. 2006. Multicellularity and the functional interdependence of motility and molecular transport. PNAS 103:1353–1358.

Solari CA, Kessler JO, Michod RE. 2006. A hydrodynamics approach to the evolution of multicellularity: flagellar motility and germ-soma differentiation in volvocalean green algae. Am Nat 167:537–554.

Strassmann JE, Zhu Y, Queller DC. 2000. Altruism and social cheating in the social amoeba *Dictyostelium discoideum*. Nature 408:965–967.

Thompson CRL, Fu Q, Buhay C, Kay RR, Shaulsky G. 2004. A bZIP/bRLZ transcription factor required for DIF signaling in *Dictyostelium*. Development 131:513–523.

True JR, Carroll SB. 2002. Gene co-option in physiological and morphological evolution. Annu Rev Cell Dev Biol 18:53–80.

Umen JG. 2005. The elusive sizer. Curr Opin Cell Biol 17:435–441.

Wilson KE, Krol M, Hüner NPA. 2003. Temperature-induced greening of *Chlorella vulgaris*. The role of the cellular energy balance and zeaxanthin-dependent nonphotochemical quenching. Planta 217:616–627.

Wittkopp PJ, Kalay G. 2012. *Cis*-regulatory elements: molecular mechanisms and evolutionary processes underlying divergence. Nat Rev Genet 13:59–69.

Wu C-Y, Rolfe PA, Gifford DK, Fink GR. 2010. Control of transcription by cell size. PLoS Biol 8:e1000523.

Curriculum Vitae

CANDIDATE'S FULL NAME: Stephan Georg König

UNIVERSITIES ATTENDED: University of Heidelberg, *Diplom* in Biology, 2005

PUBLICATIONS:

Wirtz M, Birke H, Heeg C, Müller C, Hosp F, Throm C, König S, Feldman-Salit A, Rippe K, Petersen G, et al. 2010. Structure and function of the hetero-oligomeric cysteine synthase complex in plants. J Biol Chem 285:32810–32817.

CONFERENCE PRESENTATIONS:

König SG, Nedelcu AM. 2011. New insights into the regulation of *regA* expression in *Volvox carteri*. First International *Volvox* Conference (Talk)

König SG, and Nedelcu AM. 2010. Investigations on the regulation of *regA*—the gene responsible for somatic cell differentiation in *Volvox carteri*. 14th International Conference on the Cell and Molecular Biology of Chlamydomonas (Poster presentation)

König SG, Nedelcu,AM. 2009. Investigating the regulatory elements of *regA*–the gene responsible for reproductive altruism in the green alga *Volvox carteri*. Canadian Society for Ecology and Evolution Meeting (Poster presentation)